A NEW CONTINUUM BASED NON-LINEAR
FINITE ELEMENT FORMULATION FOR MODELING OF
DYNAMIC RESPONSE OF DEEP WATER RISER BEHAVIOR

A thesis submitted for the degree of Doctor of Philosophy

by

Seyed Ali Hosseini Kordkheili

Mechanical Engineering Department, School of Engineering and Design
Brunel University

February 2009

Abstract

The principal objective of this investigation is to develop a nonlinear continuum based finite element formulation to examine dynamic response of flexible riser structures with large displacement and large rotation. Updated Lagrangian incremental approach together with the 2nd Piola-Kirchhoff stress tensor and the Green-Lagrange strain tensor is employed to derive the nonlinear finite element formulation. The 2nd Piola-Kirchhoff stress and the Green-Lagrange strain tensors are energy conjugates. These two Lagrangian tensors are not affected by rigid body rotations. Thus, they are used to describe the equilibrium equation of the body independent of rigid rotations. While the current configuration in Updated Lagrangian incremental approach is unknown, the resulting equation becomes strongly nonlinear and has to be modified to a linearized form. The main contribution of this work is to obtain a modified linearization method during development of incremental Updated Lagrangian formulation for large displacement and large rotation analysis of riser structures. For this purpose, the Green-Lagrange strain and the 2nd Piola-Kirchhoff stress tensors are decomposed into two second-order six termed functions of through-the-thickness parameters. This decomposition makes it possible to explicitly account for the nonlinearities in the direction along the riser thickness, as well. It is noted that using this linearization scheme avoids inaccuracies normally associated with other linearization schemes. The effects of buoyancy force, riser-seabed interaction as well as steady-state current loading are considered in the finite element solution for riser structure response.

An efficient riser problem fluid-solid interaction Algorithm is also developed to maintain the quality of the mesh in the vicinity of the riser surface during riser and fluid mesh movements. To avoid distortions in the fluid mesh two different approaches are proposed to modify fluid mesh movement governing elasticity equation matrices values; 1) taking the element volume into account 2) taking both element volume and distance between riser centre and element centre into account.

The formulation has been implemented in a nonlinear finite element code and the results are compared with those obtained from other schemes reported in the literature.

Acknowledgements

To Shokoufe, Hesam and Soha, with love...

Keywords

Table of Contents

Chapter 2

Non-Linear Finite Element Formulation for Flexible Risers in Presence   12
of Buoyancy Force and Seabed Interaction Boundary Condition

List of Figures

Chapter 5

Nomenclature

(x, y, z)	Global Cartesian system
(r, s, t)	Natural coordinate system
(ξ, η, ζ)	Local curvilinear coordinate system
(u_1, u_2, u_3)	Translation components
$(\theta_1, \theta_2, \theta_3)$	Rotation components
k	Indicates node number
a^k	Thickness for node k
τ	Left superscript; indicates previous time step
$\tau + \Delta\tau$	Left superscript; indicates current time step
$h_k(r)$	Interpolation (shape) function corresponding to nodal point k
$(V_{sx}^k, V_{sy}^k, V_{sz}^k)$	Local normal vector components at node k in directions s
$(V_{tx}^k, V_{ty}^k, V_{tz}^k)$	Local normal vector components at node k in directions t
$\left(\varepsilon_{\eta\eta}\right)_{ov}$	Pipe cross sectional circumferential strain component
$\left(\varepsilon_{\xi\xi}\right)_{ov}$	Pipe cross sectional longitudinal strain component
w_R	Local displacement of the pipe wall
ϕ	Measure the angular position
ω_ζ	Radial displacement
σ_{ij}	Cauchy stress tensor components
S_{ij}	2nd Piola-Kirchhoff stress tensor

E_{ij}	Green-Lagrange strain tensor
$\Re$	External virtual work
e_{ij}	Linear part of the strain tensor
η_{ij}	Nonlinear part of the strain tensor
C_{ijrs}	Components of the material property tensor
$\mathbf{H}$	Displacement interpolation matrix
$\mathbf{K_L}$	Linear stiffness matrix
$\mathbf{K_{NL}}$	Nonlinear stiffness matrix
$\mathbf{R}$	External load vector
$\mathbf{F}$	Internal force vector
$\mathbf{R}_{Buy}$	Buoyancy force vector
$\mathbf{q}_{current}$	Steady-state current force vector
$\mathbf{M}$	Mass matrix
$\mathbf{B}_L$	Linear strain-displacement matrix
$\mathbf{B}_{NL}$	Nonlinear strain-displacement matrix
$\widehat{\mathbf{S}}$	2nd Piola-Kirchhoff stress vector
$\widehat{\boldsymbol{\sigma}}$	Cauchy stress vector
Δ	Stands for the incremental values
J_{mn}	Jacobian matrix components
V	Element volume
$\tilde{r}$	Distance between riser centre and element centre

Chapter 1

Introduction

1.1 General introduction

Flexible risers are slender marine structures which are widely used in offshore production to convey fluids between the well-head and the surface unit. In deep-water applications, because of the low bending stiffness when compared to axial and torsional stiffness, a flexible pipe can suffer large displacements and large rotations which demand special geometrically nonlinear analysis.

Deepwater and ultra deepwater riser fatigue failure due to vortex induced vibration (VIV) is currently considered by the oil industry to be a very significant unresolved problem. This is essentially a coupled fluid-solid interaction phenomenon that accompanies a highly nonlinear dynamic behavior of a flexible riser with large displacement and rotation.

1.2 Flexible riser structure

Marine risers are classified into two categories: drilling and production risers. A drilling riser is used for exploratory drilling, is made of steel and contains the drill string and drilling mud. A production riser consists of a cluster of flow-lines, which transfer the crude oil from seabed to sea-surface. Traditional production marine risers are vertical rigid steel structures, which are prevented from buckling by the application of a tensile force to its top end. This makes these structures suitable for shallow water applications. Flexible risers, as modern production risers, withstand much greater vessel motions than rigid steel risers and do not require external tensile force at their extremes [1].

Flexible riser was introduced to the marine market in the early 70's [2]. The flexible risers are classified as unbonded flexible risers, without adhesive agents between the layers, and bonded flexible risers, with the reinforce bonded to an elastomeric matrix [3]. Withstanding significant flexure together with maintaining the required axial strength and pressure integrity makes unbonded flexible risers a unique structure suitable for ultra deepwater applications [4].

A flexible riser structures contains several different layers. Starting from the most inner layer, these include a carcass, an internal pressure sheath made of polymeric material, an interlocked pressure armour layer, an anti-wear layer, two tensile armour layers and an outer sheath with each layer having a particular function [5]. All layers are free to slide with respect to each other. The external plastic sheath layer protects the riser from surrounding seawater intrusion, external damages during handling and corrosion. The internal plastic sheath layer ensures internal fluid integrity and is made from polymer.

1.3 Problem statement

The growing utilization of flexible risers in deep water applications demands new and more efficient analysis techniques to achieve more reliable and more economic production. A new nonlinear finite element formulation is required to increase the accuracy of the solution during study of riser structures behavior subjected to fluid loading and also for studying

vortex induced vibration (VIV), an important phenomena which can lead to failure of the riser in service.

1.4 Research objectives

The present work aims to develop a new continuum based finite element formulation to simulate large displacement and large rotation in flexible riser structures. Also in order to simulate the fluid-solid interaction phenomena in the riser application, an efficient algorithm will be developed to transfer data between these two domains. A generalized nonlinear finite element formulation is also to be developed to analyze unbonded multilayer flexible riser using a constitutive model of the flexible riser.

1.5 Main contributions of the work

An updated Lagrangian finite element formulation for nonlinear dynamic analysis of flexible riser structure has been developed. A modified linearization scheme has also been formulated to linearize highly nonlinear governing equation. The resulting modified formulation significantly reduces the errors normally associated with other linearization schemes in the literature. Also a constitutive model that describes a very detailed behavior of the unbonded flexible riser [6] is used together with a generalized finite element formulation to solve for the dynamic response of the flexible riser structures.

1.6 Literature survey for nonlinear analysis of structures

The development of efficient computational procedures for the nonlinear analysis of structures has for a long time been the subject of many research endeavors. This is partially motivated by the need to model new materials such as composite and functionally graded materials [7-14] or structures with highly nonlinear behavior [15-17]. In large displacement analysis of structures with strong nonlinear behavior, as in the case of flexible risers, an

efficient linearization technique should be adopted. A survey in the literature reveals a number of linearization methods which have been implemented in nonlinear finite element formulations [18-21].

Bathe et al. [21] derived a finite element incremental formulation for nonlinear static and dynamic analysis of structures. Employing an isoparametric finite element discretization they achieved a numerical solution for continuum mechanic equations. Also, using a simple pipe elbow element, Bathe et al [22] proposed a finite element formulation for linear analysis of pipe structures. This finite element formulation has since been extended to include some nonlinear effects [23].

Based on Bathe's standard Lagrangian finite element formulation for structures, many works have been done by researchers who have struggled to suggest new accurate and optimal strategies for geometrically nonlinear analysis of structures [24-26]. Meanwhile, other researchers have been evaluating other techniques [27-32].

Recently, Hosseini Kordkheili and Bahai [15] presented a finite element formulation for geometrically nonlinear analysis of flexible riser structures in presence of a pipe-soil interaction boundary condition, buoyancy force and steady state current loading. This formulation was based on a flexible riser element and Updated Lagrangian (UL) formulation, which has been linearized using Bathe's standard linearization approach. This formulation currently fails to model large rotations [15]. The motivation of the present work is to develop a nonlinear finite element formulation for flexible riser structures to also account for large rotations.

1.7 Literature Survey for nonlinear analysis of riser structures

The growing economic importance of structural integrity of flexible risers for deep water oil and gas industry demands new and more efficient simulation techniques. A methodology is required to significantly reduce the computational time associated with running of the finite element detailed models of riser structure. Such a capability should have significant benefits for cost effective deep water flexible riser design practice.

At a very early stage of modeling riser structures, knowledge of applied load is necessary. At the sea-surface, a riser structure is subjected to a high mean tension combined with cyclic loading, and at the seabed, it is subjected to a pipe-soil interaction boundary condition. Also, the riser is subjected to a severe external pressure, axial compression, bending and torsional moments as well as buoyancy forces in other parts. During the installation procedure however when the pipe is empty, the riser experiences high combined axial compression and bending at the touchdown point [33].

The advantages of flexible risers with respect to rigid steel risers is the much lower bending stiffness of the former, leading to smaller radiuses of curvature with the same pressure capacity, due to the complex make up of flexible risers [34, 35], in turn resulting in increased ability of undergoing large deformations under loads induced by the sea current, vortex induced-vibrations, the motion of the floating-vessel and during installation.

Very early work on analyzing riser structures goes back to 1979 by Knapp [36]. He derived an element stiffness matrix for cable elements subjected to tension and torsion by replacing the cross-section of a cable with a single element. His approach was quite general and included consideration of the geometric nonlinearities, compressibility of the core, arbitrary cross section of the core, variation of lay angles and the number of wire layers.

The static analysis procedure for the numerical determination of nonlinear static equilibrium configurations of deep-ocean risers was performed by Felippa and Chung [37]. The riser was modeled by three-dimensional beam finite elements which include axial, bending, and torsional deformations. They extended their model by taking the deformations coupled through geometrically nonlinear effects [38]. The resulting tangent-stiffness matrix included three contributions identified as linear, geometric (initial-stress) and initial-displacement stiffness matrices. For the solution, a combination of load-parameter incrimination, state updating of fluid properties and corrective Newton-Raphson iteration was used.

McNamara and Lane [39] studied the two-dimensional response of the linear and nonlinear static and dynamic motions of offshore systems such as risers and single-leg mooring towers. Their proposed method was based on the finite element approach using convected

coordinates for arbitrary large rotations and includes terms due to loads such as buoyancy, gravity, random waves, currents, ship motions and Morison's equation. They also extended their work to the three-dimensional frequency domain computational dynamic analysis of deep-water multi-line flexible risers [40]. O'Brien et al. [41] presented the three-dimensional finite element modeling of marine risers, pipelines and offshore loading towers based on the separation of the rigid body motions and deformations of elements under conditions of finite rotations. This paper treats risers as a homogenous material and includes all the nonlinear effects including geometry changes, bending-axial and bending-torsional coupling and follower forces and pressures.

A two-dimensional static and dynamic analysis of flexible risers and pipelines in the offshore environment subjected to wave loading and vessel movements was presented by McNamara et al. [42]. They developed a hybrid beam element formulation where the axial force was combined with the corresponding axial displacements via a Lagrangian constraint. The hybrid beam element was capable of applying to offshore components varying from mooring lines or cables to pipelines with finite bending stiffness. However, they failed to consider contact and frictional effects between layer components of the riser.

Hoffman et al. [43] reviewed the design technique of deep and shallow water marine riser systems as well as their dynamic analytical and numerical analysis and the nonlinearities arising from hydrodynamic loading and dynamic boundary conditions. This paper contains design methodology criteria, parameters and procedures of flexible riser systems while treating the riser as one homogenous material layer. Atadan et al. [44] studied dynamic three-dimensional response of risers in the presence of ocean waves and ocean currents undergoing large deflections and rotations. They included shear effects based on nonlinear elastic theory in their formulation. It was concluded that the length of the riser is the most important parameter which affects the deflections of the marine-riser. Chai et al. [45] proposed a three-dimensional lump-mass formulation for riser structure analysis which is capable of handling irregular seabed interaction. They adopted a simplified model by replacing the seabed surface with an elastic foundation with independent elastic springs having an arbitrary thickness which maybe critically damped.

Ong and Pellegrino [46] studied the nonlinear dynamic behavior of mooring cables in the frequency domain. They ignored the effects of friction and impact between the cable and the seabed. Their proposed method models the time-varying boundary condition at the touchdown by replacing the section of cable interacting with the seabed with a system of coupled linear springs. They decomposed the seabed interaction into axial stretching of laid riser and the catenary action at the touchdown using a linear stress-strain relationship. Catenary action is the liftoff-and-touchdown behavior of the pipe lying on the seabed.

Zhang *et al.* [47] discussed analytical tools for improving the performance of unbonded flexible pipe. This work uses an equivalent linear bending stiffness which is derived from experimental data to calculate the maximum bending angle range. It contains reports on irregular wave fatigue analysis, collapse, axial compression and bird-caging for riser systems. The authors are of the opinion that the combined bending, axial compression and torsion could lead to the tendon being separate from the cylinder in a helix layer, and may lead to out of plane buckling. However the assumption of equivalent linear bending stiffness neglects all the interactions between layer components of an unbonded flexible riser and makes it to behave as a bonded riser.

Willden and Graham [48] reported results from two strip theory CFD investigations of the Vortex-Induced Vibrations of model riser pipes of which the first one is concerned with the vibrations of a vertical riser pipe that was subjected to a stepped current profile, and the second one is concerned with the simultaneous in-plane and out-of-plane vibrations of a model steel catenary riser that was subjected to a uniform current profile. Their method was based on computing the fluid flow in multiple two-dimensional planes that are positioned at intervals along the length of a body. It was found that six to seven simulation planes are required per half-wavelength of pipe vibration in order to obtain convergence. This work is based on modeling of steel risers and ignores the effects of friction between layers and does not capture any energy dissipation due to contact between layers.

Hibbitt et al. [49] presented nonlinear analysis of marine pipelines, involving both geometric nonlinearity and frictional effects caused by the pipeline lying directly on the seabed. The motions, caused by moving the already laid down pipelines into a correct position, typically involve very large translations and rotations. The authors are of the

opinion that the usual stiffness formulation is not practicable due to the slender characteristics of the pipelines. Their method is based on numerical models for the components of the system (pipeline, friction, drag chains, towing cable) which lead to the efficient solution of typical problems. Due to the strong path dependency of the system, a nonlinear incremental scheme has been used.

Nielsen *et al.* [50] presented the capability to predict the service life of dynamic flexible risers which was conducted by three organizations. They reviewed static and dynamic analyses of the riser, each stage performed by one organization. It is a practical application of the hysteresis model proposed by Witz and Tan [51] to analysis of fatigue. The model is based on a slip onset criterion for bending loading only. The work of Nielsen *et al.* further estimates the service life of dynamic flexible risers based on results obtained from Flex riser 4 program, which is a package originally developed for the Chevron Spain Montanozo project.

Out *et al.* [3] studied the integrity of flexible pipe. In their study, they searched for an inspection strategy by using a certain technique to look at the structure and assessing its suitability. This work discusses the type of defects and degradation in all phases of the pipe's life. The design of flexible riser systems for mechanical deterioration is not fully proven and the governing failure modes are quantitatively uncertain. It has been stipulated that acoustic emission is suitable for the inspection of flexible pipe for wear damage. For the inspection of flexible pipe for fractured outer tensile armours radiography, magnetic stray flux and eddy current are the best methods. Finally, eddy current and acoustic emissions were considered suitable for the inspection of flexible pipes for fatigue cracking of the pressure reinforcing.

Patel and Seyed [52] reported a comprehensive overview of status of analysis techniques for flexible riser design as well as a historical overview of the development of hydrodynamic analysis techniques. This work discusses the models which are being exploited in the optimization of pipe construction and highlights key issues addressed during these developments including the effects of internal and external hydrostatic pressures. This work concludes by highlighting the potential gaps in this filed of study which is the effects of structural damping, tangential hydrodynamic drag loads, and seabed

interaction effects, the effects of vortex shedding and out of plane oscillations of mid-water buoys. It also expresses concern about the lack of sufficiently wide ranging and openly available model testing and full-scale data on flexible risers [52].

Yazdchi and Crisfield used a simple two-dimensional lower-order beam element formulation for static nonlinear analysis of riser structures including the effects of buoyancy, steady-state current loading and riser top-tension. They assumed linearly elastic material property for the riser by employing a constant modulus of elasticity. They studied the static behavior of flexible pipelines and marine risers, using the types of finite elements that had been developed for conventional non-linear analysis [17]. The same authors continued their research by using a beam finite element formulation based on Reissner–Simo beam theory for the static and dynamic non-linear analysis of three-dimensional flexible pipes and riser systems in present of hydrostatic and hydrodynamic forces. Employing a linearly elastic material property, their work concentrates on the nonlinearities due to the fluid loading and the associated large deformations and considers hydrodynamic forces due to effects such as wave, drag and current action [16].

Recent developments on the fatigue analysis of unbonded flexible risers reveal the necessity of a comprehensive global dynamic analysis together with the detailed hysteresis damping of the riser loading response and the three-dimensional local stress analysis. Smith *et al.* [53] presented an application based on a fatigue reassessment of a riser system and claimed that the advanced fatigue methods produce longer fatigue lives than the current state-of-practice methods, despite the fact that their method was based on an elastoplastic model of riser bending response.

Lacarbonara and Pacitti [54] proposed a geometrically exact formulation for dynamic analysis of cables undergoing axial stretching and flexural curvature. In this model they considered material nonlinearity and general loading condition. They then employed two different numerical methods to solve some particular cases of horizontal and inclined cables with linear material properties.

According to this literature survey, modeling the flexible riser structure for dynamic loading in large displacement and large rotation regime is important.

Hosseini Kordkheili and Bahai [15, 55] presented a finite element formulation for geometrically nonlinear analysis of flexible riser structures in presence of a pipe-soil interaction boundary condition, buoyancy force and steady state current loading. This formulation was based on a pipe element and Updated Lagrangian (UL) formulation, which was linearized using Bathe's standard linearization approach. The formulation in its presented form in [15, 55] could not model large rotations. The authors were of the opinion that using a modified linearization technique during derivation of the UL formulation leads to developing a more accurate incremental nonlinear finite element formulation that also can account for large rotations. Therefore, using a particular linearization method, Hosseini Kordkheili and Bahai [56-58] presented a modified finite element formulation for geometrically nonlinear dynamic analysis of flexible riser structures with both large displacement and large rotation.

1.8 Motivation

Since many years ago it has been recognized that increasing extent of the capability of performing effective nonlinear analysis can be a very important asset in the design of structures [59]. The reliability of a structure can be increased and the cost reduced if an accurate analysis can be performed. Accordingly, this work has been motivated by a need for an accurate and efficient non-linear finite element formulation together with the buoyancy force effects, current load as well as seabed model for more accurate analysis of the dynamics behavior of riser structures. Therefore, in this thesis a finite element formulation is presented for geometrically nonlinear analysis of flexible riser structures in together with a pipe-soil interaction model, buoyancy force and steady state current loading. This formulation is based on a four-node and twenty four-degrees of freedom annular section beam element and Updated Lagrangian (UL) formulation.

1.9 Layout of the thesis

The first chapter is an introduction and the identification of the research problem. It also gives a brief description of the objectives of the research. The chapter also contains a literature review in which previous studies and research on nonlinear analysis of the structures and flexible riser are reviewed. In the second chapter, a nonlinear finite element formulation for flexible risers in presence of buoyancy force and seabed interaction boundary condition will be presented. The third chapter contains an updated Lagrangian finite element formulation for large displacement dynamic analysis of three-dimensional flexible riser structures. This chapter clearly explains the modified linearization scheme which was employed during modified formulation development.

In chapter four, an efficient riser problem fluid-solid interaction Algorithm is developed. The main focus in this chapter is on preventing fluid fine meshes from distortion while the fluid domain relocates with riser movement. Chapter five discusses a generalized nonlinear finite element formulation to analysis unbonded multilayer flexible riser using a transitional constitutive model. In chapter six some results from the nonlinear finite element code, which has been developed by author, will be verified using those available in the literature. Conclusions and future works are discussed in Chapter seven, followed by a list of references and publications by author.

Chapter 2

Non-Linear Finite Element Formulation for Flexible Risers in Presence of Buoyancy Force and Seabed Interaction Boundary Condition

2.1 Introduction

In this chapter, a non-linear finite element formulation for large displacements of flexible risers is presented. A pipe-soil interaction model is used to represent seabed boundary condition. The effects of buoyancy force as well as steady-state current loading are considered in the finite element solution for riser structural response.

The riser structure consists of a long flexible pipe which may have part of its length supported on the seabed surface. Chai et al. [45] proposed a three-dimensional lump-mass formulation for riser structure analysis which is capable of handling irregular seabed interaction. They adopted a simplified model by replacing the seabed surface with an elastic foundation with independent elastic springs having an arbitrary stiffness which maybe critically damped. Yazdchi and Crisfield [17] used a simple two-dimensional lower-order beam element formulation for nonlinear analysis of riser structures. They included in their

formulation the effects of buoyancy, steady-state current loading and riser top-tension but they did not consider sea-bed effects. Laver et al. [60] proposed a pipe-soil interaction model based upon some test data and information from some existing published data. Their model is currently being used in many Gulf of Mexico deepwater projects. To use the Laver et al.'s [60] proposed model, some knowledge on consolidation properties of marine clay is needed. Chu et al. [61] investigated the consolidation and permeability characteristics for marine clay. Their work gives a good understanding on soil property parameters and their range of values.

The existing non-linear capabilities for effective large displacement analysis of flexible risers cannot address all the features which characterise the dynamic behaviour of these risers.

The safety of riser structures may be increased and the associated costs reduced, if an accurate analysis can be performed. In this chapter a particular seabed model together with a continuum three-dimensional annular section beam element for more accurate analyzing the riser structures is presented. The chapter also deals with the riser's boundary condition and the touch-down effects on riser behavior. The finite element formulation presented deals with geometrically nonlinear features of flexible riser structures in presence of a pipe-soil interaction model, buoyancy force and steady state current loading. This formulation is based on a four-node and twenty four-degrees of freedom element and an Updated Lagrangian (UL) formulation.

2.2 Kinematics of flexible riser element

The element employed in the present work is a four-nodded, twenty four degrees of freedom annular section beam element, Figure 2.1. This element is a continuum based element which has been introduced in some published finite element documents, for example [20, 22]. The proposed element can represent axial, torsional and bending displacements as well as rotations. It can also represent the sectional ovalization effects, internal pressure stiffening effects as well as the interaction effects. The element can be

extended to model geometrically nonlinear (large deformation and rotation) behaviour. This element can also accurately predict the significant deformations and stresses in various curved pipe segments [15, 20].

This element is formulated using three different coordinate systems; the global Cartesian system (x, y, z), the natural coordinate system (r, s, t) and local curvilinear coordinate system (ξ, η, ζ).
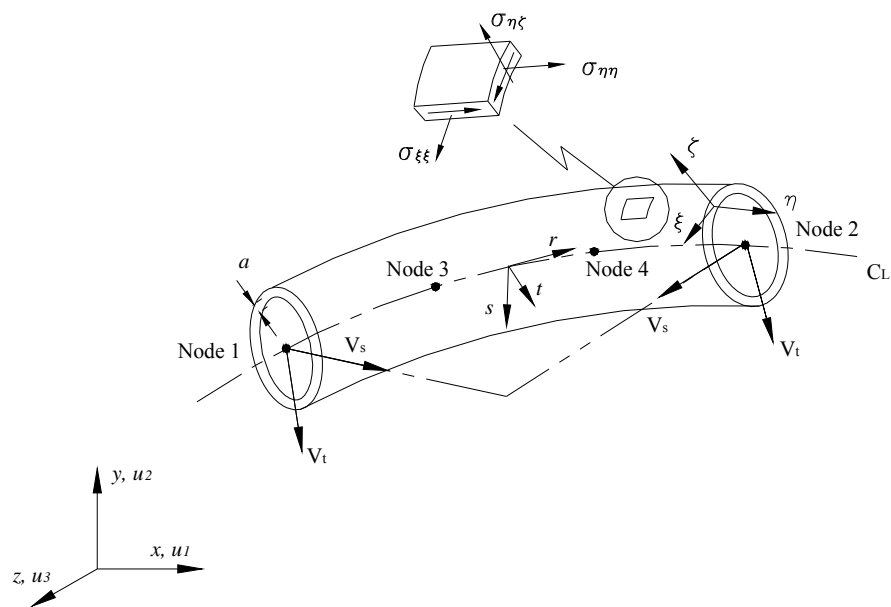
Figure 2.1: Flexible riser element together with coordinate systems and local normal vectors
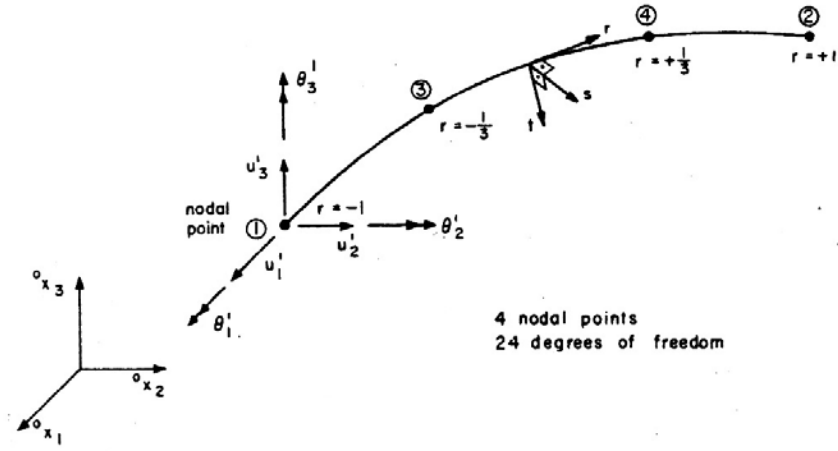
Figure 2.2: Position for third and forth nodes

In the 3-D space, three vectors are required to define the geometry of this element. One vector expresses the configuration of the pipe mid-line and the two other vectors, called the unit normal vectors, express any position between the inner and the outer surfaces of the pipe in directions s and t. The mid-line of the element which corresponds to $s = t = 0$ is parameterized using curvilinear coordinate r. In this manner, all terms derived in this study are referred to the natural coordinates (r, s, t). In this element each node has six degrees of freedom, three translations (u_1, u_2, u_3) and three rotations $(\theta_1, \theta_2, \theta_3)$ with respect to the global stationary Cartesian axes. After finite element discretization on the middle line of the continuum pipe, the configuration of the element having thickness a^k for node k can be expressed by

$$^\tau x(r,s,t) = \sum_{k=1}^{4} h_k(r)\,^\tau x^k + s\sum_{k=1}^{4} h_k(r)\,a^k\,^\tau V_{sx}^k + t\sum_{k=1}^{4} h_k(r)\,a^k\,^\tau V_{tx}^k \qquad (2.1)$$

$$^\tau y(r,s,t) = \sum_{k=1}^{4} h_k(r)\,^\tau y^k + s\sum_{k=1}^{4} h_k(r)\,a^k\,^\tau V_{sy}^k + t\sum_{k=1}^{4} h_k(r)\,a^k\,^\tau V_{ty}^k \qquad (2.2)$$

15

$$^{\tau}z(r,s,t) = \sum_{k=1}^{4} h_k(r)\,{}^{\tau}z^k + s\sum_{k=1}^{4} h_k(r)\,a^k\,{}^{\tau}V_{sz}^k + t\sum_{k=1}^{4} h_k(r)\,a^k\,{}^{\tau}V_{tz}^k \tag{2.3}$$

where $^{\tau}x$, $^{\tau}y$ and $^{\tau}z$ are Cartesian coordinates of any point in the element at time τ and $^{\tau}x^k$, $^{\tau}y^k$ and $^{\tau}z^k$ are Cartesian coordinates of nodal point k at time τ. Also $h_k(r)$ is the interpolation (shape) function corresponding to nodal point k. These shape functions interpolate varying parameters cubically along the length (using those nodal values). According to the given position for third and forth node shown in Figure 2.2, $h_k(r)$ are given below

$$h_1 = \frac{1}{16}\left(-9r^3 + 9r^2 + r - 1\right) \tag{2.4}$$

$$h_2 = \frac{1}{16}\left(9r^3 + 9r^2 - r - 1\right) \tag{2.5}$$

$$h_3 = \frac{1}{16}\left(27r^3 - 9r^2 - 27r + 9\right) \tag{2.6}$$

$$h_4 = \frac{1}{16}\left(-27r^3 - 9r^2 + 27r + 9\right) \tag{2.7}$$

Also, in Equations (2.1)-(2.3), $({}^{\tau}V_{sx}^k, {}^{\tau}V_{sy}^k, {}^{\tau}V_{sz}^k)$ and $({}^{\tau}V_{tx}^k, {}^{\tau}V_{ty}^k, {}^{\tau}V_{tz}^k)$ are the local normal vector components at node k in directions s and t, respectively. Using these equations the displacement field of the riser flexible element at time $\tau + \Delta\tau$ are obtained as

$$^{\tau+\Delta\tau}u_1(r,s,t) = {}^{\tau+\Delta\tau}x - {}^{\tau}x \tag{2.8}$$

$$^{\tau+\Delta\tau}u_2(r,s,t) = {}^{\tau+\Delta\tau}y - {}^{\tau}y \tag{2.9}$$

16

$$^{\tau+\Delta\tau}u_3(r,s,t) = {}^{\tau+\Delta\tau}z - {}^{\tau}z \tag{2.10}$$

Substituting from (2.1)-(2.3) into (2.8)-(2.10) results

$$^{\tau+\Delta\tau}u_1(r,s,t) = \sum_{k=1}^{4} h_k(r) \, {}^{\tau+\Delta\tau}u_1^k + t\sum_{k=1}^{4} a^k h_k(r) \, V_{tx}^k + s\sum_{k=1}^{4} a^k h_k(r) \, V_{sx}^k \tag{2.11}$$

$$^{\tau+\Delta\tau}u_2(r,s,t) = \sum_{k=1}^{4} h_k(r) \, {}^{\tau+\Delta\tau}u_2^k + t\sum_{k=1}^{4} a^k h_k(r) \, V_{ty}^k + s\sum_{k=1}^{4} a^k h_k(r) \, V_{sy}^k \tag{2.12}$$

$$^{\tau+\Delta\tau}u_3(r,s,t) = \sum_{k=1}^{4} h_k(r) \, {}^{\tau+\Delta\tau}u_3^k + t\sum_{k=1}^{4} a^k h_k(r) \, V_{tz}^k + s\sum_{k=1}^{4} a^k h_k(r) \, V_{sz}^k \tag{2.13}$$

where $V_{ti}^k = {}^{\tau+\Delta\tau}V_{ti}^k - {}^{\tau}V_{ti}^k$ and $V_{si}^k = {}^{\tau+\Delta\tau}V_{si}^k - {}^{\tau}V_{si}^k$ which can be approximated using the rotational degrees of freedom $\boldsymbol{\theta}^k$ as follows

$$\mathbf{V_t^k} = {}^{\tau+\Delta\tau}\boldsymbol{\theta}^k \times {}^{\tau}\mathbf{V_t^k} + \frac{1}{2}{}^{\tau+\Delta\tau}\boldsymbol{\theta}^k \times ({}^{\tau+\Delta\tau}\boldsymbol{\theta}^k \times {}^{\tau}\mathbf{V_t^k}) \tag{2.14}$$

$$\mathbf{V_s^k} = {}^{\tau+\Delta\tau}\boldsymbol{\theta}^k \times {}^{\tau}\mathbf{V_s^k} + \frac{1}{2}{}^{\tau+\Delta\tau}\boldsymbol{\theta}^k \times ({}^{\tau+\Delta\tau}\boldsymbol{\theta}^k \times {}^{\tau}\mathbf{V_s^k}) \tag{2.15}$$

where $^{\tau+\Delta\tau}\boldsymbol{\theta}^k$ is a vector of nodal point rotations at nodal point k, i.e.

$$^{\tau+\Delta\tau}\boldsymbol{\theta}^k = \left\{ \begin{array}{c} {}^{\tau+\Delta\tau}\theta_1^k \\ {}^{\tau+\Delta\tau}\theta_2^k \\ {}^{\tau+\Delta\tau}\theta_3^k \end{array} \right\} \tag{2.16}$$

While the rotation angles are small, relations (2.14) and (2.15) can be used directly to calculate V_{ti}^k and V_{si}^k. But for more accurate results in large deformation analysis the direction cosines of the new nodal point's vectors can be evaluated using:

17

$$^{\tau+\Delta\tau}\mathbf{V_t^k} = {}^{\tau}\mathbf{V_t^k} + \int_{\theta^k} d\theta^k \times {}^{\tau}\mathbf{V}_t^k + \frac{1}{2}\int_{\theta^k} d\theta^k \times (d\theta^k \times {}^{\tau}\mathbf{V}_t^k) \tag{2.17}$$

$$^{\tau+\Delta\tau}\mathbf{V_s^k} = {}^{\tau}\mathbf{V_s^k} + \int_{\theta^k} d\theta^k \times {}^{\tau}\mathbf{V}_s^k + \frac{1}{2}\int_{\theta^k} d\theta^k \times (d\theta^k \times {}^{\tau}\mathbf{V}_s^k) \tag{2.18}$$

Using Equations (2.11)-(2.13) we obtain:

$$^{\tau+\Delta\tau}\mathbf{U} = {}^{\tau+\Delta\tau}_{\tau+\Delta\tau}\mathbf{H}\ {}^{\tau+\Delta\tau}\mathbf{u}^k \tag{2.19}$$

where ${}^{\tau+\Delta\tau}_{\tau+\Delta\tau}\mathbf{H}$ is displacement interpolation matrix which is given as follow

$$^{\tau+\Delta\tau}\mathbf{U} = \begin{bmatrix} \cdots & {}^{\tau+\Delta\tau}_{\tau+\Delta\tau}\mathbf{H}^{(k)} & \cdots \end{bmatrix} \begin{Bmatrix} \vdots \\ u_1^k \\ u_2^k \\ u_3^k \\ \theta_1^k \\ \theta_2^k \\ \theta_3^k \\ \vdots \end{Bmatrix} \tag{2.20}$$

and

$$^{\tau+\Delta\tau}_{\tau+\Delta\tau}\mathbf{H}^{(k)} = \begin{bmatrix} h_k & 0 & 0 & 0 & a_k h_k(t^{\tau+\Delta\tau}V_{t3}^k + s^{\tau+\Delta\tau}V_{s3}^k) & -a_k h_k(t^{\tau+\Delta\tau}V_{t2}^k + s^{\tau+\Delta\tau}V_{s2}^k) \\ 0 & h_k & 0 & -a_k h_k(t^{\tau+\Delta\tau}V_{t3}^k + s^{\tau+\Delta\tau}V_{s3}^k) & 0 & a_k h_k(t^{\tau+\Delta\tau}V_{t1}^k + s^{\tau+\Delta\tau}V_{s1}^k) \\ 0 & 0 & h_k & a_k h_k(t^{\tau+\Delta\tau}V_{t2}^k + s^{\tau+\Delta\tau}V_{s2}^k) & -a_k h_k(t^{\tau+\Delta\tau}V_{t1}^k + s^{\tau+\Delta\tau}V_{s1}^k) & 0 \end{bmatrix}$$

$$\tag{2.21}$$

In the recent formulas as well as in this work, the super-left-script indicates the time step that the variable is calculating on also, the lower-left-script indicates the time that the variable is calculated in respect with that configuration.

18

2.3 Ovalization effects

Figure 2.3 shows the ovalization of the cross section in a typical pipe element. In analysis of pipe elements together with ovalization effects, two additional strain components also need to be considered which are due to ovalization of the cross section. These strain components are a pipe cross sectional circumferential strain, $\left(\varepsilon_{\eta\eta}\right)_{ov}$, which is due to deformation of the cross section, and, a longitudinal strain, $\left(\varepsilon_{\xi\xi}\right)_{ov}$, which is due to change in the curvature of the pipe itself [22]. Using the von Karman analysis and the assumptions that the pipe wall thickness (δ) is small in comparison to the pipe external radius (i.e., $\delta/a \ll 1$) and the pipe external radius is much smaller than the pipe curveture (i.e., $a/R \ll 1$), the longitudinal strain due to distortion of the cross section is:

$$\left(\varepsilon_{\eta\eta}\right)_{ov} = \frac{w_R}{R} \tag{2.22}$$
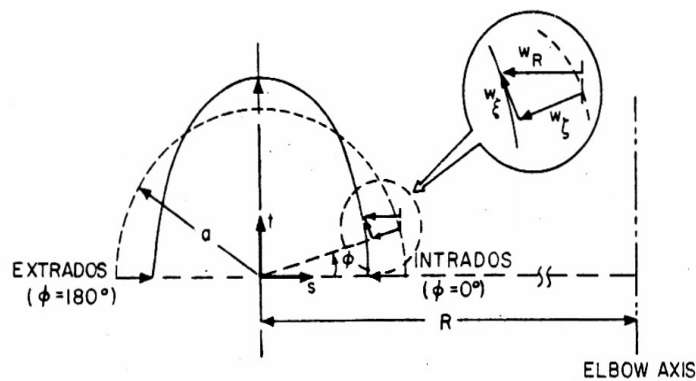
Figure 2.3: Cross sectional displacement due to ovalization

19

where w_R is the local displacement of the pipe wall in the curvature radial direction. This longitudinal strain is also assumed to be of constant magnitude through the pipe wall thickness. Also, the tangential strain component is

$$\left(\varepsilon_{\xi\xi}\right)_{ov}=-\frac{1}{a^2}\left[\omega_\zeta+\frac{d^2\omega_\zeta}{d\phi^2}\right]\zeta \qquad (2.23)$$

where ϕ is measure the angular position considered as shown in Figure 2.3, and ω_ζ is the radial displacement which is estimated using tangential displacement as follow

$$\omega_\zeta=-\frac{d\omega_\xi}{d\phi} \qquad (2.24)$$

where von Karman assumed the following function for in-plane bending of the element

$$\omega_\xi=\sum_{n=1}^{N}c_i\sin(2n\phi) \qquad (2.25)$$

using a Ritz analysis, the parameters c_i can be obtained. Considering the von Karman analysis, a geometric factor λ, where $\lambda=R\delta/a^2$, plays an important role in the determination of the number of trial functions that should be included in the analysis [22]. For example, for geometric range $\lambda\geq0.5$ number of trial functions is, $N=1$.

In a condition that both in-plane and out of plane bending are considered, the following function can be used to find displacement ω_ξ for the four noded riser element Figure 2.1.

$$\omega_\xi\left(r,\phi\right)=\sum_{m=1}^{Nc}\sum_{k=1}^{4}h_k(r)c_m^k\sin(2m\phi)+\sum_{m=1}^{Nd}\sum_{k=1}^{4}h_k(r)d_m^k\cos(2m\phi) \qquad (2.26)$$

20

The first term represents in-plane bending and the second term is for out of plane bending. In Equation (2.26) c_m and d_m are the unknown generalized ovalization displacements. Depending on the pipe geometry, and the type of loading, it may be sufficient to include only the first term, or first two terms of one or both double summations in Equation (2.26), as discussed before.

The total riser element displacements are the sum of the displacements given in Equations (2.11)-(2.13) and Equation (2.26). Therefore a typical nodal point of a three-dimensional pipe element can have from 6 to 12 degrees of freedom at each node, depending on whether the ovalization displacements are included and which ovalization patterns are used. Thus a typical nodal point k will have the following generalized displacement vector:

$$\mathbf{U}^T = \left\{ u_1^k \quad u_2^k \quad u_3^k \quad \theta_1^k \quad \theta_2^k \quad \theta_3^k \quad c_1^k \quad c_2^k \quad c_3^k \quad d_1^k \quad d_2^k \quad d_3^k \right\} \tag{2.27}$$

2.4 Pressure stiffening effects

The effect of internal pressure on the stiffness of a riser is significant when thin pipes are considered. The formulation for the riser element in Figure 2.1 can also be simply extended to include internal pressure stiffening effects. Consider the element in Figure 2.4 subjected to an internal pressure p. In this case, the internal pressure acts against the external loading to prevent changes in the cross-sectional area. Therefore the work done due to the internal pressure is

$$W_{pr} = -\int_{-1}^{+1} \int_0^{2\pi} p \frac{(R - a\cos\phi)\theta}{2} \, dA(r, \phi) \, dr \tag{2.28}$$

where p is the internal pressure, $(R - a\cos\phi)$ is the longitudinal arc length the mid-surface of the bend, r is the isoparametric longitudinal coordinate, and $dA(r, \phi)$ is the differential
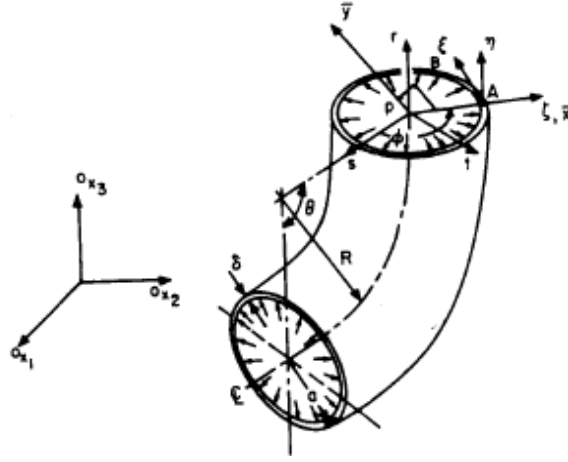
Figure 2.4: Riser (pipe) element in subjected to an internal pressure p

change in the cross sectional area of the pipe bend. Considering the displacements ω_ζ and ω_ξ into the ζ and ξ directions and also with the assumption that the circumferential strains vanish at the mid-surface of the bend Equation (2.28) simplifies to:

$$W_{pr} = -\frac{p}{8} \int_{-1}^{+1} \int_{0}^{2\pi} \left(w_\xi^2 - \left(d^2 w_\xi / d\phi^2 \right)^2 \right) (R - a\cos\phi)\, \theta\, d\phi\, dr \qquad (2.29)$$

Using the ovalization displacement interpolation relation of the element, i.e. Equation (2.26), we obtain the following pressure stiffness matrix [23]

$$\mathbf{K}_{pr} = \frac{p}{2} \int_{-1}^{+1} \int_{0}^{2\pi} \left(\mathbf{G}_{p1}^T \mathbf{G}_{p1} - \mathbf{G}_{p2}^T \mathbf{G}_{p2} \right) \frac{(R - a\cos\phi)\,\theta}{2}\, d\phi\, dr \qquad (2.30)$$

where

$$\mathbf{G}_{p1} = \left[\dots\dots\ \ \bar{a}_1^k\ \ \bar{a}_2^k\ \ \bar{a}_3^k\ \ \bar{b}_1^k\ \ \bar{b}_2^k\ \ \bar{b}_3^k\ \ \dots\dots \right] \qquad (2.31)$$

22

$$\bar{a}_m^k = -(2m)^2 h_k \sin 2m\phi \tag{2.32}$$

$$\bar{b}_m^k = -(2m)^2 h_k \cos 2m\phi \tag{2.33}$$

$$\mathbf{G}_{p2} = \begin{bmatrix} .... & \tilde{a}_1^k & \tilde{a}_2^k & \tilde{a}_3^k & \tilde{b}_1^k & \tilde{b}_2^k & \tilde{b}_3^k & .... \end{bmatrix} \tag{2.34}$$

$$\tilde{a}_m^k = h_k \sin 2m\phi \tag{2.35}$$

$$\tilde{b}_m^k = h_k \cos 2m\phi \tag{2.36}$$

and $\mathbf{K}_{pr}$ is defined to describe the ovalization degrees of freedom, i.e.

$$\mathbf{U}^T = \left\{ .... \quad c_1^k \quad c_2^k \quad c_3^k \quad d_1^k \quad d_2^k \quad d_3^k \quad .... \right\} \tag{2.37}$$

2.5 Nonlinear finite element method for continua

In the linear analysis approach it is assumed that a continuum represents infinitesimally small displacements and that the material is linearly elastic. In this case the displacement response is a linear function of the applied load and the configuration of the structure remains the same after undergoing infinitesimal displacements. But the configuration of the structure with large deformations is changing during the nonlinear analysis; therefore in a nonlinear analysis the challenge is to find the state of equilibrium of the structure to the applied load. For this purpose, the externally applied loads are considered as a function of time (step) and an incremental solution with a number of load steps requires finding state of equilibrium at each increment. Therefore, the equilibrium condition for applied external loads is

$${}^{\tau}\mathbf{R}-{}^{\tau}\mathbf{F}=0 \tag{2.38}$$

where ${}^{\tau}\mathbf{R}$ is the externally applied load vector in the configuration at time (step) τ and ${}^{\tau}\mathbf{F}$ is the reaction force vector that corresponds to the stresses in this configuration. The basic approach in an incremental step-by-step solution is to assume that the solution for the discrete time τ is known, and that the solution for the discrete time $\tau+\Delta\tau$ is required. $\Delta\tau$ is a chosen time increment. Hence, considering (2.38) at time $\tau+\Delta\tau$ we obtain:

$${}^{\tau+\Delta\tau}\mathbf{R}-{}^{\tau+\Delta\tau}\mathbf{F}=0 \tag{2.39}$$

In view of the fact that, the solution is known at time τ, we therefore have:

$${}^{\tau+\Delta\tau}\mathbf{F}={}^{\tau}\mathbf{F}+\mathbf{F} \tag{2.40}$$

where $\mathbf{F}$ is the increment in nodal forces as a result of the increment in stresses from time τ to time $\tau+\Delta\tau$. This vector can be approximated as follow:

$$\mathbf{F}\doteq{}^{\tau}\mathbf{K}\mathbf{U} \tag{2.41}$$

where $^\tau\mathbf{K}$ is a tangent stiffness matrix related to geometric and material condition at time τ and U is a vector of incremental nodal displacements. Using (2.40) and (2.41) into (2.39) results in:

$$^\tau\mathbf{KU}=^{\tau+\Delta\tau}\mathbf{R}-^\tau\mathbf{F} \tag{2.42}$$

Solving (2.42) for U results in nodal displacement at time $\tau+\Delta\tau$

$$^{\tau+\Delta\tau}\mathbf{U}=^\tau\mathbf{U}+\mathbf{U} \tag{2.43}$$

Due to assumption in (2.41), the displacement from (2.42) is an approximated value. Using this displacement field, an approximation to the stresses and corresponding nodal forces at time $\tau+\Delta\tau$ can be evaluated. These values then can be used for the next time increment calculations. However, because of the assumptions in (2.41) accumative errors can be induced in the results and depending on the load step size, may render the solution to become unstable. In practice, an iterative process is necessary until sufficient accuracy in the results is achieved. For this purpose, the modified Newton-Raphson iteration method is commonly used in the literature to formulate the iterative process. The equations which are used in this method are

$$^\tau\mathbf{K}\Delta\mathbf{U}^{(i)}=^{\tau+\Delta\tau}\mathbf{R}-^{\tau+\Delta\tau}\mathbf{F}^{(i-1)}$$

$$^{\tau+\Delta\tau}\mathbf{U}=^{\tau+\Delta\tau}\mathbf{U}^{(i-1)}+\Delta\mathbf{U}^{(i)} \tag{2.44}$$

25

$$^{\tau+\Delta\tau}\mathbf{U}^{(0)} = {}^{\tau}\mathbf{U}, \qquad ^{\tau+\Delta\tau}\mathbf{F}^{(0)} = {}^{\tau}\mathbf{F} \tag{2.45}$$

where relations in (2.45) are initial conditions.

2.6 Equations of motion for continua

The motion for a continuum with large deformations in a stationary Cartesian coordinate system, as shown in Figure 2.5, is considered. To develop an appropriate solution method, assume that all static and kinematic variables have been obtained for all time steps from *0* to time τ. Then approximating the solutions for the next step, at time $\tau+\Delta\tau$, using the previous known variables leads to an iterative procedure until convergence is achieved. This approach in which the particles of a continuum follow their motion from their original position to their final configuration is called the Lagrangian formulation.

Large deformation of a continuum can be decomposed into a rigid body motion and pure deformation. The existencing constitutive models in the literature are not capable to model this rigid body motion. However, in a continuum without rigid body motion there is no geometric nonlinearity in the governing equations of the motion. In nonlinear motions, the configuration of the body is changing continuously; consequently the current configuration is always unknown. Continuously changing configuration of the continuum is the difference between the geometric linear and nonlinear types of analyses. Having a current unknown configuration requires an incremental procedure to solve the nonlinear equations of equilibrium. For this purpose, one of the previous known equilibrium configurations may be used as a reference configuration to derive the Lagrangian governing equations.
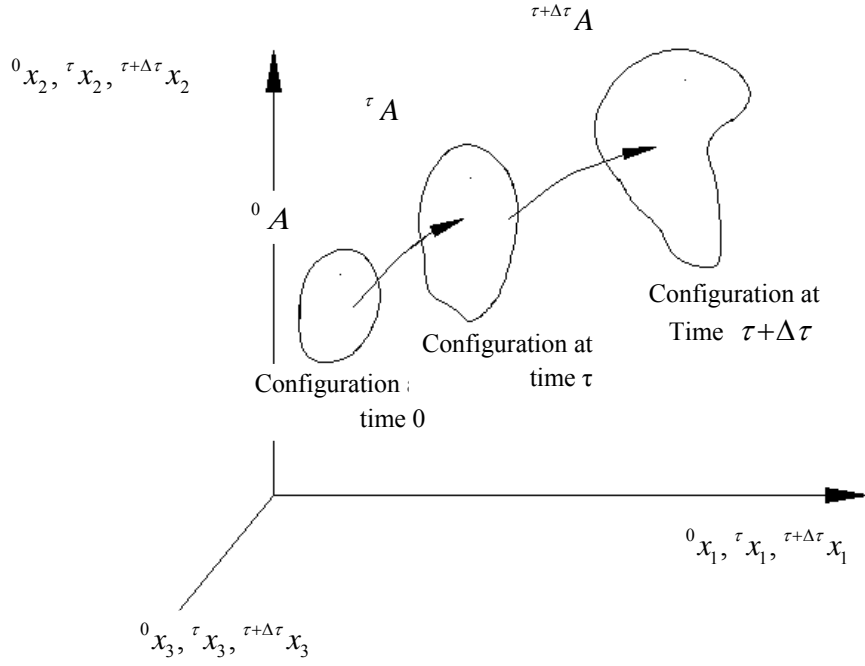
Figure 2.5: Large deformations for a body in a stationary Cartesian coordinate system

In the Lagrangian incremental analysis approach, the equilibrium of a deforming body at time $\tau+\Delta\tau$ is expressed by using the principle of virtual displacements as follows [20]

$$\int_{\tau+\Delta\tau_V} {}^{\tau+\Delta\tau}\sigma_{ij}\delta_{\tau+\Delta\tau}e_{ij}{}^{\tau+\Delta\tau}dV={}^{\tau+\Delta\tau}\mathfrak{R} \tag{2.46}$$

where ${}^{\tau+\Delta\tau}\sigma_{ij}$ are components of the Cauchy stress tensor and ${}_{\tau+\Delta\tau}e_{ij}$ are components of the strain tensor. The left hand side of (2.46) is the virtual work performed when the body is

27

subjected to a virtual displacement at time $\tau+\Delta\tau$. Also, $^{\tau+\Delta\tau}\mathfrak{R}$ is the external virtual work expressed by

$$^{\tau+\Delta\tau}\mathfrak{R}= \int\limits_{^{\tau+\Delta\tau}V} {}^{\tau+\Delta\tau}f_i^B\,\delta u_i\,{}^{\tau+\Delta\tau}dV+ \int\limits_{^{\tau+\Delta\tau}S} {}^{\tau+\Delta\tau}f_i^S\,\delta u_i\,{}^{\tau+\Delta\tau}dS \qquad (2.47)$$

where $^{\tau+\Delta\tau}f_i^B$ and $^{\tau+\Delta\tau}f_i^S$ are components of the externally applied body and surface force vectors respectively, and δu_i is the ith component of the virtual displacement vector.

The continuous change in the configuration of the body, when it undergoes large deformations, entails some important consequences for the development of an incremental analysis procedure. Since the configuration of the body at time $\tau+\Delta\tau$ is unknown, it is difficult to apply Equation (2.46) in its general form. In addition, this change of configuration is often accompanied by rigid body rotation of material particles and the $^{\tau+\Delta\tau}\sigma_{ij}$ components are affected by rigid body motions. Therefore, the Cauchy stresses at time $\tau+\Delta\tau$ cannot be obtained by simply adding to the Cauchy stresses at time τ plus a stress increment value, i.e. $^{\tau+\Delta\tau}\sigma_{ij}\neq{}^{\tau}\sigma_{ij}+{}_{\tau}\sigma_{ij}$.

In order to describe the equilibrium equation of the body correctly, suitable conjugate pair of stress and strain tensors should be used [62]. There are various pairs of tensors that, in principle, could be used for this purpose. In the present work, the 2nd Piola-Kirchhoff stress tensor is used. This is defined by

$$^{\tau+\Delta\tau}_{\tau}S_{ij}=\frac{^{\tau}\rho}{^{\tau+\Delta\tau}\rho}\,{}_{\tau+\Delta\tau}^{\tau}x_{i,m}\,{}^{\tau+\Delta\tau}\sigma_{mn}\,{}_{\tau+\Delta\tau}^{\tau}x_{j,n} \qquad (2.48)$$

where $_{\tau+\Delta\tau}^{\quad\tau}x_{i,m} = \partial^\tau x_i / \partial^{\tau+\Delta\tau}x_m$, and $^\tau\rho / ^{\tau+\Delta\tau}\rho$ represent the ratio of the mass densities at time τ and time $\tau+\Delta\tau$. The 2nd Piola-Kirchhoff stress and the Green-Lagrange strain tensors are energy conjugates [20, 62]. Therefore, for the present finite element formulation the Green-Lagrange strain tensor is used as

$$^{\tau+\Delta\tau}_{\tau}\varepsilon_{ij} = \frac{1}{2}\left(^{\tau+\Delta\tau}_{\tau}u_{i,j} + ^{\tau+\Delta\tau}_{\tau}u_{j,i} + ^{\tau+\Delta\tau}_{\tau}u_{k,i} \, ^{\tau+\Delta\tau}_{\tau}u_{k,j} \right) \qquad (2.49)$$

The 2nd Piola-Kirchhoff stress and the Green-Lagrange strain are Lagrangian tensors that are not affected by rigid body rotations. Thus, these two tensors are used to describe the equilibrium equation of the body independent of rigid rotations. It is also recognised that the 2nd Piola-Kirchhoff stress tensor has a little physical meaning and in practice the Cauchy stress values are calculated in each increment and then using Equation (2.48) the incremental values for 2nd Piola-Kirchhoff stress tensor determined.

2.7 Updated Lagrangian formulation

In large deformation analysis, the incremental form of the equilibrium equation has to be derived in order to solve the nonlinear equations. For this purpose, we can employ Equation (2.46) to refer the stresses and strains to one of the known equilibrium configurations. In theory, any one of the already calculated equilibrium configurations could be used. Yet in practice, the total Lagrangian (TL) or updated Lagrangian (UL) formulations are used. In the total Lagrangian formulation all static and kinematic variables are referred to the initial configuration at time 0 . But in updated Lagrangian formulation all variables are referred to the configuration at time t . Both these formulations include all kinematic nonlinear effects due to large displacements, large rotations and large strains. The only advantage of using one formulation rather than the other lies in its greater numerical efficiency. However, in

practice, the updated Lagrangian approach requires less numerical effort. Thus, it is more computationally efficient.

Using the 2nd Piola-Kirchhoff stress and the Green-Lagrange strain tensors in Equation (2.46) together with an updated Lagrangian description, we obtain the incremental equation of motion as follows

$$\int_{^\tau V} {}^{\tau+\Delta\tau}_{\tau}S_{ij}\,\delta\,{}^{\tau+\Delta\tau}_{\tau}\varepsilon_{ij}\,{}^\tau dV = {}^{\tau+\Delta\tau}\Re \tag{2.50}$$

2.8 Linearization of updated Lagrangian formulation for incremental solution

While the current configuration is unknown, Equation (2.50) is strongly nonlinear and in order to obtain an incremental solution, the equation has to be modified to a linearized form.   Some linearization techniques proposed by other researchers can be found in the literature [18, 20, 21, 63]. In order to proceed using an incremental scheme, incremental decompositions of stresses and strains have to be used in the following forms

$$ {}^{\tau+\Delta\tau}_{\tau}S_{ij} = {}^\tau\sigma_{ij} + {}_\tau S_{ij} \tag{2.51}$$

$$ {}^{\tau+\Delta\tau}_{\tau}\varepsilon_{ij} = {}_\tau\varepsilon_{ij} \;,\qquad {}_\tau\varepsilon_{ij} = {}_\tau e_{ij} + {}_\tau\eta_{ij} \tag{2.52}$$

where ${}_\tau^\tau S_{ij} = {}^\tau \sigma_{ij}$, ${}_\tau e_{ij}$ and ${}_\tau \eta_{ij}$ stand for the linear and nonlinear parts of the incremental strain components respectively. At the incremental level a constitutive equation of the form ${}_\tau S_{ij} = {}_\tau C_{ijrs} e_{rs}$ is used by Bathe [20], where $\delta {}_\tau \varepsilon_{ij} = \delta {}_\tau e_{ij}$. Also, ${}_\tau C_{ijrs}$ are components of the material property tensor at time t. Using (2.51) and (2.52), the equation of motion (2.50) can be written as

$$\int_{{}^\tau V} {}_\tau C_{ijrs} \, {}_\tau e_{rs} \delta \, {}_\tau e_{ij} \, {}^\tau dV + \int_{{}^t V} {}^\tau \sigma_{ij} \delta \, {}_\tau \eta_{ij} \, {}^\tau dV = {}^{\tau+\Delta\tau}\Re - \int_{{}^\tau V} {}^\tau \sigma_{ij} \delta \, {}_\tau e_{ij} \, {}^\tau dV \qquad (2.53)$$

The right hand side of (2.53) represents the "out-of-balance virtual work". In order to reduce the error of the solution, an iterative procedure is adopted in each increment. For this purpose, using the modified Newton-Raphson iterative method to solve Equation (2.53), the expression for this equation at iteration i is written as

$$\int_{{}^\tau V} {}_\tau C_{ijrs} \, {}_\tau e_{rs} \delta \, {}_\tau \overset{(i)}{e}_{ij} \, {}^\tau dV + \int_{{}^\tau V} {}^\tau \sigma_{ij} \delta \, {}_\tau \overset{(i)}{\eta}_{ij} \, {}^\tau dV$$
$$= {}^{\tau+\Delta\tau}\Re - \int_{{}^\tau V} {}^\tau \sigma_{ij} \delta \, {}_\tau \overset{(i)}{e}_{ij} \, {}^\tau dV \qquad (2.54)$$

During this linearization process a significant loss occurs in accuracy of the Lagrangian formulation [18, 57, 63]. In this work and in Chapter 3 a particular linearization scheme is also proposed to avoid such inaccuracies.

2.9 Updated Lagrangian finite element formulation

Using Equation (2.54), the incremental finite element equation of equilibrium can be written as

$$\left({}^{\tau+\Delta\tau}_{\tau+\Delta\tau}\mathbf{K}_{L}^{(i)} + {}^{\tau+\Delta\tau}_{\tau+\Delta\tau}\mathbf{K}_{NL}^{(i-1)} \right) \Delta \overset{(i)}{\mathbf{U}} = {}^{\tau+\Delta\tau}\mathbf{R} - {}^{\tau+\Delta\tau}_{\tau+\Delta\tau}\mathbf{F}^{(i-1)} \tag{2.55}$$

where ${}^{\tau}_{\tau}\mathbf{K}_{L}$ and ${}^{\tau}_{\tau}\mathbf{K}_{NL}$ are the linear and nonlinear (due to large deformation) stiffness matrices and ${}^{\tau+\Delta\tau}\mathbf{R} - {}^{\tau+\Delta\tau}_{\tau+\Delta\tau}\mathbf{F}^{(i-1)}$ is the incremental load from time t to $\tau+\Delta\tau$. Also, $\mathbf{R}$ denotes the external load vector and $\mathbf{F}$ is the internal force vector. These matrices and vectors are obtained based on equilibrium Equation (2.54) as follow

$$ {}^{\tau}_{\tau}\mathbf{K}_{\mathbf{L}} = \int_{{}^{\tau}V} {}^{\tau}_{\tau}\mathbf{B}_{\mathbf{L}}^{\mathbf{T}} \, {}_{\tau}\mathbf{C} \, {}^{\tau}_{\tau}\mathbf{B}_{\mathbf{L}} \, {}^{\tau}dV \tag{2.56}$$

$$ {}^{\tau+\Delta\tau}_{\tau+\Delta\tau}\mathbf{K}_{NL} = \int_{{}^{\tau+\Delta\tau}V} {}^{\tau+\Delta\tau}_{\tau+\Delta\tau}\mathbf{B}_{NL}^{\mathbf{T}} \, {}^{\tau+\Delta\tau}_{\tau+\Delta\tau}\boldsymbol{\sigma} \, {}^{\tau+\Delta\tau}_{\tau+\Delta\tau}\mathbf{B}_{NL} \, d^{\tau+\Delta\tau}V \tag{2.57}$$

$$ {}^{\tau+\Delta\tau}_{\tau+\Delta\tau}\mathbf{F} = \int_{{}^{\tau+\Delta\tau}V} {}^{\tau+\Delta\tau}_{\tau+\Delta\tau}\mathbf{B}_{L}^{\mathbf{T}} \, {}^{\tau+\Delta\tau}\hat{\boldsymbol{\sigma}} \, d^{\tau+\Delta\tau}V \tag{2.58}$$

$$ {}^{\tau+\Delta\tau}\mathbf{R} = \int_{{}^{0}V} \mathbf{H}^{\mathbf{T}} \, {}^{\tau+\Delta\tau}_{0}\mathbf{f}^{\mathbf{B}} \, {}^{0}dV + \int_{{}^{0}S} \mathbf{H}^{\mathbf{ST}} \, {}^{\tau+\Delta\tau}_{0}\mathbf{f}^{\mathbf{S}} \, {}^{0}dS \tag{2.59}$$

Figure 2.6: Newton-Cotes formula's integration point positions

In this work to evaluate these stiffness matrices and internal force vector, a reduced numerical integration scheme using Newton-Cotes formula with the following orders is employed; 3-point integration through the wall thickness, 5-point integration along the length and 8-point integration around the circumference. Figure 2.6 shows the positions of these integral points.

2.10 Buoyancy force

The buoyancy force is equal to the weight of the displaced fluid and acts on floating riser in vertical direction opposite to the body force. Using this definition the following relation is developed to estimate the buoyancy force vector, $^{\tau+\Delta\tau}\mathbf{R}_{Buy}$, consistent with the presented flexible riser finite element formulation.

$$^{\tau+\Delta\tau}\mathbf{R}_{Buy} = \int_{^{\tau+\Delta\tau}l} {}^{\tau+\Delta\tau}_{\tau+\Delta\tau}\mathbf{H}_a^{\mathrm{T}} {}^{\tau+\Delta\tau}\mathbf{q}_{Buy} \, d^{\tau+\Delta\tau}s \tag{2.60}$$

where

$$^{\tau+\Delta\tau}\mathbf{q}_{Buy} = \begin{bmatrix} \cdots & ^{\tau+\Delta\tau}\mathbf{q}_{Buy}^{(k)} & \cdots \end{bmatrix}_{k=1\ldots4} \tag{2.61}$$

and

$$^{\tau+\Delta\tau}\mathbf{q}_{Buy}^{(k)} = \left\{ \begin{matrix} 0 \\ 0 \\ \dfrac{\rho_w}{^{\tau+\Delta\tau}l}\displaystyle\int_{^{\tau+\Delta\tau}\widehat{V}} d\,^{\tau+\Delta\tau}\widehat{V} \end{matrix} \right\} = \left\{ \begin{matrix} 0 \\ 0 \\ \dfrac{a_0\rho_w}{^{\tau+\Delta\tau}l}\displaystyle\int_{-1}^{1} \left| ^{\tau+\Delta\tau}\mathbf{J}_{(r),s=0,t=0} \right| dr \end{matrix} \right\} \tag{2.62}$$

Therefore

$$^{\tau+\Delta\tau}\mathbf{R}_{Buy} = \int_{-1}^{1} {}^{\tau+\Delta\tau}_{\tau+\Delta\tau}\mathbf{H}_a^{\mathrm{T}}\,^{\tau+\Delta\tau}\mathbf{q}_{Buy} \left| ^{\tau+\Delta\tau}\mathbf{J}_{(r),s=0,t=0} \right| dr \tag{2.63}$$

In Equation (2.62), ρ_w is water density, $^{\tau+\Delta\tau}l$ stands for the element length at $\tau+\Delta\tau$ and $^{\tau+\Delta\tau}\widehat{V}$ is displaced water volume. Also, a_0 is defined as

$$a_0 = \pi\left(1-\left(r_i/r_o\right)^2\right) \tag{2.64}$$

34

2.11 Steady state current loading

A displacement-dependent (follower) external load due to steady state current can be expressed as

$$^{\tau+\Delta\tau}\mathbf{R}_{Current} = \int_{^{\tau+\Delta\tau}l} {}^{\tau+\Delta\tau}_{\tau+\Delta\tau}\mathbf{H}_a^{\mathrm{T}}\,{}^{\tau+\Delta\tau}\mathbf{q}_{Current}\,d\,{}^{\tau+\Delta\tau}s \tag{2.65}$$

where

$$^{\tau+\Delta\tau}\mathbf{q}_{Current} = \left[\cdots \quad {}^{\tau+\Delta\tau}\mathbf{q}_{Current}^{(k)} \quad \cdots\right]_{k=1\ldots4} \tag{2.66}$$

$\mathbf{q}_{current}$ is the steady-state current force due to fluid-structure interaction (using Morison's equation) which can be decomposed into two vectors: transverse drag load vector and skin friction or tangential drag vector. The transverse drag load vector per unit length is given by:

$$^{\tau+\Delta\tau}\mathbf{q}_{Dn}^{(k)} = \frac{1}{2\,{}^{\tau+\Delta\tau}l}\rho_w\,D\,C_{Dn}\,{}^{\tau+\Delta\tau}\vec{\mathbf{V}}_{cn}\left|{}^{\tau+\Delta\tau}\vec{\mathbf{V}}_{cn}\right| \tag{2.67}$$

and skin friction or tangential drag vector per unit length is defined as:

35

$$\tau+\Delta\tau\,\mathbf{q}_{Dt}^{(k)} = \frac{1}{2^{\,\tau+\Delta\tau}l}\,\rho_w\,D\,C_{Dt}\,^{\tau+\Delta\tau}\vec{\mathbf{V}}_{ct}\left|^{\tau+\Delta\tau}\vec{\mathbf{V}}_{ct}\right| \tag{2.68}$$

C_{Dn} and C_{Dt} are drag coefficients which are obtained from experiments and are functions of Reynolds number of the current. $\vec{\mathbf{V}}_c$ is steady state current velocity vector. $^{\tau+\Delta\tau}\vec{\mathbf{V}}_{cn}(=\vec{\mathbf{V}}_c - ^{\tau+\Delta\tau}\vec{\mathbf{V}}_{ct})$ and $^{\tau+\Delta\tau}\vec{\mathbf{V}}_{ct}(=(\vec{\mathbf{V}}_c^T\,^{\tau+\Delta\tau}\mathbf{V}_r)\,^{\tau+\Delta\tau}\mathbf{V}_r)$ are normal and tangential components of $\vec{\mathbf{V}}_c$ which are acting on the riser at time increment $\tau+\Delta\tau$. Using Equations (2.67) and (2.68) and assuming a uniform variation of current velocity with respect to water depth results in

$$\tau+\Delta\tau\,\mathbf{q}_{Current}^{(k)} = {}^{\tau+\Delta\tau}\mathbf{q}_{Dn}^{(k)} + {}^{\tau+\Delta\tau}\mathbf{q}_{Dt}^{(k)} = \frac{\rho_w D}{2^{\,\tau+\Delta\tau}l}\left\{\begin{array}{l} C_{Dn}\,^{\tau+\Delta\tau}V_{cn1}\left|^{\tau+\Delta\tau}\vec{\mathbf{V}}_{cn}\right| + C_{Dt}\,^{\tau+\Delta\tau}V_{ct1}\left|^{\tau+\Delta\tau}\vec{\mathbf{V}}_{ct}\right| \\ C_{Dn}\,^{\tau+\Delta\tau}V_{cn2}\left|^{\tau+\Delta\tau}\vec{\mathbf{V}}_{cn}\right| + C_{Dt}\,^{\tau+\Delta\tau}V_{ct2}\left|^{\tau+\Delta\tau}\vec{\mathbf{V}}_{ct}\right| \\ C_{Dn}\,^{\tau+\Delta\tau}V_{cn3}\left|^{\tau+\Delta\tau}\vec{\mathbf{V}}_{cn}\right| + C_{Dt}\,^{\tau+\Delta\tau}V_{ct3}\left|^{\tau+\Delta\tau}\vec{\mathbf{V}}_{ct}\right| \end{array}\right\} \tag{2.69}$$

Therefore

$$\tau+\Delta\tau\,\mathbf{R}_{Current} = \int_{-1}^{1}\,^{\tau+\Delta\tau}\mathbf{H}_a^{T\,\tau+\Delta\tau}\mathbf{q}_{Current}\left|^{\tau+\Delta\tau}\mathbf{J}_{(r),s=0,t=0}\right|dr \tag{2.70}$$

2.12 Seabed soil-riser interaction modeling

The pipe-soil interaction model (Figure 2.7) adopted in this study has been proposed by Laver et. al. [60]. This model is based on some experiments which were conducted to investigate the effects of pull-out rate, pipe diameter, consolidation time and consolidation load.

Q_s (Uplift resident

force per unit length)

Max.
Uplift
resistance
force; $Q_{S, Max}$

Pipe displacement (m)

Break out

$0.075\Delta_B$ $0.7\Delta_B$ displacement, Δ_B
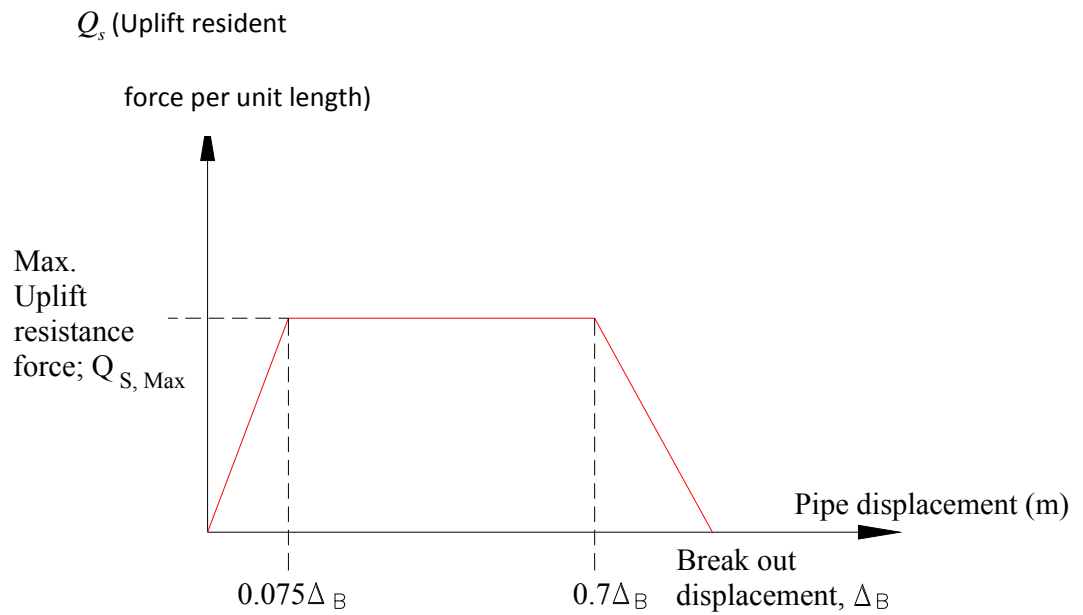
Figure 2.7: Pipe-soil interaction model

The model profile has three linear phases as shown in Figure 2.7. From this figure, when the pipe initially moves upwards the suction force (Q_s) increases from zero to the maximum value then the suction force remains constant as the pipe moves further upwards finally under further upward movement the suction force reduces from its maximum value to zero at the break-out displacement. The soil suction model has two defined limits the maximum uplift resistance force per unit length, $Q_{S,MAX}$, and the break-out displacement, Δ_B which are estimated using the formulas below [60]

$$Q_{S,MAX} = k_c k_F \left(\frac{V_p}{D} \right)^{n_F} \left(0.00033 \, \frac{F_C \sqrt{c_V t}}{LD^2} + 0.9 \right) N \, D \, S_U \qquad (2.71)$$

$$\Delta_B = k_D V_p^{n_D} \, D \left(0.0009 \, \frac{F_C \sqrt{c_V t}}{LD^2} + 0.8 \right) \qquad (2.72)$$

where k_c is cyclic loading factor (=1.0 for slow drift motion) and k_F, n_F, k_D and n_D are empirically derived constants; for onsoy clay $k_F=1.12$, $n_F=0.18$, $k_D=0.98$, $n_D=0.26$ and for watchet clay $k_F=0.98$, $n_F=0.21$, $k_D=0.83$, $n_D=0.19$. Also, V is pull-out velocity (between 0.005-0.2 m/s), D is external diameter of riser, F_C is consolidation force (N), c_V is coefficient of consolidation ($m^2/year$), t is the consolidation time (years) and S_u is un-drained shear strength of soil. In Equation (2.71) $N=\text{Min}[5.14+1.18\sqrt{z/B}, 7.5]$ where z is depth of riser invert and B is its bearing width. The bearing width of a pipe is typically equal to its external diameter ($B=D$), but for the pipe penetration depth less than $\frac{1}{2}D$, $B=2\sqrt{Dz-z^2}$. In this paper, in the large deformation finite-element context the seabed interaction is applied as a follower external load. For this purpose for those elements with seabed interaction and initial penetration, a force vector at each time step of incremental solution is defined as

$$\prescript{\tau+\Delta\tau}{\tau+\Delta\tau}{\mathbf{R}}_{Bed} = \int\limits_{\prescript{\tau+\Delta\tau}{}{\widehat{L}}} \prescript{\tau+\Delta\tau}{\tau+\Delta\tau}{\mathbf{H}}_L^{\mathrm{T}} \, \prescript{\tau+\Delta\tau}{}{\mathbf{q}}_{Bed} \, d \, \prescript{\tau+\Delta\tau}{}{\widehat{L}} \qquad (2.73)$$

where

$$
{}^{\tau+\Delta\tau}\mathbf{q}_{Bed} = \left\{ \begin{array}{l} Q_s \displaystyle\int_{{}^{\tau+\Delta\tau}\widehat{l}} d\, {}^{\tau+\Delta\tau}\widehat{l}\; \mathbf{e}_z \cdot {}^{\tau+\Delta\tau}\mathbf{V}_r \\[3mm] Q_s \displaystyle\int_{{}^{\tau+\Delta\tau}\widehat{l}} d\, {}^{\tau+\Delta\tau}\widehat{l}\; \mathbf{e}_z \cdot {}^{\tau+\Delta\tau}\mathbf{V}_s \\[3mm] Q_s \displaystyle\int_{{}^{\tau+\Delta\tau}\widehat{l}} d\, {}^{\tau+\Delta\tau}\widehat{l}\; \mathbf{e}_z \cdot {}^{\tau+\Delta\tau}\mathbf{V}_t \end{array} \right\}
\tag{2.74}
$$

where $\widehat{l}$ is length of those part of element which has interaction with seabed.

2.13 Solution Algorithm

The nonlinear finite element formulation derived in the previous sections has been coded in a finite element program using an appropriate algorithm; Figure 2.8 gives an overview of this algorithm. In this algorithm the outer loop carries out the incremental solution of the problem and the external load vector is calculated in each increment. This figure illustrates that in order to achieve convergence in each increment an iterative solution procedure has to be employed in which in all iterations the stiffness matrices as well as the nodal force vector should be updated for all integration points of every element. After calculating the assembled global stiffness matrix and nodal force vector of the structure, the incremental displacement vector will be calculated. In the next step, the geometry of the structure will be updated using calculated incremental displacement values. Then, the stress and strain tensors will be calculated for all integration points. These iterative solutions will continue until the convergence criterion is satisfied.

Start

Read data (initial configuration, loading & ...)

Do 100 Incs=1, No. of increments

Cal. External Load vectro (R) using: $^{t+\Delta t}_{0}\mathbf{R} = \int_{0_V} \mathbf{H}^{\mathbf{T}} {}^{t+\Delta t}_{0}\mathbf{f}^{\mathbf{B}} \, {}^{0}dV + \int_{0_S} \mathbf{H}^{\mathbf{ST}} {}^{t+\Delta t}_{0}\mathbf{f}^{\mathbf{S}} \, {}^{0}dS$

Do 110 Iter=1, No. of iterations

Do 120 NELE=1, No. of elements

Do 130 Nint=1, No. of integration points

Call stifness matrix & nodal force SUBROUTINE

130 Continue

120 Continue

SUBROUTINE: Stifness matrix & nodal force

Calculation linear stifness matrix using: $^{t}_{t}\mathbf{K}_{\mathbf{L}} = {}^{t}_{t}\mathbf{K}_{\mathbf{L}} + {}^{t}_{t}\mathbf{B}^{\mathbf{T}}_{\mathbf{L}} \, {}^{t}_{t}\mathbf{C} \, {}^{t}_{t}\mathbf{B}_{\mathbf{L}}$

Calculation nonlinear stifness matrix using: $^{t}_{t}\mathbf{K}_{\mathbf{NL}} = {}^{t}_{t}\mathbf{K}_{\mathbf{NL}} + {}^{t}_{t}\mathbf{B}^{\mathbf{T}}_{\mathbf{NL}} \, {}^{t}\sigma \, {}^{t}_{t}\mathbf{B}_{\mathbf{NL}}$

Assemblage the stifness matrices into global stiffness matrix

Calculation nodal force vector using: $^{t}_{t}\mathbf{F} = {}^{t}_{t}\mathbf{F} + {}^{t}_{t}\mathbf{B}^{\mathbf{T}}_{\mathbf{L}} \, {}^{t}\hat{\sigma}$

Call solver (finding displacement vector U by solving: $\left({}^{t}_{t}\mathbf{K}_{\mathbf{L}} + {}^{t}_{t}\mathbf{K}_{\mathbf{NL}} \right) \Delta \mathbf{U}^{(t)} = {}^{t+\Delta t}\mathbf{R} - {}^{t+\Delta t}_{t+\Delta t}\mathbf{F}^{(i-1)}$ **)**

Geometry update

Do 140 NELE=1, No. of elements

Do 150 Nint=1, No. of integration points

Call stress & strain SUBROUTINE

150 Continue

140 Continue

If Error<Convegence Criteria goto 999

110 Continue

999 Write output files

100 Continue

End

SUBROUTINE: stress & strain

Calculation increment in strain tensor using: $_{t}\varepsilon_{ij} = \frac{1}{2}\left({}_{t}u_{i,j} + {}_{t}u_{j,i} + {}_{t}u_{k,i} \, {}_{t}u_{k,j} \right)$

Calculation increment in 2ed Piola-Kirchhoff stress tensor using: $_{t}S_{ij} = {}_{t}C_{ijrs}\varepsilon_{rs}$

Calculation 2ed Piola-Kirchhoff stress tensor using: $^{t+\Delta t}_{t}S_{ij} = {}^{t}\sigma_{ij} + {}_{t}S_{ij}; \; \left({}^{t}_{t}S_{ij} = {}^{t}\sigma_{ij} \right)$

Calculation Cauchy stress tensor using: $\sigma = \frac{1}{|\mathbf{F}|}\mathbf{F}\,\mathbf{S}_{2}\mathbf{F}^{\mathbf{T}}$

Figure 2.8: Nonlinear solution algorithm

40

Chapter 3

An Updated Lagrangian Finite Element Formulation for Large Displacement Dynamic Analysis of Three-Dimensional Flexible Riser Structures

3.1 Introduction

The finite element formulation that was presented in Chapter 2 can be used for modeling large rigid body motion, large displacement with small rotations. In a case problem with large rotation, due to some singularity in rotational degrees of freedom the formulation fails to model finite deformation [15, 57]. In this chapter, an updated Lagrangian finite element formulation of a three-dimensional annular section flexible riser element is presented for large displacement and large rotation dynamic analysis of flexible riser structures. In this formulation a modified linearization method is used to avoid inaccuracies normally associated with other linearization schemes.

3.2 Kinematics of three-dimensional riser element

The element employed in the present chapter is the same four-nodded, twenty four degrees of freedom flexible riser element Figure 2.1. This element is a continuum based element whose displacement field at time $\tau + \Delta\tau$ is obtained as

$$^{\tau+\Delta\tau}u_i(r,s,t) = \sum_{k=1}^{4} h_k(r) \,^{\tau+\Delta\tau}u_i^k + t\sum_{k=1}^{4} a^k h_k(r) \, V_{ti}^k + s\sum_{k=1}^{4} a^k h_k(r) \, V_{si}^k ; \; i = 1,2,3 \tag{3.1}$$

where all parameters in this equation were defined in Chapter 2.

3.3 An incremental solution for flexible riser element using a novel linearization approach

According to detail explanations from Chapter 2, in the UL incremental analysis approach, the equilibrium equations of a deforming body at time $\tau + \Delta\tau$ are expressed using the principle of virtual displacements as:

$$\int_{\tau_V} \,^{\tau+\Delta\tau}_{\tau}S_{ij} \, \delta(^{\tau+\Delta\tau}_{\tau}E_{ij}) \, dV = \,^{\tau+\Delta\tau}_{\tau}\tilde{\Re} \tag{3.2}$$

where $^{\tau+\Delta\tau}_{\tau}S_{ij}$ is the 2nd Piola-Kirchhoff stress, $^{\tau+\Delta\tau}_{\tau}E_{ij}$ is the Green-Lagrange strain and parameter $^{\tau+\Delta\tau}_{\tau}\tilde{\Re}$ represents the external virtual work. An expression for $^{\tau+\Delta\tau}_{\tau}\tilde{\Re}$ includes all external loadings applied to the body (flexible riser) such as current loading, buoyancy force as well as inertia force. Writing (3.2) for dynamic analysis of body by excluding inertia force from $^{\tau+\Delta\tau}_{\tau}\tilde{\Re}$ results in:

$$\int_{\tau+\Delta\tau_V} \rho \,^{\tau+\Delta\tau}\ddot{u}_i \, \delta u_i \, dV + \int_{\tau_V} \,^{\tau+\Delta\tau}_{\tau}S_{ij} \, \delta(^{\tau+\Delta\tau}_{\tau}E_{ij}) \, dV = \,^{\tau+\Delta\tau}_{\tau}\Re \tag{3.3}$$

42

In Equation (3.3) the 2nd Piola-Kirchhoff stress and Green-Lagrange strain tensors are an energy conjugate pair [62], both of which are unaffected by rigid body rotations. The incremental form of the Green-Lagrange strain tensor is as follows:

$$
{}^{\tau+\Delta\tau}_{\tau}E_{ij}=\frac{1}{2}\left({}^{\tau+\Delta\tau}_{\tau}u_{i,j}+{}^{\tau+\Delta\tau}_{\tau}u_{j,i}+{}^{\tau+\Delta\tau}_{\tau}u_{k,i}\;{}^{\tau+\Delta\tau}_{\tau}u_{k,j}\right)
\tag{3.4}
$$

Also, the relation between the 2nd Piola-Kirchhoff stress components S_{ij} and the Cauchy stress components σ_{mn} is written as follows:

$$
{}^{\tau+\Delta\tau}\sigma_{mn}=\det\left({}^{\tau+\Delta\tau}_{\tau}x_{m,i}\right)\;{}^{\tau+\Delta\tau}_{\tau}x_{m,i}\;{}^{\tau+\Delta\tau}_{\tau}S_{ij}\;{}^{\tau+\Delta\tau}_{\tau}x_{n,j}
\tag{3.5}
$$

where ${}^{\tau+\Delta\tau}_{\tau}x_{m,i}=\partial\,{}^{\tau+\Delta\tau}x_{m}/\partial\,{}^{\tau}x_{i}$ represents the deformation gradient of the increment. Substitution of displacement field (3.1) into Equation (3.4) yields a second order function for expressing the Green-Lagrange strain tensor as follows [57]

$$
\begin{aligned}
{}^{\tau+\Delta\tau}_{\tau}E_{ij}(r,s,t)=&\;{}^{\tau+\Delta\tau}_{\tau}E_{ij}^{(0)}(r)+s\,{}^{\tau+\Delta\tau}_{\tau}E_{ij}^{(1)}(r)+t\,{}^{\tau+\Delta\tau}_{\tau}E_{ij}^{(2)}(r)\\
&+st\,{}^{\tau+\Delta\tau}_{\tau}E_{ij}^{(3)}(r)+s^{2}\,{}^{\tau+\Delta\tau}_{\tau}E_{ij}^{(4)}(r)+t^{2}\,{}^{\tau+\Delta\tau}_{\tau}E_{ij}^{(5)}(r)
\end{aligned}
\tag{3.6}
$$

where

$$
\begin{aligned}
2\,{}^{\tau+\Delta\tau}_{\tau}E_{ij}^{(0)}=&\sum_{k=1}^{4}J_{j1}^{-1}h_{,r}^{k}\,{}^{\tau}u_{i}^{k}+\sum_{k=1}^{4}J_{j2}^{-1}h^{k}a^{k}V_{si}^{k}+\sum_{k=1}^{4}J_{j3}^{-1}h^{k}a^{k}V_{ti}^{k}+\sum_{k=1}^{4}J_{i1}^{-1}h_{,r}^{k}\,{}^{\tau}u_{j}^{k}+\sum_{k=1}^{4}J_{i2}^{-1}h^{k}a^{k}V_{sj}^{k}\\
&+\sum_{k=1}^{4}J_{i3}^{-1}h^{k}a^{k}V_{tj}^{k}+\left(\sum_{k=1}^{4}J_{i1}^{-1}h_{,r}^{k}\,{}^{\tau}u_{k}^{k}+\sum_{k=1}^{4}J_{i2}^{-1}h^{k}a^{k}V_{sk}^{k}+\sum_{k=1}^{4}J_{i3}^{-1}h^{k}a^{k}V_{tk}^{k}\right)\\
&\qquad\qquad\times\left(\sum_{k=1}^{4}J_{j1}^{-1}h_{,r}^{k}\,{}^{\tau}u_{k}^{k}+\sum_{k=1}^{4}J_{j2}^{-1}h^{k}a^{k}V_{sk}^{k}+\sum_{k=1}^{4}J_{j3}^{-1}h^{k}a^{k}V_{tk}^{k}\right)
\end{aligned}
$$

$$
\tag{3.7}
$$

$$2\,{}_{\tau}^{\tau+\Delta\tau}E_{ij}^{(1)}=\sum_{k=1}^{4}J_{j1}^{-1}h_{,r}^{k}\,a^{k}\,V_{si}^{k}+\sum_{k=1}^{4}J_{i1}^{-1}h_{,r}^{k}\,a^{k}\,V_{sj}^{k}$$

$$+\left(\sum_{k=1}^{4}J_{i1}^{-1}h_{,r}^{k}\,{}^{\tau}u_{k}^{k}+\sum_{k=1}^{4}J_{i2}^{-1}h^{k}a^{k}\,V_{sk}^{k}+\sum_{k=1}^{4}J_{i3}^{-1}h^{k}a^{k}\,V_{tk}^{k}\right)\times\left(\sum_{k=1}^{4}J_{j1}^{-1}h_{,r}^{k}\,a^{k}\,V_{sk}^{k}\right)$$

$$+\left(\sum_{k=1}^{4}J_{i1}^{-1}h_{,r}^{k}\,a^{k}\,V_{sk}^{k}\right)\times\left(\sum_{k=1}^{4}J_{j1}^{-1}h_{,r}^{k}\,{}^{\tau}u_{k}^{k}+\sum_{k=1}^{4}J_{j2}^{-1}h^{k}a^{k}\,V_{sk}^{k}+\sum_{k=1}^{4}J_{j3}^{-1}h^{k}a^{k}\,V_{tk}^{k}\right) \qquad (3.8)$$

$$2\,{}_{\tau}^{\tau+\Delta\tau}E_{ij}^{(2)}=\sum_{k=1}^{4}J_{j1}^{-1}h_{,r}^{k}a^{k}\,V_{ti}^{k}+\sum_{k=1}^{4}J_{i1}^{-1}h_{,r}^{k}a^{k}\,V_{tj}^{k}$$

$$+\left(\sum_{k=1}^{4}J_{i1}^{-1}h_{,r}^{k}\,{}^{\tau}u_{k}^{k}+\sum_{k=1}^{4}J_{i2}^{-1}h^{k}a^{k}\,V_{sk}^{k}+\sum_{k=1}^{4}J_{i3}^{-1}h^{k}a^{k}\,V_{tk}^{k}\right)\times\left(\sum_{k=1}^{4}J_{j1}^{-1}h_{,r}^{k}\,a^{k}\,V_{tk}^{k}\right)$$

$$+\left(\sum_{k=1}^{4}J_{i1}^{-1}h_{,r}^{k}\,a^{k}\,V_{tk}^{k}\right)\times\left(\sum_{k=1}^{4}J_{j1}^{-1}h_{,r}^{k}\,{}^{\tau}u_{k}^{k}+\sum_{k=1}^{4}J_{j2}^{-1}h^{k}a^{k}\,V_{sk}^{k}+\sum_{k=1}^{4}J_{j3}^{-1}h^{k}a^{k}\,V_{tk}^{k}\right) \qquad (3.9)$$

$$\,{}_{\tau}^{\tau+\Delta\tau}E_{ij}^{(3)}=\sum_{k=1}^{4}J_{i1}^{-1}\,h_{,r}^{k}\,a^{k}\,V_{sk}^{k}\,V_{tk}^{k}\times\sum_{k=1}^{4}J_{j1}^{-1}h_{,r}^{k}\,a^{k}\,V_{sk}^{k}\,V_{tk}^{k} \qquad (3.10)$$

$$\,{}_{\tau}^{\tau+\Delta\tau}E_{ij}^{(4)}=\frac{1}{2}\sum_{k=1}^{4}J_{i1}^{-1}\,h_{,r}^{k}\,a^{k}\,V_{sk}^{k}\times\sum_{k=1}^{4}J_{j1}^{-1}\,h_{,r}^{k}\,a^{k}\,V_{sk}^{k} \qquad (3.11)$$

$$\,{}_{\tau}^{\tau+\Delta\tau}E_{ij}^{(5)}=\frac{1}{2}\sum_{k=1}^{4}J_{i1}^{-1}\,h_{,r}^{k}\,a^{k}\,V_{tk}^{k}\times\sum_{k=1}^{4}J_{j1}^{-1}\,h_{,r}^{k}\,a^{k}\,V_{tk}^{k} \qquad (3.12)$$

J_{mn} are the Jacobian matrix components referred to configuration at time τ. Using Equation (3.6) together with stress-strain relation $\,{}_{\tau}^{\tau+\Delta\tau}S_{ij}=\,{}_{\tau}^{\tau+\Delta\tau}C_{ijkl}\,{}_{\tau}^{\tau+\Delta\tau}E_{kl}$, the 2nd Piola-Kirchhoff stress tensor can be written as

$$
\begin{aligned}
{}_{\tau}^{\tau+\Delta\tau}S_{ij}(r,s,t) = {}&{}_{\tau}^{\tau+\Delta\tau}S_{ij}^{(0)}(r)+s\,{}_{\tau}^{\tau+\Delta\tau}S_{ij}^{(1)}(r)+t\,{}_{\tau}^{\tau+\Delta\tau}S_{ij}^{(2)}(r) \\
&+st\,{}_{\tau}^{\tau+\Delta\tau}S_{ij}^{(3)}(r)+s^{2}\,{}_{\tau}^{\tau+\Delta\tau}S_{ij}^{(4)}(r)+t^{2}\,{}_{\tau}^{\tau+\Delta\tau}S_{ij}^{(5)}(r)
\end{aligned}
\tag{3.13}
$$

where

$$
{}_{\tau}^{\tau+\Delta\tau}S_{ij}^{(P)}(r) = {}_{\tau}^{\tau+\Delta\tau}C_{ijkl}\; {}_{\tau}^{\tau+\Delta\tau}E_{kl}^{(P)}(r) \; ; \qquad \text{P=0}\cdots5
\tag{3.14}
$$

Also, in view of Equation (3.14) and using Equation (3.5), the Cauchy stress components, can be written as

$$
{}^{\tau+\Delta\tau}\sigma_{mn}^{(P)}(r) = \det\left({}_{\tau}^{\tau+\Delta\tau}x_{m,i}\right)\,{}_{\tau}^{\tau+\Delta\tau}x_{m,i}\;{}_{\tau}^{\tau+\Delta\tau}S_{ij}^{(P)}(r)\;{}_{\tau}^{\tau+\Delta\tau}x_{n,j} \; ; \qquad \text{P=0}\cdots5
\tag{3.15}
$$

In order to develop an incremental solution for nonlinear Equation (3.2), the stress and strain tensors are decomposed into:

$$
{}_{\tau}^{\tau+\Delta\tau}S_{ij} = {}^{\tau}S_{ij}+\Delta S_{ij} = {}^{\tau}\sigma_{ij}+\Delta S_{ij}
\tag{3.16}
$$

$$
{}_{\tau}^{\tau+\Delta\tau}E_{ij} = \Delta E_{ij}=\Delta e_{ij}+\Delta\eta_{ij}
\tag{3.17}
$$

where operator Δ stands for the incremental values. The parameters Δe_{ij} and $\Delta\eta_{ij}$ are the linear and nonlinear parts of the incremental Green-Lagrange strain tensor and ΔS_{ij} is the incremental 2nd Piola-Kirchhoff stress tensor. Using Equations (3.13) and (3.16) we obtain

$$
\begin{aligned}
{}_{\tau}^{\tau+\Delta\tau}S_{ij} = {}&({}^{\tau}\sigma_{ij}^{(0)}+\Delta S_{ij}^{(0)})+s({}^{\tau}\sigma_{ij}^{(1)}+\Delta S_{ij}^{(1)})+t({}^{\tau}\sigma_{ij}^{(2)}+\Delta S_{ij}^{(2)})+st({}^{\tau}\sigma_{ij}^{(3)}+\Delta S_{ij}^{(3)}) \\
&+s^{2}({}^{\tau}\sigma_{ij}^{(4)}+\Delta S_{ij}^{(4)})+t^{2}({}^{\tau}\sigma_{ij}^{(5)}+\Delta S_{ij}^{(5)})
\end{aligned}
\tag{3.18}
$$

Substituting Equations (3.17) and (3.18) into nonlinear Equation (3.2) and after some manipulation, the equilibrium equation of a deforming riser body at time $\tau+\Delta\tau$ is obtained as

45

$$\int\limits_{\tau+\Delta\tau V} \rho\,{}^{\tau+\Delta\tau}\ddot{u}_i\,\delta u_i\,dV + \int\limits_{\tau V} S_{ij}^{(0)}\,\delta(\Delta e_{ij})dV$$

$$+ \int\limits_{\tau V} \left({}^{\tau+\Delta\tau}_{\tau}S_{ij}^{(0)} + s\,{}^{\tau+\Delta\tau}_{\tau}S_{ij}^{(1)} + t\,{}^{\tau+\Delta\tau}_{\tau}S_{ij}^{(2)} + st\,{}^{\tau+\Delta\tau}_{\tau}S_{ij}^{(3)} + s^2\,{}^{\tau+\Delta\tau}_{\tau}S_{ij}^{(4)} + t^2\,{}^{\tau+\Delta\tau}_{\tau}S_{ij}^{(5)}\right)\delta(\Delta\eta_{ij})dV$$

$$= {}^{\tau+\Delta\tau}_{\tau}\Re - \int\limits_{\tau V}\left({}^{\tau}_{\tau}\sigma_{ij}^{(0)} + s\,{}^{\tau+\Delta\tau}_{\tau}S_{ij}^{(1)} + t\,{}^{\tau+\Delta\tau}_{\tau}S_{ij}^{(2)} + st\,{}^{\tau+\Delta\tau}_{\tau}S_{ij}^{(3)} + s^2\,{}^{\tau+\Delta\tau}_{\tau}S_{ij}^{(4)} + t^2\,{}^{\tau+\Delta\tau}_{\tau}S_{ij}^{(5)}\right)\delta(\Delta e_{ij})dV$$

$$(3.19)$$

In Equation (3.19), the second term in the left hand side which is a nonlinear term, is linearized using a Taylor series expansion as follows

$$\int\limits_{\tau V} S_{ij}^{(0)}\,\delta(\Delta e_{ij})dV = \int\limits_{\tau V}\left(\underbrace{\left.\frac{\partial(S_{ij}^{(0)})}{\partial(E_{rs}^{(0)})}\right|_t}_{C_{ijrs}}\,(\underbrace{\Delta e_{rs}^{(0)}}_{\approx\Delta e_{rs}} + \underbrace{\Delta\eta_{rs}^{(0)}}_{Neglect}) + \underbrace{high\,order\,terms}_{Neglect}\right)\delta(\Delta e_{ij})dV$$

$$\square \int\limits_{\tau V} C_{ijrs}\,\Delta e_{rs}\,\delta(\Delta e_{ij})dV$$

$$(3.20)$$

Therefore, a linearized incremental virtual work equation is obtained in the form of

$$\int\limits_{\tau+\Delta\tau V} \rho\,{}^{\tau+\Delta\tau}\ddot{u}_i\,\delta u_i\,dV + \int\limits_{\tau V} \Delta C_{ijrs}\,\Delta e_{rs}\,\delta(\Delta e_{ij})dV$$

$$+ \int\limits_{\tau V} \left({}^{\tau+\Delta\tau}_{\tau}S_{ij}^{(0)} + s\,{}^{\tau+\Delta\tau}_{\tau}S_{ij}^{(1)} + t\,{}^{\tau+\Delta\tau}_{\tau}S_{ij}^{(2)} + st\,{}^{\tau+\Delta\tau}_{\tau}S_{ij}^{(3)} + s^2\,{}^{\tau+\Delta\tau}_{\tau}S_{ij}^{(4)} + t^2\,{}^{\tau+\Delta\tau}_{\tau}S_{ij}^{(5)}\right)\delta(\Delta\eta_{ij})dV$$

$$= {}^{\tau+\Delta\tau}_{\tau}\Re - \int\limits_{\tau V}\left({}^{\tau}_{\tau}\sigma_{ij}^{(0)} + s\,{}^{\tau+\Delta\tau}_{\tau}S_{ij}^{(1)} + t\,{}^{\tau+\Delta\tau}_{\tau}S_{ij}^{(2)} + st\,{}^{\tau+\Delta\tau}_{\tau}S_{ij}^{(3)} + s^2\,{}^{\tau+\Delta\tau}_{\tau}S_{ij}^{(4)} + t^2\,{}^{\tau+\Delta\tau}_{\tau}S_{ij}^{(5)}\right)\delta(\Delta e_{ij})dV$$

$$(3.21)$$

The right hand side of Equation (3.21) is the out-of-balance virtual work. During the numerical solution process, an iterative scheme is performed in each increment of the solution based on the modified Newton-Raphson method to get the equilibrium state. Hence, in iteration i Equation (3.21) is represented as:

$$\int\limits_{\tau+\Delta\tau V} \rho \, {}^{\tau+\Delta\tau}\overset{(i)}{\ddot{u}_i} \, \delta u_i \, dV + \int\limits_{\tau V} \Delta C_{ijrs} \overset{(i)}{\Delta e}_{rs} \, \delta(\Delta e_{ij}) dV$$

$$+ \int\limits_{\tau V} \left({}^{\tau+\Delta\tau}_{\tau}\overset{(i-1)}{S_{ij}^{(0)}} + s \, {}^{\tau+\Delta\tau}_{\tau}\overset{(i-1)}{S_{ij}^{(1)}} + t \, {}^{\tau+\Delta\tau}_{\tau}\overset{(i-1)}{S_{ij}^{(2)}} + st \, {}^{\tau+\Delta\tau}_{\tau}\overset{(i-1)}{S_{ij}^{(3)}} + s^2 \, {}^{\tau+\Delta\tau}_{\tau}\overset{(i-1)}{S_{ij}^{(4)}} + t^2 \, {}^{\tau+\Delta\tau}_{\tau}\overset{(i-1)}{S_{ij}^{(5)}} \right) \delta(\Delta \eta_{ij}) dV$$

$$= {}^{\tau+\Delta\tau}\Re - \int\limits_{\tau V} \left({}^{\tau}_{\tau}\sigma_{ij}^{(0)} + s \, {}^{\tau+\Delta\tau}_{\tau}\overset{(i-1)}{S_{ij}^{(1)}} + t \, {}^{\tau+\Delta\tau}_{\tau}\overset{(i-1)}{S_{ij}^{(2)}} + st \, {}^{\tau+\Delta\tau}_{\tau}\overset{(i-1)}{S_{ij}^{(3)}} + s^2 \, {}^{\tau+\Delta\tau}_{\tau}\overset{(i-1)}{S_{ij}^{(4)}} + t^2 \, {}^{\tau+\Delta\tau}_{\tau}\overset{(i-1)}{S_{ij}^{(5)}} \right) \delta(\Delta e_{ij}) dV$$

$$(3.22)$$

3.4 Nonlinear Dynamic Finite Element Formulation for Flexible Riser Structures

Using Equation (3.22) a finite element formulation for geometrically nonlinear dynamic analysis of riser structures is developed. The incremental form of this finite element formulation for iteration i at time step $\tau+\Delta\tau$ is

$$\overset{(i)}{\mathbf{M}} \overset{(i)}{\ddot{\mathbf{U}}} + (\overset{(i)}{\mathbf{K}_L} + \overset{(i-1)}{\mathbf{K}_{NL}}) \overset{(i)}{\mathbf{U}} = \mathbf{R} - \overset{(i-1)}{\mathbf{F}} \tag{3.23}$$

Where $\mathbf{M}$ is time dependent mass matrix, $\mathbf{K}_L$ and $\mathbf{K}_{NL}$ are the linear and nonlinear (due to large deformation) stiffness matrices. Also, $\mathbf{R}$ denotes the external load vector and $\mathbf{F}$ is the internal force vector. These matrices and vector are obtained based on equilibrium Equation (3.22), i.e.

$$\mathbf{M} = \int\limits_{\tau+\Delta\tau V} \rho \, \mathbf{H}^{\mathrm{T}} \mathbf{H} \, dV \tag{3.24}$$

$$\mathbf{K}_L = \int\limits_{\tau+\Delta\tau V} \mathbf{B}_L^{\mathrm{T}}(r,s,t) \Delta \mathbf{C} \, \mathbf{B}_L(r,s,t) \, dV \tag{3.25}$$

$$\mathbf{K}_{NL}=$$
$$\int\limits_{\tau+\Delta\tau_V}\mathbf{B}_{NL}^{\mathrm{T}}(r,s,t)\left({}_{\tau}^{\tau+\Delta\tau}\mathbf{S}^{(\mathbf{0})}+s\,{}_{\tau}^{\tau+\Delta\tau}\mathbf{S}^{(\mathbf{1})}+t\,{}_{\tau}^{\tau+\Delta\tau}\mathbf{S}^{(\mathbf{2})}+st\,{}_{\tau}^{\tau+\Delta\tau}\mathbf{S}^{(\mathbf{3})}+s^2\,{}_{\tau}^{\tau+\Delta\tau}\mathbf{S}^{(\mathbf{4})}+t^2\,{}_{\tau}^{\tau+\Delta\tau}\mathbf{S}^{(\mathbf{5})}\right)\mathbf{B}_{NL}(r,s,t)\,dV$$

$$(3.26)$$

$$\mathbf{F}=\int\limits_{\tau+\Delta\tau_V}\mathbf{B}_{L}^{\mathrm{T}}(r,s,t)\left({}^{\tau}\widehat{\boldsymbol{\sigma}}^{(\mathbf{0})}+s\,{}_{\tau}^{\tau+\Delta\tau}\widehat{\mathbf{S}}^{(\mathbf{1})}+t\,{}_{\tau}^{\tau+\Delta\tau}\widehat{\mathbf{S}}^{(\mathbf{2})}+st\,{}_{\tau}^{\tau+\Delta\tau}\widehat{\mathbf{S}}^{(\mathbf{3})}+s^2\,{}_{\tau}^{\tau+\Delta\tau}\widehat{\mathbf{S}}^{(\mathbf{4})}+t^2\,{}_{\tau}^{\tau+\Delta\tau}\widehat{\mathbf{S}}^{(\mathbf{5})}\right)dV \quad (3.27)$$

where $\mathbf{H}$ is displacement interpolation matrix which is given in Equation (2-21), $\Delta\mathbf{C}$ is the incremental material properties matrix, $\mathbf{S}$ the 2nd Piola-Kirchhoff stress tensor, and $\widehat{\mathbf{S}}$ and $\widehat{\boldsymbol{\sigma}}$ are vectors containing the components of the 2nd Piola-Kirchhoff and Cauchy stress tensors, respectively. It is noted that all these matrices and vectors are independent of the s and t parameters. Also, $\mathbf{H}$ together with $\mathbf{B}_{L}$ and $\mathbf{B}_{NL}$ which are the linear and nonlinear strain-displacement matrices, respectively, are the only s and t -dependent matrices which can be decomposed as

$$\mathbf{H}(r,s,t)=\mathbf{H}_{\mathbf{a}}(r)+s\,\mathbf{H}_{\mathbf{b}}(r)+t\,\mathbf{H}_{\mathbf{c}}(r) \tag{3.28}$$

$$\mathbf{B}_{L}(r,s,t)=\mathbf{B}_{L\mathbf{a}}(r)+s\,\mathbf{B}_{L\mathbf{b}}(r)+t\,\mathbf{B}_{L\mathbf{c}}(r) \tag{3.29}$$

$$\mathbf{B}_{NL}(r,s,t)=\mathbf{B}_{NL\mathbf{a}}(r)+s\,\mathbf{B}_{NL\mathbf{b}}(r)+t\,\mathbf{B}_{NL\mathbf{c}}(r) \tag{3.30}$$

where the new matrices in Equations (3.28)-(3.30) are defined as follow

$$\mathbf{H}_{a}(r)=\left[\cdots\;\mathbf{H}_{a}^{(k)}(r)\;\cdots\right]_{k=1\ldots4},\qquad \mathbf{H}_{a}^{(k)}(r)=\begin{bmatrix} h_k & 0 & 0 & 0 & 0 & 0 \\ 0 & h_k & 0 & 0 & 0 & 0 \\ 0 & 0 & h_k & 0 & 0 & 0 \end{bmatrix} \tag{3.31}$$

$$\mathbf{H}_{b}(r)=\left[\cdots\;\mathbf{H}_{b}^{(k)}(r)\;\cdots\right]_{k=1\ldots4},\qquad \mathbf{H}_{b}^{(k)}(r)=a_k\,h_k\begin{bmatrix} 0 & 0 & 0 & 0 & {}^{\tau+\Delta\tau}V_{s3}^{k} & -{}^{\tau+\Delta\tau}V_{s2}^{k} \\ 0 & 0 & 0 & -{}^{\tau+\Delta\tau}V_{s3}^{k} & 0 & {}^{\tau+\Delta\tau}V_{s1}^{k} \\ 0 & 0 & 0 & {}^{\tau+\Delta\tau}V_{s2}^{k} & -{}^{\tau+\Delta\tau}V_{s1}^{k} & 0 \end{bmatrix} \tag{3.32}$$

48

$$\mathbf{H}_c(r) = \left[\cdots \; \mathbf{H}_c^{(k)}(r) \; \cdots \right]_{k=1\ldots4}, \qquad \mathbf{H}_c^{(k)}(r) = a_k\, h_k \begin{bmatrix} 0 & 0 & 0 & 0 & {}^{\tau+\Delta\tau}V_{t3}^k & -{}^{\tau+\Delta\tau}V_{t2}^k \\ 0 & 0 & 0 & -{}^{\tau+\Delta\tau}V_{t3}^k & 0 & -{}^{\tau+\Delta\tau}V_{t1}^k \\ 0 & 0 & 0 & {}^{\tau+\Delta\tau}V_{t2}^k & -{}^{\tau+\Delta\tau}V_{t1}^k & 0 \end{bmatrix} \quad (3.33)$$

$$\mathbf{B}_{La}(r) = \left[\cdots \; \mathbf{B}_{La}^{(k)}(r) \; \cdots \right]_{k=1\ldots4},$$

$$\mathbf{B}_{La}^{(k)}(r) = \begin{bmatrix} h_{k,1} & 0 & 0 & (\Phi1)_{11}^k & (\Phi2)_{11}^k & (\Phi3)_{11}^k \\ 0 & h_{k,2} & 0 & (\Phi1)_{22}^k & (\Phi2)_{22}^k & (\Phi3)_{22}^k \\ 0 & 0 & h_{k,3} & (\Phi1)_{33}^k & (\Phi2)_{33}^k & (\Phi3)_{33}^k \\ h_{k,2} & h_{k,1} & 0 & (\Phi1)_{12}^k+(\Phi1)_{21}^k & (\Phi2)_{12}^k+(\Phi2)_{21}^k & (\Phi3)_{12}^k+(\Phi3)_{21}^k \\ 0 & h_{k,3} & h_{k,2} & (\Phi1)_{23}^k+(\Phi1)_{32}^k & (\Phi2)_{23}^k+(\Phi2)_{32}^k & (\Phi3)_{23}^k+(\Phi3)_{32}^k \\ h_{k,3} & 0 & h_{k,1} & (\Phi1)_{13}^k+(\Phi1)_{31}^k & (\Phi2)_{13}^k+(\Phi2)_{31}^k & (\Phi3)_{13}^k+(\Phi3)_{31}^k \end{bmatrix} \quad (3.34)$$

$$\mathbf{B}_{Lb}(r) = \left[\cdots \; \mathbf{B}_{Lb}^{(k)}(r) \; \cdots \right]_{k=1\ldots4},$$

$$\mathbf{B}_{Lb}^{(k)}(r) = \begin{bmatrix} 0 & 0 & 0 & (\hat\Phi1)_{11}^k & (\hat\Phi2)_{11}^k & (\hat\Phi3)_{11}^k \\ 0 & 0 & 0 & (\hat\Phi1)_{22}^k & (\hat\Phi2)_{22}^k & (\hat\Phi3)_{22}^k \\ 0 & 0 & 0 & (\hat\Phi1)_{33}^k & (\hat\Phi2)_{33}^k & (\hat\Phi3)_{33}^k \\ 0 & 0 & 0 & (\hat\Phi1)_{12}^k+(\hat\Phi1)_{21}^k & (\hat\Phi2)_{12}^k+(\hat\Phi2)_{21}^k & (\hat\Phi3)_{12}^k+(\hat\Phi3)_{21}^k \\ 0 & 0 & 0 & (\hat\Phi1)_{23}^k+(\hat\Phi1)_{32}^k & (\hat\Phi2)_{23}^k+(\hat\Phi2)_{32}^k & (\hat\Phi3)_{23}^k+(\hat\Phi3)_{32}^k \\ 0 & 0 & 0 & (\hat\Phi1)_{13}^k+(\hat\Phi1)_{31}^k & (\hat\Phi2)_{13}^k+(\hat\Phi2)_{31}^k & (\hat\Phi3)_{13}^k+(\hat\Phi3)_{31}^k \end{bmatrix} \quad (3.35)$$

$$\mathbf{B}_{Lc}(r) = \left[\cdots \; \mathbf{B}_{Lc}^{(k)}(r) \; \cdots \right]_{k=1\ldots4},$$

$$\mathbf{B}_{Lc}^{(k)}(r)=\begin{bmatrix} 0 & 0 & 0 & (\bar{\Phi}1)_{11}^{k} & (\bar{\Phi}2)_{11}^{k} & (\bar{\Phi}3)_{11}^{k} \\ 0 & 0 & 0 & (\bar{\Phi}1)_{22}^{k} & (\bar{\Phi}2)_{22}^{k} & (\bar{\Phi}3)_{22}^{k} \\ 0 & 0 & 0 & (\bar{\Phi}1)_{33}^{k} & (\bar{\Phi}2)_{33}^{k} & (\bar{\Phi}3)_{33}^{k} \\ 0 & 0 & 0 & (\bar{\Phi}1)_{12}^{k}+(\bar{\Phi}1)_{21}^{k} & (\bar{\Phi}2)_{12}^{k}+(\bar{\Phi}2)_{21}^{k} & (\bar{\Phi}3)_{12}^{k}+(\bar{\Phi}3)_{21}^{k} \\ 0 & 0 & 0 & (\bar{\Phi}1)_{23}^{k}+(\bar{\Phi}1)_{32}^{k} & (\bar{\Phi}2)_{23}^{k}+(\bar{\Phi}2)_{32}^{k} & (\bar{\Phi}3)_{23}^{k}+(\bar{\Phi}3)_{32}^{k} \\ 0 & 0 & 0 & (\bar{\Phi}1)_{13}^{k}+(\bar{\Phi}1)_{31}^{k} & (\bar{\Phi}2)_{13}^{k}+(\bar{\Phi}2)_{31}^{k} & (\bar{\Phi}3)_{13}^{k}+(\bar{\Phi}3)_{31}^{k} \end{bmatrix} \tag{3.36}$$

$$\mathbf{B}_{NLa}(r)=\left[\cdots \ \mathbf{B}_{NLa}^{(k)}(r) \ \cdots\right]_{k=1\ldots4}, \quad \mathbf{B}_{NLa}^{(k)}(r)=\begin{bmatrix} h_{k,1} & 0 & 0 & (\Phi1)_{11}^{k} & (\Phi2)_{11}^{k} & (\Phi3)_{11}^{k} \\ h_{k,2} & 0 & 0 & (\Phi1)_{12}^{k} & (\Phi2)_{12}^{k} & (\Phi3)_{12}^{k} \\ h_{k,3} & 0 & 0 & (\Phi1)_{13}^{k} & (\Phi2)_{13}^{k} & (\Phi3)_{13}^{k} \\ 0 & h_{k,1} & 0 & (\Phi1)_{21}^{k} & (\Phi2)_{21}^{k} & (\Phi3)_{21}^{k} \\ 0 & h_{k,2} & 0 & (\Phi1)_{22}^{k} & (\Phi2)_{22}^{k} & (\Phi3)_{22}^{k} \\ 0 & h_{k,3} & 0 & (\Phi1)_{23}^{k} & (\Phi2)_{23}^{k} & (\Phi3)_{23}^{k} \\ 0 & 0 & h_{k,1} & (\Phi1)_{31}^{k} & (\Phi2)_{31}^{k} & (\Phi3)_{31}^{k} \\ 0 & 0 & h_{k,2} & (\Phi1)_{32}^{k} & (\Phi2)_{32}^{k} & (\Phi3)_{32}^{k} \\ 0 & 0 & h_{k,3} & (\Phi1)_{33}^{k} & (\Phi2)_{33}^{k} & (\Phi3)_{33}^{k} \end{bmatrix} \tag{3.37}$$

$$\mathbf{B}_{NLb}(r)=\left[\cdots \ \mathbf{B}_{NLb}^{(k)}(r) \ \cdots\right]_{k=1\ldots4}, \quad \mathbf{B}_{NLb}^{(k)}(r)=\begin{bmatrix} 0 & 0 & 0 & (\hat{\Phi}1)_{11}^{k} & (\hat{\Phi}2)_{11}^{k} & (\hat{\Phi}3)_{11}^{k} \\ 0 & 0 & 0 & (\hat{\Phi}1)_{12}^{k} & (\hat{\Phi}2)_{12}^{k} & (\hat{\Phi}3)_{12}^{k} \\ 0 & 0 & 0 & (\hat{\Phi}1)_{13}^{k} & (\hat{\Phi}2)_{13}^{k} & (\hat{\Phi}3)_{13}^{k} \\ 0 & 0 & 0 & (\hat{\Phi}1)_{21}^{k} & (\hat{\Phi}2)_{21}^{k} & (\hat{\Phi}3)_{21}^{k} \\ 0 & 0 & 0 & (\hat{\Phi}1)_{22}^{k} & (\hat{\Phi}2)_{22}^{k} & (\hat{\Phi}3)_{22}^{k} \\ 0 & 0 & 0 & (\hat{\Phi}1)_{23}^{k} & (\hat{\Phi}2)_{23}^{k} & (\hat{\Phi}3)_{23}^{k} \\ 0 & 0 & 0 & (\hat{\Phi}1)_{31}^{k} & (\hat{\Phi}2)_{31}^{k} & (\hat{\Phi}3)_{31}^{k} \\ 0 & 0 & 0 & (\hat{\Phi}1)_{32}^{k} & (\hat{\Phi}2)_{32}^{k} & (\hat{\Phi}3)_{32}^{k} \\ 0 & 0 & 0 & (\hat{\Phi}1)_{33}^{k} & (\hat{\Phi}2)_{33}^{k} & (\hat{\Phi}3)_{33}^{k} \end{bmatrix} \tag{3.38}$$

$$\mathbf{B}_{NLc}(r)=\Big[\cdots\ \mathbf{B}_{NLc}^{(k)}(r)\ \cdots\Big]_{k=1\ldots4},\qquad \mathbf{B}_{NLc}^{(k)}(r)=\begin{bmatrix} 0 & 0 & 0 & (\bar{\Phi}1)_{11}^{k} & (\bar{\Phi}2)_{11}^{k} & (\bar{\Phi}3)_{11}^{k} \\ 0 & 0 & 0 & (\bar{\Phi}1)_{12}^{k} & (\bar{\Phi}2)_{12}^{k} & (\bar{\Phi}3)_{12}^{k} \\ 0 & 0 & 0 & (\bar{\Phi}1)_{13}^{k} & (\bar{\Phi}2)_{13}^{k} & (\bar{\Phi}3)_{13}^{k} \\ 0 & 0 & 0 & (\bar{\Phi}1)_{21}^{k} & (\bar{\Phi}2)_{21}^{k} & (\bar{\Phi}3)_{21}^{k} \\ 0 & 0 & 0 & (\bar{\Phi}1)_{22}^{k} & (\bar{\Phi}2)_{22}^{k} & (\bar{\Phi}3)_{22}^{k} \\ 0 & 0 & 0 & (\bar{\Phi}1)_{23}^{k} & (\bar{\Phi}2)_{23}^{k} & (\bar{\Phi}3)_{23}^{k} \\ 0 & 0 & 0 & (\bar{\Phi}1)_{31}^{k} & (\bar{\Phi}2)_{31}^{k} & (\bar{\Phi}3)_{31}^{k} \\ 0 & 0 & 0 & (\bar{\Phi}1)_{32}^{k} & (\bar{\Phi}2)_{32}^{k} & (\bar{\Phi}3)_{32}^{k} \\ 0 & 0 & 0 & (\bar{\Phi}1)_{33}^{k} & (\bar{\Phi}2)_{33}^{k} & (\bar{\Phi}3)_{33}^{k} \end{bmatrix} \tag{3.39}$$

in Equations (3.34)-(3.39), parameters $(\Phi_m)_{in}^{k}$, $(\hat{\Phi}_m)_{in}^{k}$ and $(\bar{\Phi}_m)_{in}^{k}$ are defined as follow

$$(\Phi_m)_{in}^{k}=\left(J_{n2}^{-1}(\hat{\phi})_{mi}^{k}+J_{n3}^{-1}(\bar{\phi})_{mi}^{k}\right)h_k \tag{3.40}$$

$$(\hat{\Phi}_m)_{in}^{k}=\left(J_{n1}^{-1}(\hat{\phi})_{mi}^{k}\right)\frac{\partial h_k}{\partial r} \tag{3.41}$$

$$(\bar{\Phi}_m)_{in}^{k}=\left(J_{n1}^{-1}(\bar{\phi})_{mi}^{k}\right)\frac{\partial h_k}{\partial r} \tag{3.42}$$

where, nonzero values for $\hat{\phi}$ and $\bar{\phi}$ are

$$(\hat{\phi})_{12}^{k}=-(\hat{\phi})_{21}^{k}=-0.5a^{k\ \tau+\Delta\tau}V_{s3}^{k} \tag{3.43}$$

$$(\hat{\phi})_{13}^{k}=-(\hat{\phi})_{31}^{k}=0.5a^{k\ \tau+\Delta\tau}V_{s2}^{k} \tag{3.44}$$

$$\left(\hat{\phi}\right)^k_{23} = -\left(\hat{\phi}\right)^k_{32} = -0.5a^k \; ^{\tau+\Delta\tau}V^k_{s1} \tag{3.45}$$

$$\left(\bar{\phi}\right)^k_{12} = -\left(\bar{\phi}\right)^k_{21} = -0.5a^k \; ^{\tau+\Delta\tau}V^k_{t3} \tag{3.46}$$

$$\left(\bar{\phi}\right)^k_{13} = -\left(\bar{\phi}\right)^k_{31} = 0.5a^k \; ^{\tau+\Delta\tau}V^k_{t2} \tag{3.47}$$

$$\left(\bar{\phi}\right)^k_{23} = -\left(\bar{\phi}\right)^k_{32} = -0.5a^k \; ^{\tau+\Delta\tau}V^k_{t1} \tag{3.48}$$

Now, substitution of Equations (3.28)-(3.30) into Equations (3.24)-(3.27) results in

$$\mathbf{M} = \int_{^{\tau+\Delta\tau}V} \rho\left(\mathbf{M}_a(r)+s\mathbf{M}_b(r)+t\mathbf{M}_c(r)+st\mathbf{M}_d(r)+s^2\mathbf{M}_e(r)+t^2\mathbf{M}_f(r)\right)dV \tag{3.49}$$

$$\mathbf{K}_L = \int_{^{\tau+\Delta\tau}V} \left(\mathbf{K}_{La}(r)+s\mathbf{K}_{Lb}(r)+t\mathbf{K}_{Lc}(r)+st\mathbf{K}_{Ld}(r)+s^2\mathbf{K}_{Le}(r)+t^2\mathbf{K}_{Lf}(r)\right)dV \tag{3.50}$$

$$\begin{aligned}\mathbf{K}_{NL} = \int_{^{\tau+\Delta\tau}V} \Big(&\mathbf{K}_{NLa}(r)+s\mathbf{K}_{NLb}(r)+t\mathbf{K}_{NLc}(r)+st\mathbf{K}_{NLd}(r)+s^2\mathbf{K}_{NLe}(r)+t^2\mathbf{K}_{NLf}(r)\\ &+s^2t\mathbf{K}_{NLg}(r)+st^2\mathbf{K}_{NLh}(r)+s^3\mathbf{K}_{NLi}(r)+t^3\mathbf{K}_{NLj}(r)+s^2t^2\mathbf{K}_{NLk}(r)\\ &+s^3t\mathbf{K}_{NLl}(r)+st^3\mathbf{K}_{NLm}(r)+s^4\mathbf{K}_{NLn}(r)+t^4\mathbf{K}_{NLo}(r)\Big)dV\end{aligned} \tag{3.51}$$

$$\begin{aligned}\mathbf{F} = \int_{^{\tau+\Delta\tau}V} \Big(&\mathbf{F}_a(r)+s\mathbf{F}_b(r)+t\mathbf{F}_c(r)+st\mathbf{F}_d(r)+s^2\mathbf{F}_e(r)+t^2\mathbf{F}_f(r)\\ &+s^2t\mathbf{F}_g(r)+st^2\mathbf{F}_h(r)+s^3\mathbf{F}_i(r)+t^3\mathbf{F}_j(r)\Big)dV\end{aligned} \tag{3.52}$$

the new matrices and vectors in these equations are defined as follows

$$\mathbf{M}_a(r) = \mathbf{H}_a^T\mathbf{H}_a \tag{3.53}$$

$$\mathbf{M}_b(r) = \mathbf{H}_a^{\mathrm{T}} \mathbf{H}_b + \mathbf{H}_b^{\mathrm{T}} \mathbf{H}_a \qquad (3.54)$$

$$\mathbf{M}_c(r) = \mathbf{H}_a^{\mathrm{T}} \mathbf{H}_c + \mathbf{H}_c^{\mathrm{T}} \mathbf{H}_a \qquad (3.55)$$

$$\mathbf{M}_d(r) = \mathbf{H}_b^{\mathrm{T}} \mathbf{H}_c + \mathbf{H}_c^{\mathrm{T}} \mathbf{H}_b \qquad (3.56)$$

$$\mathbf{M}_e(r) = \mathbf{H}_b^{\mathrm{T}} \mathbf{H}_b \qquad (3.57)$$

$$\mathbf{M}_f(r) = \mathbf{H}_c^{\mathrm{T}} \mathbf{H}_c \qquad (3.58)$$

$$\mathbf{K}_{La}(r) = \mathbf{B}_{La}^{\mathrm{T}} \mathbf{C} \mathbf{B}_{La} \qquad (3.59)$$

$$\mathbf{K}_{Lb}(r) = \mathbf{B}_{La}^{\mathrm{T}} \mathbf{C} \mathbf{B}_{Lb} + \mathbf{B}_{Lb}^{\mathrm{T}} \mathbf{C} \mathbf{B}_{La} \qquad (3.60)$$

$$\mathbf{K}_{Lc}(r) = \mathbf{B}_{La}^{\mathrm{T}} \mathbf{C} \mathbf{B}_{Lc} + \mathbf{B}_{Lc}^{\mathrm{T}} \mathbf{C} \mathbf{B}_{La} \qquad (3.61)$$

$$\mathbf{K}_{Ld}(r) = \mathbf{B}_{Lb}^{\mathrm{T}} \mathbf{C} \mathbf{B}_{Lc} + \mathbf{B}_{Lc}^{\mathrm{T}} \mathbf{C} \mathbf{B}_{Lb} \qquad (3.62)$$

$$\mathbf{K}_{Le}(r) = \mathbf{B}_{Lb}^{\mathrm{T}} \mathbf{C} \mathbf{B}_{Lb} \qquad (3.63)$$

$$\mathbf{K}_{Lf}(r) = \mathbf{B}_{Lc}^{\mathrm{T}} \mathbf{C} \mathbf{B}_{Lc} \qquad (3.64)$$

$$\mathbf{K}_{NLa}(r) = \mathbf{B}_{NLa}^{\mathrm{T}} \mathbf{S}^{(0)} \mathbf{B}_{NLa} \qquad (3.65)$$

$$\mathbf{K}_{NLb}(r) = \mathbf{B}_{NLa}^{\mathrm{T}} \mathbf{S}^{(1)} \mathbf{B}_{NLa} + \mathbf{B}_{NLb}^{\mathrm{T}} \mathbf{S}^{(0)} \mathbf{B}_{NLa} + \mathbf{B}_{NLa}^{\mathrm{T}} \mathbf{S}^{(0)} \mathbf{B}_{NLb} \qquad (3.66)$$

$$\mathbf{K}_{NLc}(r) = \mathbf{B}_{NLa}^{\mathrm{T}} \mathbf{S}^{(2)} \mathbf{B}_{NLa} + \mathbf{B}_{NLc}^{\mathrm{T}} \mathbf{S}^{(0)} \mathbf{B}_{NLa} + \mathbf{B}_{NLa}^{\mathrm{T}} \mathbf{S}^{(0)} \mathbf{B}_{NLc} \qquad (3.67)$$

$$\mathbf{K}_{NLd}(r) = \mathbf{B}_{NLa}^{\mathrm{T}}\mathbf{S}^{(1)}\mathbf{B}_{NLc} + \mathbf{B}_{NLa}^{\mathrm{T}}\mathbf{S}^{(2)}\mathbf{B}_{NLb} + \mathbf{B}_{NLb}^{\mathrm{T}}\mathbf{S}^{(0)}\mathbf{B}_{NLc} + \mathbf{B}_{NLc}^{\mathrm{T}}\mathbf{S}^{(0)}\mathbf{B}_{NLb}$$
$$+ \mathbf{B}_{NLc}^{\mathrm{T}}\mathbf{S}^{(1)}\mathbf{B}_{NLa} + \mathbf{B}_{NLa}^{\mathrm{T}}\mathbf{S}^{(3)}\mathbf{B}_{NLa} + \mathbf{B}_{NLb}^{\mathrm{T}}\mathbf{S}^{(2)}\mathbf{B}_{NLa} \tag{3.68}$$

$$\mathbf{K}_{NLe}(r) = \mathbf{B}_{NLb}^{\mathrm{T}}\mathbf{S}^{(0)}\mathbf{B}_{NLb} + \mathbf{B}_{NLa}^{\mathrm{T}}\mathbf{S}^{(4)}\mathbf{B}_{NLa} + \mathbf{B}_{NLb}^{\mathrm{T}}\mathbf{S}^{(1)}\mathbf{B}_{NLa} + \mathbf{B}_{NLa}^{\mathrm{T}}\mathbf{S}^{(1)}\mathbf{B}_{NLb} \tag{3.69}$$

$$\mathbf{K}_{NLf}(r) = \mathbf{B}_{NLa}^{\mathrm{T}}\mathbf{S}^{(2)}\mathbf{B}_{NLc} + \mathbf{B}_{NLc}^{\mathrm{T}}\mathbf{S}^{(0)}\mathbf{B}_{NLc} + \mathbf{B}_{NLa}^{\mathrm{T}}\mathbf{S}^{(5)}\mathbf{B}_{NLa} + \mathbf{B}_{NLc}^{\mathrm{T}}\mathbf{S}^{(2)}\mathbf{B}_{NLa} \tag{3.70}$$

$$\mathbf{K}_{NLg}(r) = \mathbf{B}_{NLa}^{\mathrm{T}}\mathbf{S}^{(3)}\mathbf{B}_{NLb} + \mathbf{B}_{NLa}^{\mathrm{T}}\mathbf{S}^{(4)}\mathbf{B}_{NLc} + \mathbf{B}_{NLb}^{\mathrm{T}}\mathbf{S}^{(1)}\mathbf{B}_{NLc} + \mathbf{B}_{NLb}^{\mathrm{T}}\mathbf{S}^{(2)}\mathbf{B}_{NLb}$$
$$+ \mathbf{B}_{NLc}^{\mathrm{T}}\mathbf{S}^{(1)}\mathbf{B}_{NLb} + \mathbf{B}_{NLc}^{\mathrm{T}}\mathbf{S}^{(4)}\mathbf{B}_{NLa} + \mathbf{B}_{NLb}^{\mathrm{T}}\mathbf{S}^{(3)}\mathbf{B}_{NLa} \tag{3.71}$$

$$\mathbf{K}_{NLh}(r) = \mathbf{B}_{NLa}^{\mathrm{T}}\mathbf{S}^{(3)}\mathbf{B}_{NLc} + \mathbf{B}_{NLa}^{\mathrm{T}}\mathbf{S}^{(5)}\mathbf{B}_{NLb} + \mathbf{B}_{NLb}^{\mathrm{T}}\mathbf{S}^{(2)}\mathbf{B}_{NLc} + \mathbf{B}_{NLc}^{\mathrm{T}}\mathbf{S}^{(1)}\mathbf{B}_{NLc}$$
$$+ \mathbf{B}_{NLc}^{\mathrm{T}}\mathbf{S}^{(2)}\mathbf{B}_{NLb} + \mathbf{B}_{NLb}^{\mathrm{T}}\mathbf{S}^{(5)}\mathbf{B}_{NLa} + \mathbf{B}_{NLc}^{\mathrm{T}}\mathbf{S}^{(3)}\mathbf{B}_{NLa} \tag{3.72}$$

$$\mathbf{K}_{NLi}(r) = \mathbf{B}_{NLa}^{\mathrm{T}}\mathbf{S}^{(4)}\mathbf{B}_{NLb} + \mathbf{B}_{NLb}^{\mathrm{T}}\mathbf{S}^{(1)}\mathbf{B}_{NLb} + \mathbf{B}_{NLb}^{\mathrm{T}}\mathbf{S}^{(4)}\mathbf{B}_{NLa} \tag{3.73}$$

$$\mathbf{K}_{NLj}(r) = \mathbf{B}_{NLa}^{\mathrm{T}}\mathbf{S}^{(5)}\mathbf{B}_{NLc} + \mathbf{B}_{NLc}^{\mathrm{T}}\mathbf{S}^{(2)}\mathbf{B}_{NLc} + \mathbf{B}_{NLc}^{\mathrm{T}}\mathbf{S}^{(5)}\mathbf{B}_{NLa} \tag{3.74}$$

$$\mathbf{K}_{NLk}(r) = \mathbf{B}_{NLb}^{\mathrm{T}}\mathbf{S}^{(3)}\mathbf{B}_{NLc} + \mathbf{B}_{NLb}^{\mathrm{T}}\mathbf{S}^{(5)}\mathbf{B}_{NLb} + \mathbf{B}_{NLc}^{\mathrm{T}}\mathbf{S}^{(3)}\mathbf{B}_{NLb} + \mathbf{B}_{NLc}^{\mathrm{T}}\mathbf{S}^{(4)}\mathbf{B}_{NLc} \tag{3.75}$$

$$\mathbf{K}_{NLl}(r) = \mathbf{B}_{NLb}^{\mathrm{T}}\mathbf{S}^{(3)}\mathbf{B}_{NLb} + \mathbf{B}_{NLb}^{\mathrm{T}}\mathbf{S}^{(4)}\mathbf{B}_{NLc} + \mathbf{B}_{NLc}^{\mathrm{T}}\mathbf{S}^{(4)}\mathbf{B}_{NLb} \tag{3.76}$$

$$\mathbf{K}_{NLm}(r) = \mathbf{B}_{NLb}^{\mathrm{T}}\mathbf{S}^{(5)}\mathbf{B}_{NLc} + \mathbf{B}_{NLc}^{\mathrm{T}}\mathbf{S}^{(3)}\mathbf{B}_{NLc} + \mathbf{B}_{NLc}^{\mathrm{T}}\mathbf{S}^{(5)}\mathbf{B}_{NLb} \tag{3.77}$$

$$\mathbf{K}_{NLn}(r) = \mathbf{B}_{NLb}^{\mathrm{T}}\mathbf{S}^{(4)}\mathbf{B}_{NLb} \tag{3.78}$$

$$\mathbf{K}_{NLo}(r) = \mathbf{B}_{NLc}^{\mathrm{T}}\mathbf{S}^{(5)}\mathbf{B}_{NLc} \tag{3.79}$$

Equations (3.49)-(3.52) can be evaluated by a selected order of Gaussian quadrature numerical integration procedure over the annular section riser element volume. In order to make the formulation more efficient and to avoid higher order numerical integrations, and since some of the terms in Equations (3.49)-(3.52) are eliminated, an analytical integration scheme for through-the-thickness coordinates r and t is employed for solution of these equations. Thus, after explicitly integrating Equations (3.49)-(3.52), we get:

$$\mathbf{M}=\int_{-1}^{1}\rho\left(a_0\mathbf{M}_a(r)+a_1\left[\mathbf{M}_e(r)+\mathbf{M}_f(r)\right]\right)\left|\mathbf{J}_{(r),s=0,t=0}\right|dr \tag{3.80}$$

$$\mathbf{K}_L=\int_{-1}^{1}\left(a_0\mathbf{K}_{La}(r)+a_1\left[\mathbf{K}_{Le}(r)+\mathbf{K}_{Lf}(r)\right]\right)\left|\mathbf{J}_{(r),s=0,t=0}\right|dr \tag{3.81}$$

$$\mathbf{K}_{NL}=\int_{-1}^{1}\left(a_0\mathbf{K}_{NLa}(r)+a_1\left[\mathbf{K}_{NLe}(r)+\mathbf{K}_{NLf}(r)\right]\right.$$
$$\left.+a_2\left[\mathbf{K}_{NLk}(r)+3\mathbf{K}_{NLn}(r)+3\mathbf{K}_{NLo}(r)\right]\right)\left|\mathbf{J}_{(r),s=0,t=0}\right|dr \tag{3.82}$$

$$\mathbf{F}=\int_{-1}^{1}\left(a_0\mathbf{F}_a(r)+a_1\left[\mathbf{F}_e(r)+\mathbf{F}_f(r)\right]\right)\left|\mathbf{J}_{(r),s=0,t=0}\right|dr \tag{3.83}$$

where

$$a_0=\pi\left(1-(r_i/r_o)^2\right) \tag{3.84}$$

$$a_1=\frac{\pi}{4}\left(1-(r_i/r_o)^4\right) \tag{3.85}$$

$$a_2=\frac{\pi}{24}\left(1-(r_i/r_o)^6\right) \tag{3.86}$$

55

3.5 Modal (free vibration) analysis

Considering Equation (3.23), free vibration equilibrium equation for riser structure at time $\tau+\Delta\tau$ is as follow

$$\overset{(i)}{\mathbf{M}}\,\overset{(i)}{\ddot{\mathbf{U}}}+(\overset{(i)}{\mathbf{K}_L}+\overset{(i-1)}{\mathbf{K}_{NL}})\,\overset{(i)}{\mathbf{U}}=0 \qquad\qquad (3.87)$$

A solution for Equation (3.87) can be postulated to be of the form

$$^{\tau+\Delta\tau}\mathbf{U}=\boldsymbol{\varphi}\,\sin\omega(\tau+\Delta\tau) \qquad\qquad (3.88)$$

Therefore the generalized eigenproblem results as

$$(\mathbf{K}_L+\mathbf{K}_{NL})\boldsymbol{\varphi}=\omega^2\mathbf{M}\boldsymbol{\varphi} \qquad\qquad (3.89)$$

Since $\mathbf{K}=(\mathbf{K}_L+\mathbf{K}_{NL})$ is symmetric and $\mathbf{M}$ is symmetric positive definite, a simple Algorithm can be adopted to transform eigenproblem (3.89) to a standard eigenproblem. Using the Cholesky factorization results in

$$\mathbf{M}=\mathbf{R}^T\mathbf{R} \qquad\qquad (3.90)$$

where $\mathbf{R}$ is a triangular matrix. Substituting Equation (3.90) into the Equation (3.89), the generalized eigenproblem Equation (3.89) is transformed to

$$\mathbf{R}^{-T}(\mathbf{K}_L + \mathbf{K}_{NL})\mathbf{R}^{-1}(\mathbf{R}\boldsymbol{\varphi}) = \omega^2 \mathbf{M}(\mathbf{R}\boldsymbol{\varphi}) \tag{3.91}$$

Therefore we obtain the standard eigenproblem $\mathbf{K}_1\boldsymbol{\varphi}_1 = \omega^2\boldsymbol{\varphi}_1$. Compute all of the eigenvalues of the real symmetric matrix $\mathbf{K}_1 = \mathbf{R}^{-T}(\mathbf{K}_L + \mathbf{K}_{NL})\mathbf{R}^{-1}$ leads modal analysis for generalized eigenproblem (3.89).

3.6 The Newmark Method for Dynamic Solution

The most general approach for the solution of the dynamic response of structural systems is the direct numerical integration of the dynamic equilibrium equations. Newmark presented a family of single-step integration methods for the solution of structural dynamic problems. Since that many other researchers have improved the Newmark methods. Newmark's equations in standard form produces with assuming the acceleration to be linear with the time step, i.e.

$$\dddot{\mathbf{U}} = \frac{{}^{\tau+\Delta\tau}\ddot{\mathbf{U}} - {}^{\tau}\ddot{\mathbf{U}}}{2} \tag{3.92}$$

Using Equation (3.92) in Taylor's series ${}^{\tau+\Delta\tau}\mathbf{U}$ and ${}^{\tau+\Delta\tau}\dot{\mathbf{U}}$, and then after some mathematical manipulations, standard form of the Newmark's equations results;

$${}^{\tau+\Delta\tau}\dot{\mathbf{U}} = {}^{\tau}\dot{\mathbf{U}} + \left[(1-\delta)\,{}^{\tau}\ddot{\mathbf{U}} + \delta\,{}^{\tau+\Delta\tau}\ddot{\mathbf{U}}\right]\Delta\tau \tag{3.93}$$

57

$$^{\tau+\Delta\tau}\mathbf{U} = {}^{\tau}\mathbf{U} + {}^{\tau}\dot{\mathbf{U}}\Delta\tau + \left[\left(\frac{1}{2}-\alpha\right){}^{\tau}\ddot{\mathbf{U}} + \alpha \, {}^{\tau+\Delta\tau}\ddot{\mathbf{U}}\right]\Delta\tau^2 \qquad (3.94)$$

Where α and δ are parameters that can be determined to obtain integration accuracy and stability. For zero damping Newmark's method is conditionally stable if

$$0.5 \le \delta, \quad 0.25(0.5+\delta)^2 \le \alpha \le 0.5, \quad \Delta\tau \le \frac{1}{\omega_{\max}\sqrt{0.5\delta-\alpha}} \qquad (3.95)$$

where $\omega_{\max}$ is the maximum frequency in the structural system. As a summary for the Newmark method in direct integration scheme, the following steps have to be considered;

1. Select time step size $\Delta\tau$, parameters α and δ, and calculate integration constants:

$$\delta \ge 0.5, \quad \alpha \ge 0.25(0.5+\delta)^2$$

$$a_0 = \frac{1}{\alpha\,\Delta\tau^2}, \quad a_1 = \frac{\delta}{\alpha\,\Delta\tau}, \quad a_2 = \frac{1}{\alpha\,\Delta\tau}$$

$$a_3 = \frac{1}{2\alpha}-1, \quad a_4 = \frac{\delta}{\alpha}, \quad a_5 = \frac{\Delta\tau}{2}\left(\frac{\delta}{\alpha}-2\right)$$

$$a_6 = \Delta\tau(1-\delta), \quad a_7 = \delta\,\Delta\tau$$

2. Form effective stiffness matrix

$$\mathbf{K}^{eff} = \mathbf{K} + a_0\,\mathbf{M}$$

3. Calculate effective load

$$\mathbf{R}^{eff} = \mathbf{R} + \left(a_0{}^{\tau}\mathbf{U} + a_2{}^{\tau}\dot{\mathbf{U}} + a_3{}^{\tau}\ddot{\mathbf{U}}\right)\mathbf{M}$$

4. Solve for displacement

$$\mathbf{K}^{eff}\ {}^{\tau+\Delta\tau}\mathbf{U} = {}^{\tau+\Delta\tau}\mathbf{R}^{eff} - {}^{\tau+\Delta\tau}\mathbf{F}$$

5. Calculate accelerations and velocities

$${}^{\tau+\Delta\tau}\ddot{\mathbf{U}} = a_0\left({}^{\tau+\Delta\tau}\mathbf{U} - {}^{\tau}\mathbf{U}\right) - a_2{}^{\tau}\dot{\mathbf{U}} - a_3{}^{\tau}\ddot{\mathbf{U}}$$

$${}^{\tau+\Delta\tau}\dot{\mathbf{U}} = {}^{\tau}\dot{\mathbf{U}} + a_6{}^{\tau}\ddot{\mathbf{U}} + a_7\ {}^{\tau+\Delta\tau}\ddot{\mathbf{U}}$$

Chapter 4

Development of an Efficient Riser Fluid-Solid Interaction Algorithm

4.1 Introduction

The fluid-solid interaction is a significant concern in many engineering problems such as offshore and submerged structures and aerospace structures. The equations defining the structure are solved for displacement which is a Lagrangian variable and is computed from the solution of nonlinear elastic equations. The incompatibility between the moving Lagrangian mesh of the riser and the fixed Eulerian grids of the fluid is usually coupled by using an Arbitrary Lagrangian Eulerian (ALE) weak formulation between the two boundaries.

This chapter develops an efficient riser problem fluid-solid interaction Algorithm. The main focus in this chapter will be on updating fluid domain mesh and interface coupling of fluid-structure domains using localized Lagrange multipliers.

The interaction changes the dynamic characteristics of the structure and consequently its response to transient, cyclic, and stochastic excitation, significantly. Therefore, it is preferred to accurately model these diverse systems with the inclusion of the fluid-structure interaction [64].

4.2 Flexible riser problem in more detail

Figure 4.1 shows the flexible riser problem in more detail. As there is a feedback between subsystems of the problem, this is a coupled problem with two way interaction between two different subsystems of fluid and structure. This mechanical system is analyzed by decomposition which may be driven by physical, functional or computational considerations.
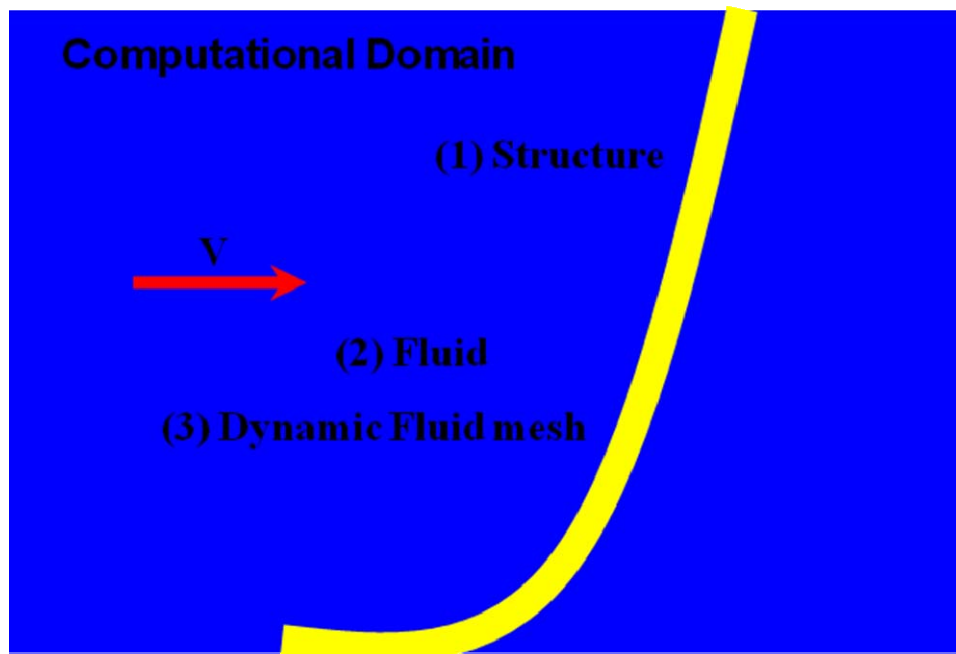
Figure 4.1: Flexible riser problem in more detail

According to this definition, the riser problem has two different types of subsystems: (1) the physical subsystems including structure and fluid (2) artificial subsystem which is the dynamic fluid mesh.

Physical subsystems (fields) have their own mathematical models to describe the fields however, the artificial subsystems are incorporated for computational solution. Figure 4.2 shows the loop (diagram) for interaction between structural and fluid meshed. According to this figure:

1- The structural mesh is solved for displacements

2- The new configuration of the fluid mesh is computed

3- Results from (2) are then used by the fluid code which is solved for pressure

4- The pressure distribution is then used as the new boundary condition for the structural model,

5- The loop is repeated
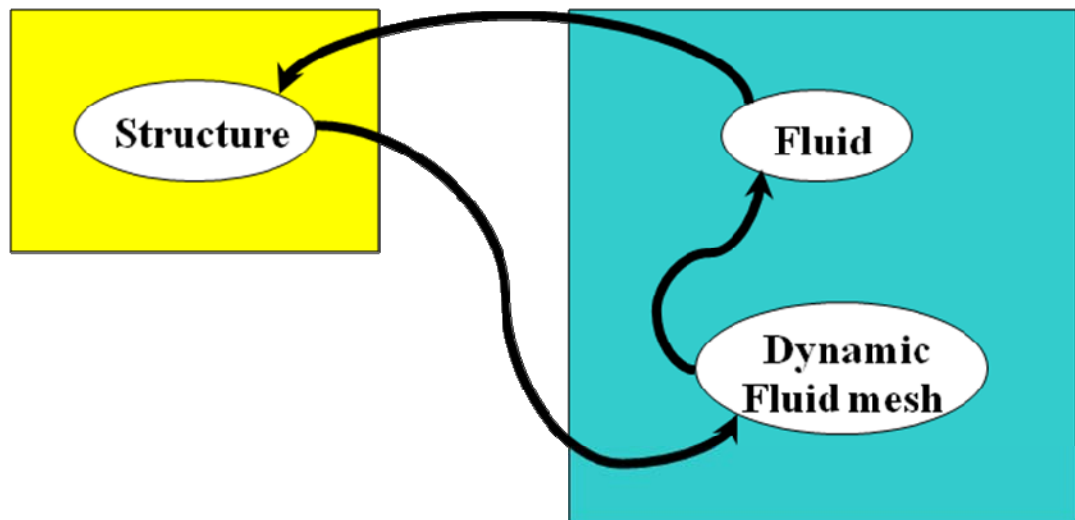
Figure 4.2: The loop (diagram) for interaction between structural and fluid meshes

4.3 Dynamic fluid mesh (ALE)

Generally, the fluid field is modeled using Eulerian method, by taking a fixed mesh over the field. However, the treatment of moving boundaries and interfaces is difficult with Eulerian elements. On the other hand, Lagrangian method is inapplicable to model fluid field but is most common for the structural analysis. Therefore, some hybrid techniques which combine the advantages of Eulerian and Lagrangian methods have been developed.

These methods which are called arbitrary Eulerian-Lagrangian formulation provide a natural solution to this coupled system problem. In this method Eulerian formulation is used in some part of the fluid filed and Lagrangian formulation is used for the structure part. Then, ALE formulation is used for some deformable part as the fluid mesh around the interface.

ALE accounts an arbitrary combination of the Lagrangian and Eulerian techniques that is specified by the user through the selection of a mesh updated (motion) method.

4.4 Mesh update using a modified elasticity equation

Using an efficient mesh movement technique is important to get adequate results in the ALE when we deal with large deformation problems. Indeed, solving mesh movement uncoupled from structure and fluid field solutions makes it possible to apply some new approaches to avoid mesh distortions. For this purpose, in this work a modified elasticity equation in which the mesh 'flow' is governed by the modified equations of the elasticity without body force and prescribed traction is used [65]

$$\tilde{\mathbf{K}}\Delta\mathbf{U}_m=\tilde{\mathbf{R}} \qquad\qquad\qquad (4.1)$$

Where, $\tilde{\mathbf{K}}$ is modified stiffness matrix and $\tilde{\mathbf{R}}$ represents the fluid boundary displacements.
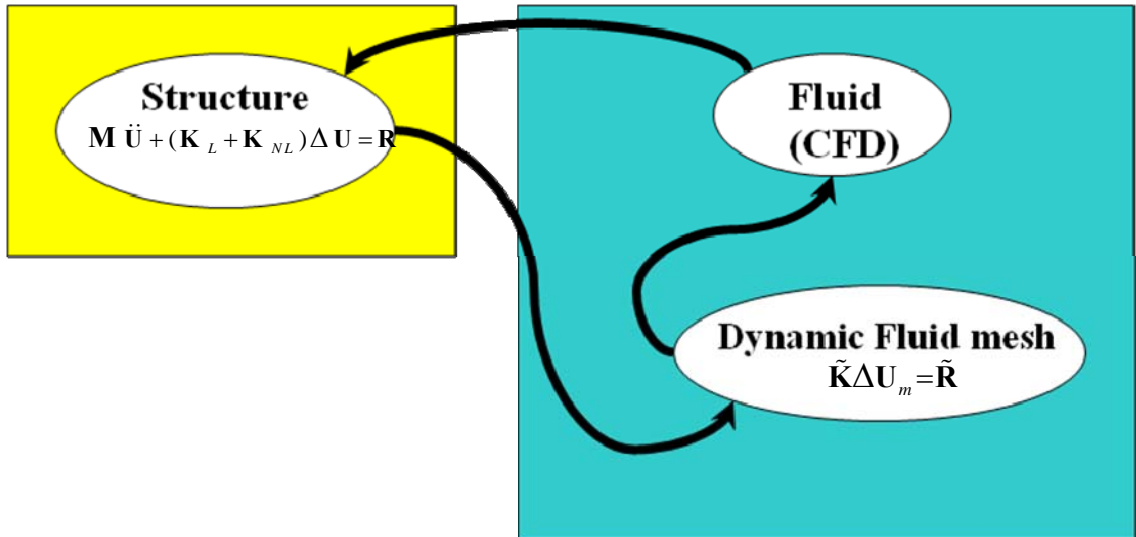
Figure 4.3: The techniques that are used for each subsystem

When mesh movement takes place, Equation (4.1) is solved to determine the internal nodal displacement of the mesh based on the given data. Figure 4.3 shows the techniques that are used for each subsystem during fluid-structure interaction uncoupled solution. After mesh motion, data is transferred from the original mesh to relocated mesh using an extrapolation procedure.

During large displacement analysis of deep water riser structure, the riser is displaced significantly by the current loading. Therefore, moving the riser to its new position results distortions in the fluid mesh. But in CFD it is important that the quality of the mesh near the riser surface (where the cells are small) remains high. In order to avoid this problem, we therefore propose two different approaches to modify elasticity equation matrices values.

1 - Taking the element volume ($^{t+\Delta t}V$) into account with a function of $1\!\!\Big/_{\!t+\Delta t V^2}$ for calculating $\tilde{\mathbf{K}}$.

2 - Taking both $^{t+\Delta t}V$ and $^{t+\Delta t}\square$ (a distance between riser centre and element centre) into account with a function of $1\!\!\Big/_{\!(^{t+\Delta t}V \; ^{t+\Delta t}\tilde{r})}$ for calculating $\tilde{\mathbf{K}}$.

Figure 4.4 shows a mesh of the fluid flow around a section of the riser structure. In Figure 4.5 this mesh updates after 0.1 m movement in horizontal direction using elasticity equation for mesh modification. According to this result the small cells near riser boundary are distorted. It is interesting to compare this result with those obtained by the modified elasticity equation where the proposed modification approaches are considered.
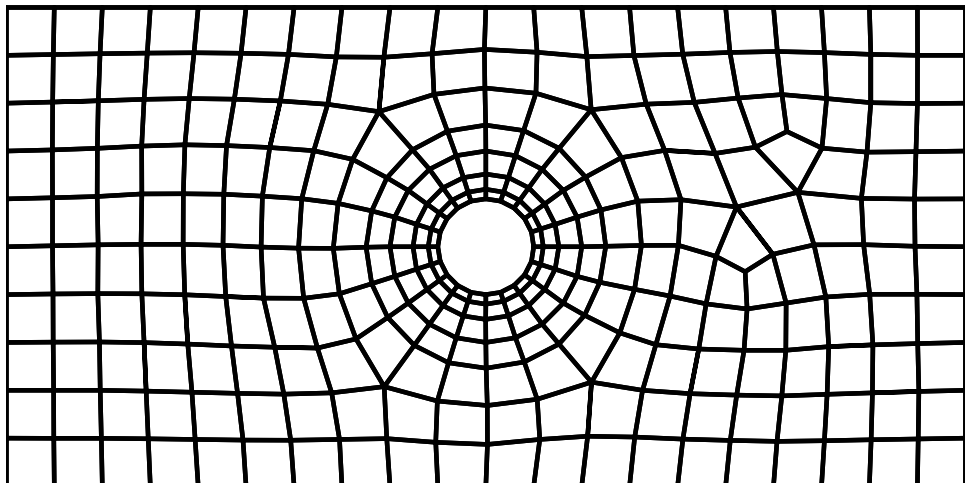
Figure 4.4: Unmoved fluid mesh
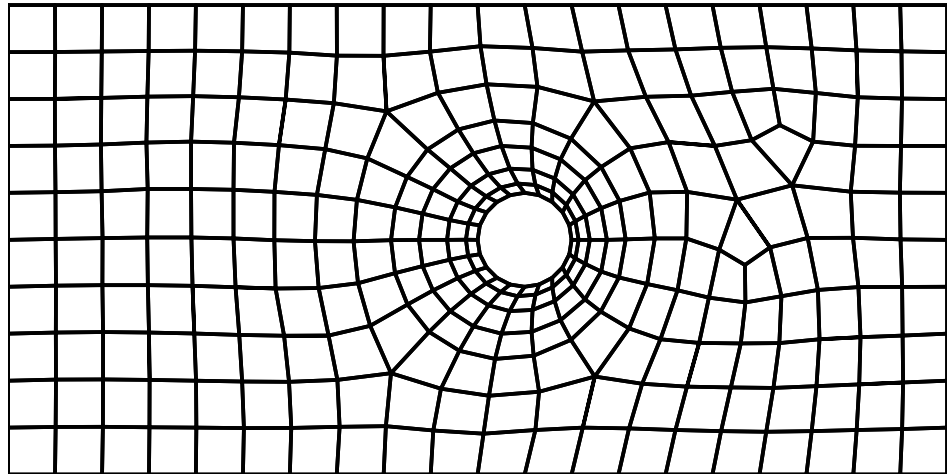
Figure 4.5: Moved fluid mesh

In this approach, the elasticity equation is modified by taking the element volume into account for calculating stiffness matrix. Figure 4.6 compares the results. In this figure red cells show the moved mesh position with no modification in elasticity equation and black cells show the moved mesh position calculated using modified equation. According to this figure less distortion occurs at the small cells (black cells) when the modified elasticity equation is used. Also, in the black mesh, most of displacements occur in elements far from the riser center where the cells have larger volumes.
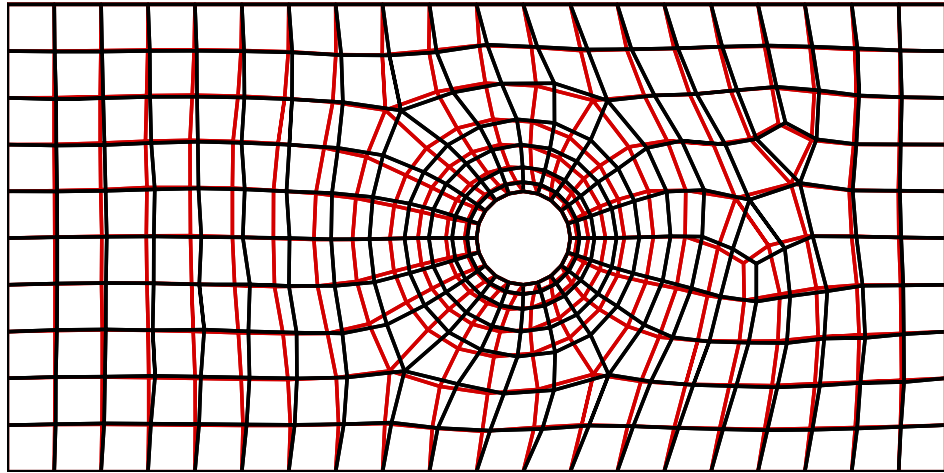
(a)
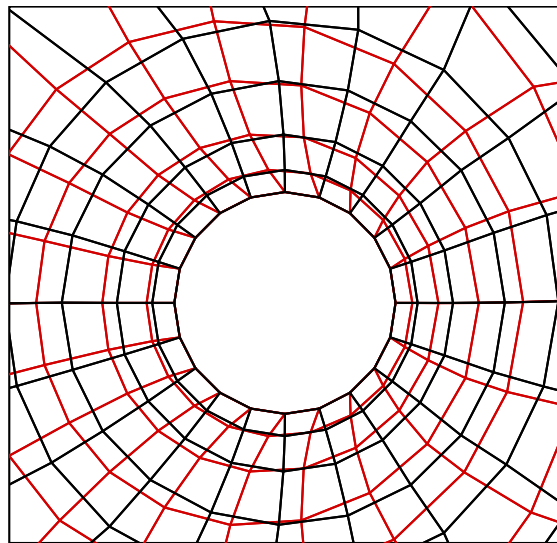
(b)

Figure 4.6: Compares the results, (a) red cells: moved mesh with no modification, black cells: moved mesh with modification. (b) Zoomed on small cells

In this section, two different proposed modifications approaches for calculating elasticity matrices during mesh movement are compared. For this purpose, the mesh shown in Figure 4.7 is considered. In Figure 4.8 a view of the initial mesh and the moved mesh is shown. In order to obtain a better view for comparison of the results from the two different methods a zoomed view is shown in Figure 4.9. In this figure blue lines show the moved mesh position for the case that modification takes place using the function of $\dfrac{1}{{}^{t+\Delta t}V^2}$ for calculating elasticity matrices and the black lines show the moved mesh position for the case that the function of $\dfrac{1}{({}^{t+\Delta t}V \; {}^{t+\Delta t}\tilde{r})}$ is used for modification.
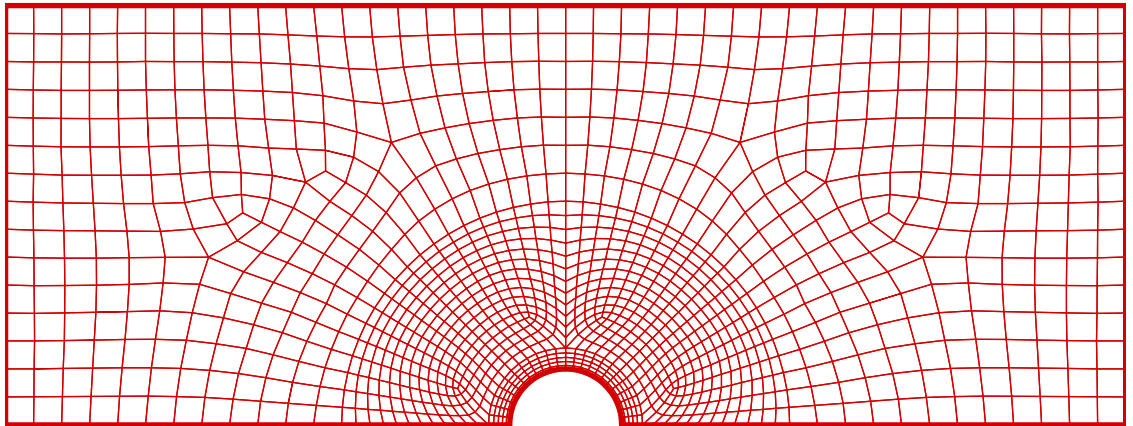
Figure 4.7: A fine mesh case
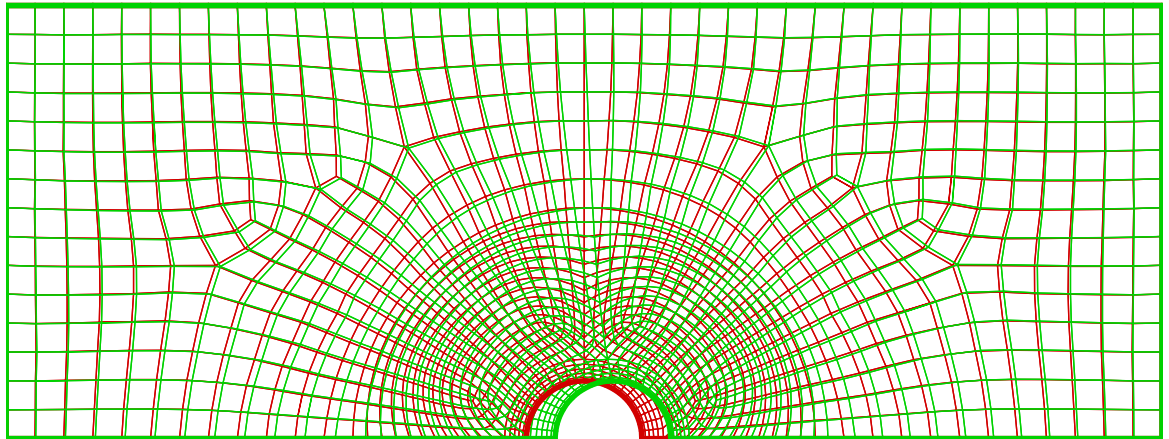
Figure 4.8: A view of the initial mesh and the moved mesh
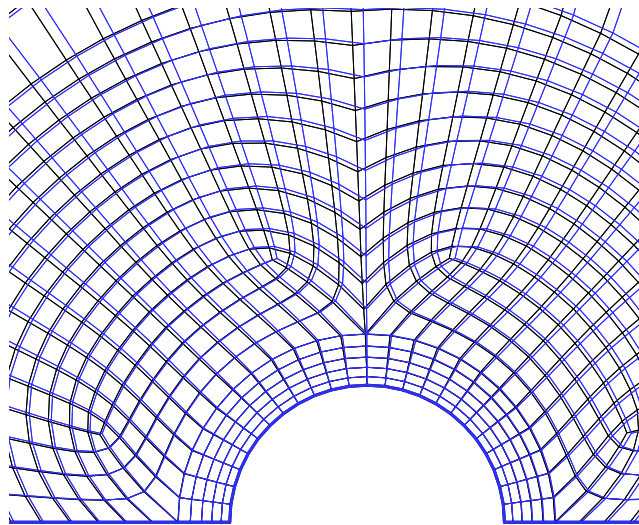
Figure 4.9: Compare the results from two different modification methods. Modification takes place using functions $1/_{t+\Delta t}V^2$ (Blue lines) and $1/(^{t+\Delta t}V \ ^{t+\Delta t}\tilde{r})$ (Black lines)

According to the Figure 4.9, for small cells near the riser surface there is no differences between two results. But it seems that when using function $\dfrac{1}{(^{t+\Delta t}V\ ^{t+\Delta t}\tilde{r})}$ for modification, the majority of the distortions is transferred far from riser center where normally use larger cells are used.

4.5 Non- matching meshes

In flexible riser fluid-structure interaction problem, the separate meshes that are used in the fluid and structure domains do not matched at their common interface. In this problem, for fluid we need a very fine mesh (Figure 4.10) specially around the riser surface to model turbulent fluid flow. However, for long length riser structure a long coarse mesh can be implemented to avoid high computational efforts.

(a)   (b)
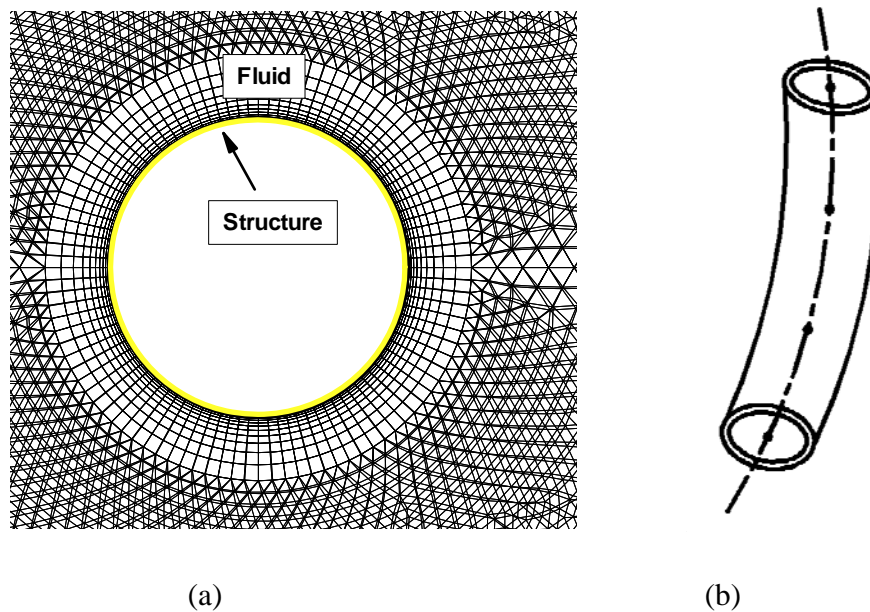
Figure 4.10: (a) Very fine fluid domain mesh, (b) High course riser mesh

4.6 Transfer data between fluid and structure non- matched meshes

At the fluid-structure interface where the two meshes are potentially non-matched, the important data has to be transfered between these incompatible meshes. Exchange of information over this interface is therefore no longer trivial. There are several methods to perform this data transformation. De Boer et al [66] have outlined six different methods. The most common method for formulation of fluid-structure interaction problems is based on using localized Lagrange multipliers [66]. In this method we introduce an interface frame between the fluid and the structure at the interaction surface (Figure 4.11). Then Local Lagrange Multipliers (LLM) links the sub-domains to the interface frame. The LLM method requires that the partitioned boundary displacements be the same as the interface frame displacements [64].
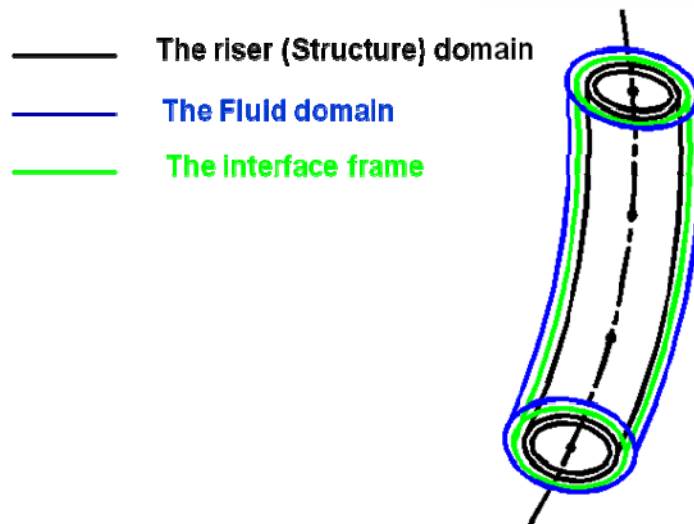
Figure 4.11: Introducing an interface frame between the fluid and structure interaction surface

4.7 Analysis of a riser system subjected to current loading

Using the element described in this work a simple case study is carried out by subjecting the nonlinear riser element to steady state flow loading (Figure 4.12). Here we are considering a simple 2D steady state flow whose governing equations are:

Conservation of Mass:
$$\frac{\partial u_i}{\partial x_i} = 0 \qquad (4.2)$$

Conservation of Momentum:
$$\rho_\infty u_j \frac{\partial u_i}{\partial x_j} - \frac{\partial}{\partial x_j}\left(-P\delta_{ij} + \mu\left(\frac{\partial u_i}{\partial x_j} + \frac{\partial u_j}{\partial x_i}\right)\right) + \rho_\infty f_i = 0 \qquad (4.3)$$

Using the dimensionless variables $u^* = \dfrac{u}{U_\infty}$, $p^* = \dfrac{p}{\rho_\infty U_\infty^{\ 2}}$ and $\mathrm{Re} = \dfrac{\rho_\infty U_\infty D}{\mu}$ as well as using Galerkin least square method by preparing the weak forms of governing equations, the mixed model of finite element formulation results in

$$\begin{bmatrix} 2\mathrm{K}_{11}+\mathrm{K}_{22}+\mathrm{C(u)} & \mathrm{K}_{21} & -\mathrm{Q}_1 \\ \mathrm{K}_{12} & \mathrm{K}_{11}+2\mathrm{K}_{22}+\mathrm{C(u)} & -\mathrm{Q}_2 \\ -\mathrm{Q}_1^{\mathrm{T}} & -\mathrm{Q}_2^{\mathrm{T}} & 0 \end{bmatrix} \begin{Bmatrix} \mathrm{u}_1 \\ \mathrm{u}_2 \\ \mathrm{P} \end{Bmatrix} = \begin{Bmatrix} \mathrm{F}_1 \\ \mathrm{F}_2 \\ 0 \end{Bmatrix} \qquad (4.4)$$

where

$$\mathrm{K}_{ij} = \int_{\Omega^e} \mu \frac{\partial \mathbf{N}}{\partial x_i} \frac{\partial \mathbf{N}^{\mathrm{T}}}{\partial x_j} dx \quad \mathrm{Q}_i = \int_{\Omega^e} \mu \frac{\partial \mathbf{N}}{\partial x_i} \mathbf{N}^{\mathrm{T}} dx \quad \mathrm{C(u)} = \int_{\Omega^e} \rho_0 \mathbf{N}(\mathbf{N}^{\mathrm{T}} u_j) \frac{\partial \mathbf{N}^{\mathrm{T}}}{\partial x_j} dx \qquad (4.5)$$

where $\mathbf{N}$ is shape function vector of element used. A square 4-node element is used for solution of the steady flow over the pipe section.
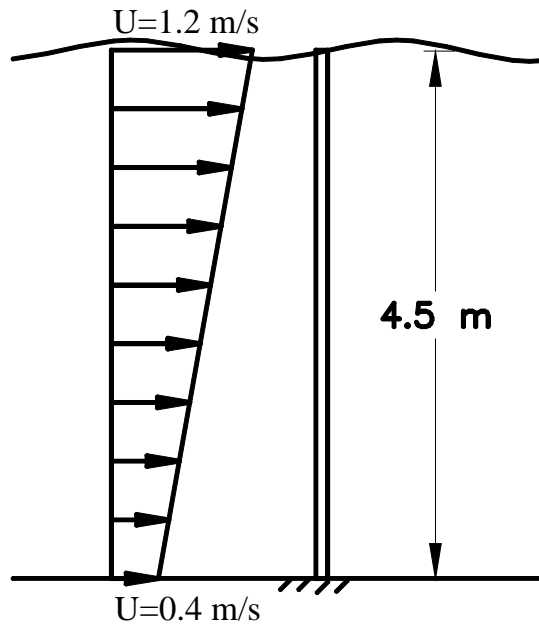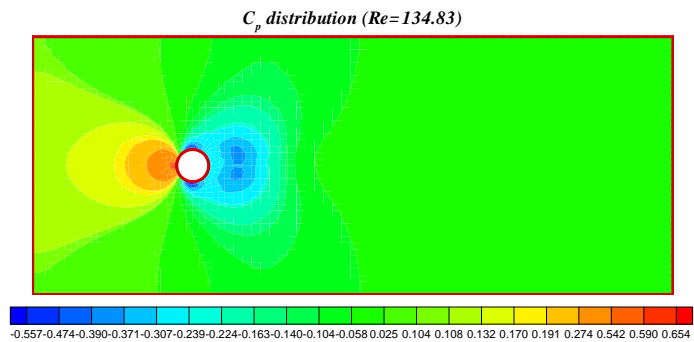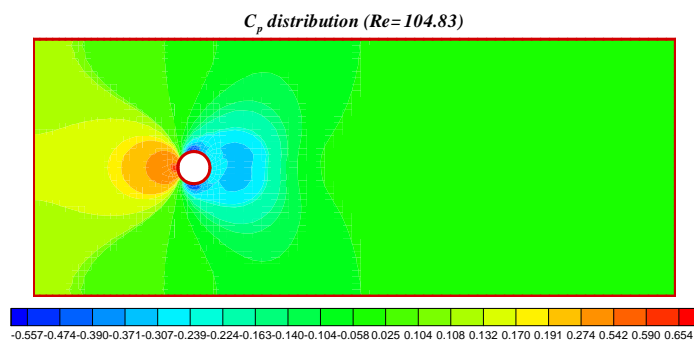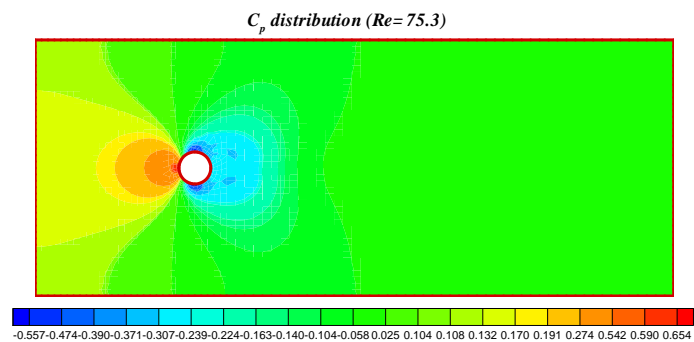
Figure 4.12: A pipe system subjected to steady state flow loading

In order to find the current loading on pipe structure the pressure coefficient (C_p) distribution has been found at four levels (Figures 4.13), and for other parts of pipe structure, a linear interpolation scheme has been used. The fluid mesh has been updated for each increment, and on starting new increment the fluid domain was re-meshed with reference to the new position of the riser and the data are interpolated from the last status. The nonlinear response of this typical pipe due to calculated current loading is illustrated in Figure 4.14.
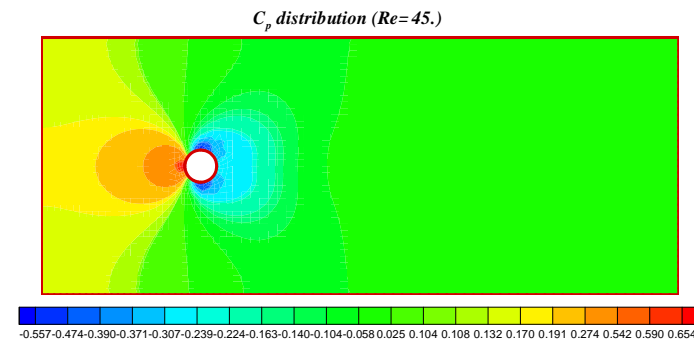
C_p distribution (Re=134.83)

-0.557-0.474-0.390-0.371-0.307-0.239-0.224-0.163-0.140-0.104-0.058 0.025 0.104 0.108 0.132 0.170 0.191 0.274 0.542 0.590 0.654

a: at top of pipe

C_p distribution (Re=104.83)

-0.557-0.474-0.390-0.371-0.307-0.239-0.224-0.163-0.140-0.104-0.058 0.025 0.104 0.108 0.132 0.170 0.191 0.274 0.542 0.590 0.654

b: in depth 1.5 m

C_p distribution (Re=75.3)

-0.557-0.474-0.390-0.371-0.307-0.239-0.224-0.163-0.140-0.104-0.058 0.025 0.104 0.108 0.132 0.170 0.191 0.274 0.542 0.590 0.654

c: in depth 3.0 m

C_p distribution (Re=45.)

-0.557-0.474-0.390-0.371-0.307-0.239-0.224-0.163-0.140-0.104-0.058 0.025 0.104 0.108 0.132 0.170 0.191 0.274 0.542 0.590 0.654

d: at bottom of pipe

Figure 4.13: The pressure coefficient (C_p) distribution at different levels

74
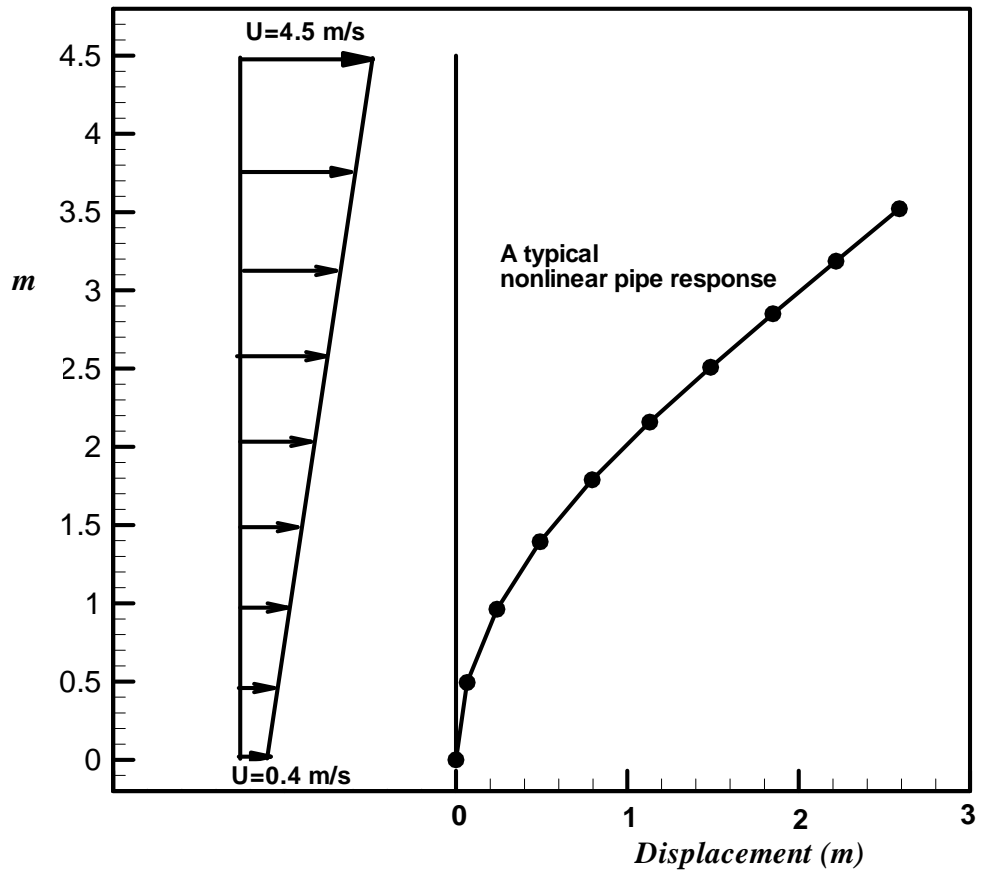
Figure 4.14: The nonlinear response of typical pipe subjected to current loading

Chapter 5

Development of a Generalized Nonlinear Finite Element Formulation to Analysis Unbounded Multilayer Flexible Riser Using a Constitutive Model

5.1 Introduction

A common approach for numerical analysis of riser structures is to use an equivalent modeling scheme to simulate the existence of various layers which make up the structure of a flexible riser. This approach fails to account for the interaction between layers, the hysteresis effects due to occurrence of inter-layer slip-stick and also the nonlinear behaviors due to friction between the unbounded layers.

Recently Bahtui et. Al. [6] presented a constitutive model for flexible riser structures. They developed this constitutive model using the response of a limited length riser to bending

moment and average internal and external pressures. An ABAQUS detailed model has been used to study the response of the limited length riser.

5.2 Geometry of the riser

Flexible risers consist of different layers (Figure 5.1), each one designed for a specific task. Main components are the helical armour layers and a set of sealing and/or anti- wear
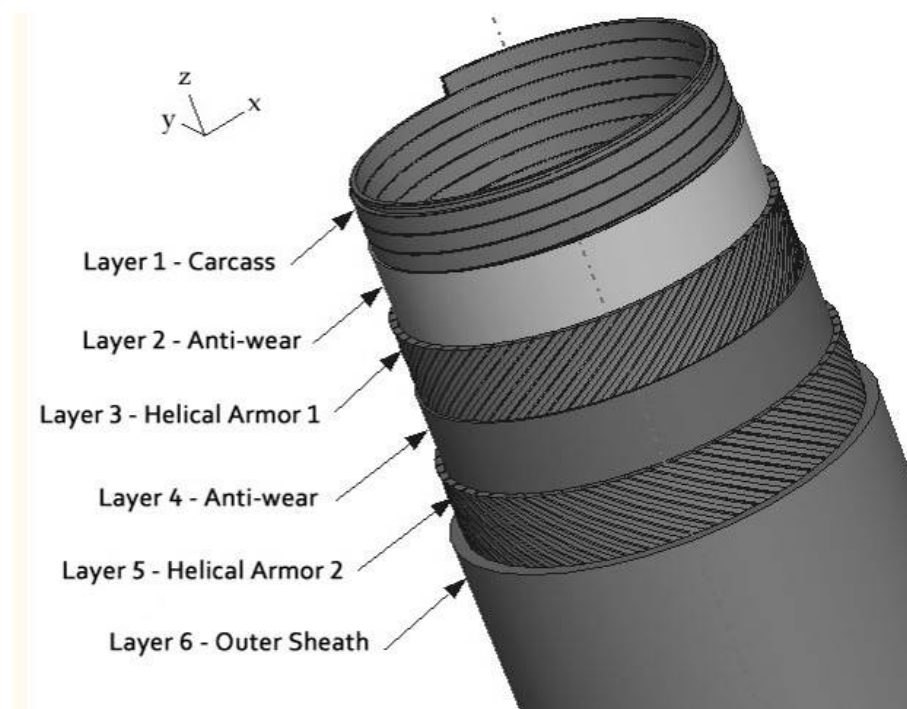

Figure 5.1: Schematic of a typical six-layer unbounded flexible riser [67]

polymer layers, while additional components which are typically present include a metallic internal 'carcass' and a pressure armour layer. The geometry of an actual flexible pipe was chosen from manufacturer as shown in Table 5.1.

Table 5.1: Flexible pipe geometrical data [67].

Layer	Type	r_i (mm)	r_o (mm)	r (mm)	t (mm)	α (degrees)
1	Carcass	85.54	90.54	88.04	5	88.44
2	Anti-wear Layer	90.76	97.46	94.11	6.7	90
3	Helical Armour 1	99.43	103.42	101.43	3.99	36.54
4	Anti-wear Layer	103.55	104.95	104.25	1.4	90
5	Helical Armour 2	105.17	109.17	107.17	4	-35.59
6	Outer Sheath	109.4	116.3	112.85	6.9	90

Definitions:

Type   - Layer description

r_i/ r_o - Radius to layer inner/ outer surface

r   - Layer mean radius

t   - Layer thickness

All layers except the carcass layer were assumed to have isotropic type of properties. The material data for the riser analysis is listed in Table 5.2. Modelling a three-dimensional carcass layer in very detail leads to excessive computational solution time. The carcass layer is thus replaced by an equivalent material and geometrically orthotropic layer.

The material property of the equivalent orthotropic layer was derived by comparing results from the actual carcass layer and results from the embedded orthotropic sheath layer. The orthotropic material properties are then evaluated using structural stability relations.

Table 5.2: Material data for the riser [67].

Layer	Type	E (N/mm^2)	v	σ_y (N/mm^2)	ρ (kg/m^3)
1	Carcass	$E_1 = 1.50E+5$ $E_2 = 1.24E+4$	0.3	250	7860
2	Anti-wear Layer	3.50E+2	0.4	21	1030
3	Helical Armour 1	2.10E+5	0.3	740	7860
4	Anti-wear Layer	3.50E+2	0.4	21	1030
5	Helical Armour 2	2.10E+5	0.3	740	7860
6	Outer Sheath	3.50E+2	0.4	21	1030

A detailed three-dimensional finite element model is then developed under a global cylindrical coordinate system with its origin located at the centre of riser bottom end. Layers were modeled individually and then assembled together [67, 68]. Three-dimensional contact interaction is also introduced between all layers, so that the layers are allowed to slide with respect to each other during all stages of loading. The load cases considered are tension, torsion, and bending. The analysis then is carried out as a geometrically non-linear problem. This nonlinearity occurs due to the presence of contact surfaces as well as large rigid body displacement taking place in the tendons of the helical armour layer. Abaqus results show the hysteresis effect in the unbounded type of flexible riser which exists in all load cases, but are particularly significant in the bending case, as shown in Figure 5.2, where the loading and unloading paths are well distinct.

The results from various solutions are subsequently used to develop a constitutive model for multilayer flexible riser structures.
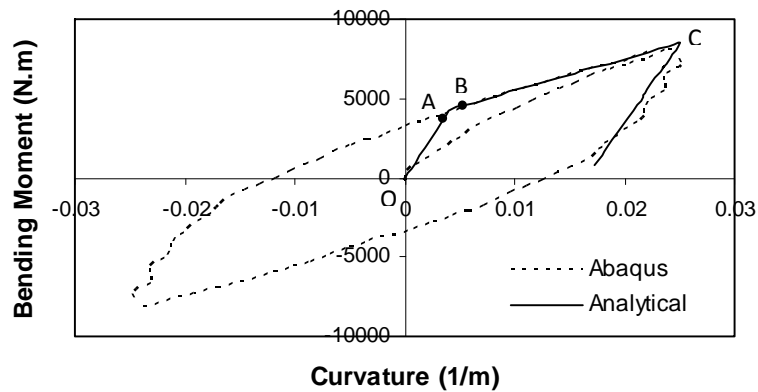
Figure 5.2: Bending moment vs. curvature [67]

5.3 Constitutive model for multilayer flexible riser

Using the finite element details model results, Bahtui et. al. [6] proposed a model which gives a relationship between generalized stress and strain components as follow

$$
\begin{bmatrix} N \\ M_x \\ M_y \\ P_u \\ P_\varepsilon \end{bmatrix} = \begin{bmatrix} D_{11} & 0 & 0 & D_{41} & D_{51} \\ & D_{22} & 0 & 0 & 0 \\ & & D_{22} & 0 & 0 \\ & sym. & & D_{44} & D_{54} \\ & & & & D_{55} \end{bmatrix} \begin{bmatrix} \varepsilon_z \\ \chi_x \\ \chi_y \\ u_r \\ \varepsilon_r \end{bmatrix}
\tag{5.1}
$$

In this model N, M_t, M_x, M_y, P_u and P_ε are the generalized stresses. The corresponding work-conjugated generalized strains are $\varepsilon_z, \phi, \chi_x, \chi_y, u_r, \varepsilon_r$, where $\varepsilon_z, \chi_x, \chi_y$ and ϕ are the axial strain, the curvatures about the x and y directions and the torsional curvature. The detailed definition of the model is given in [6]. A compact notation is conveniently introduced denoting by $\underline{\sigma}$ and $\underline{\varepsilon}$ the generalized stresses and strains:

$$
\underline{\sigma} = \begin{bmatrix} N \\ M_t \\ M_x \\ M_y \\ P_u \\ P_\varepsilon \end{bmatrix} \qquad \underline{\varepsilon} = \begin{bmatrix} \varepsilon_z \\ \phi \\ \chi_x \\ \chi_y \\ u_r \\ \varepsilon_r \end{bmatrix}
\tag{5.2}
$$

Also components D_{ij} values are given in [6]. In order to use this model, we then need to develop a generalized nonlinear finite element formulation.

5.4 Generalized nonlinear finite element formulation

Next a generalized nonlinear finite element formulation is developed based on Euler-Bernoulli beams theory with two extra degree of freedoms in riser radial and thickness directions to fulfil all the required flexible riser degrees of freedom [6]. This finite element formulation is also suitable to take the transitional constitutive model into the account for analysing flexible riser structures. Referring to Figure 5.3, displacement components u_i, v_i and w_i for node i are defined as

$$u_i = u_{0i}(x) - z \frac{\partial w_{0i}(x)}{\partial x} + y \frac{\partial u_{0i}(x)}{\partial x} \tag{5.3}$$

$$v_i = v_{0i}(x) \tag{5.4}$$

$$w_i = w_{0i}(x) \tag{5.5}$$
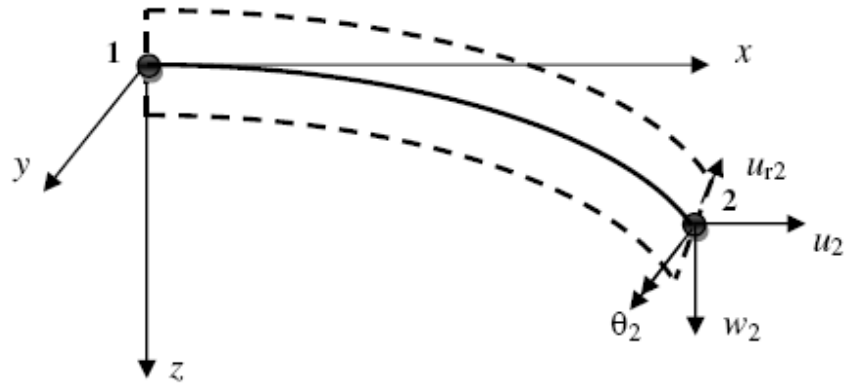
Figure 5.3: Euler-Bernoulli Beam Element with one extra degree of freedom to model riser radial displacement

where $i=1,2$ indicates the node numbers, $u_{0i}(x)$, $v_{0i}(x)$ and $w_{0i}(x)$ are the displacement of the centre-line in x, y and z directions, respectively. Also $\partial w_{0i}(x)/\partial x$ and $\partial u_{0i}(x)/\partial x$ are rotation component about y and z axis for node i. Using relations (5.3)-(5.5) the nonlinear strain–displacement relations, based on the von Karman's assumption, are

$$\varepsilon_{xx} = \frac{\partial u_0}{\partial x} + \frac{1}{2}\left(\frac{\partial w_0}{\partial x} + \frac{\partial v_0}{\partial x}\right)^2 - z\frac{\partial^2 w_0}{\partial x^2} + y\frac{\partial^2 v_0}{\partial x^2} \tag{5.6}$$

$$\varepsilon_{yy} = 0 \tag{5.7}$$

$$\varepsilon_{xy} = 0 \tag{5.8}$$

Also, referring to the cross-sectional view of the riser in Figure 5.4, the average radial strain ε_r is given by

$$\varepsilon_r = -\frac{t - t_{in}}{t_{in}} \tag{5.9}$$

where t_{in} and t denote the initial and the current thickness of the whole riser, respectively. The radial displacement of the average radius, the radial displacement of the internal layer and the radial displacement of the external layer, indicated with u_r, u_{int} and u_{ext}, respectively, are related to the radial strain and to the current thickness as follows:

$$u_{\text{int}} = u_r + \varepsilon_r\frac{t}{2}$$
$$\tag{5.10}$$
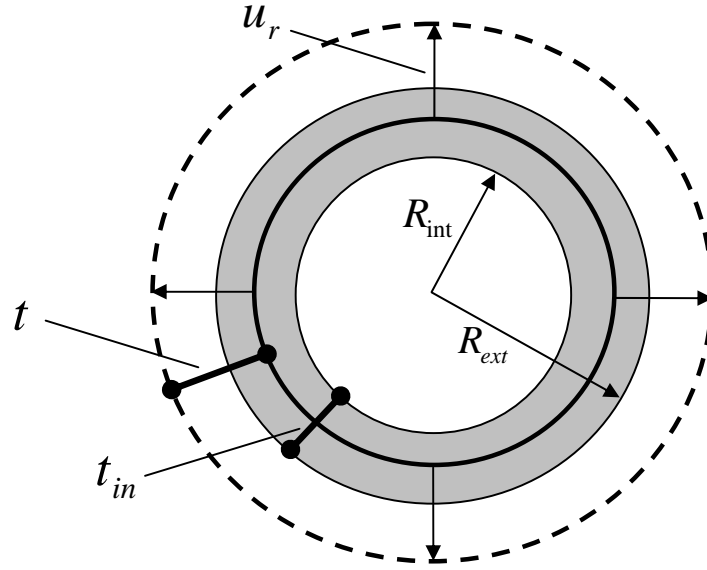$$u_{ext} = u_r - \varepsilon_r\frac{t}{2}$$

Figure 5.4: Cross view of the riser section [6]

To develop a nonlinear finite element model for this Euler-Bernoulli beam element we interpolate the displacement values as well as generalized strain components u_r and ε_r in the element field using their nodal values as follows

$$u = N_1 u_1 + N_2 u_2 \tag{5.11}$$

$$v = N_3 v_1 + N_4 v_2 + N_5 \theta_1 + N_6 \theta_2 \tag{5.12}$$

$$w = N_3 w_1 + N_4 w_2 + N_5 \theta_1 + N_6 \theta_2 \tag{5.13}$$

$$u_r = N_1 u_{r1} + N_2 u_{r2} \tag{5.14}$$

$$\varepsilon_r = N_1 \varepsilon_{r1} + N_2 \varepsilon_{r2} \tag{5.15}$$

where u_1 and u_2 are the axial nodal displacements, w_1 and w_2 are transitional displacements, θ_1 and θ_2 are nodal rotational components. Also in Equations (5.11)-(5.15), N_1 and N_2 are linear shape functions however N_3-N_6 are cubic shape function (Figure 5.5).

Here to develop governing nonlinear finite element formulation for Euler-Bernoulli beam we need to define bending curvature components, as follows

$$\chi_x = \frac{\dfrac{\partial^2 w}{\partial x^2}}{\left[1+\left(\dfrac{\partial w}{\partial x}\right)^2\right]^{3/2}} \tag{5.16}$$
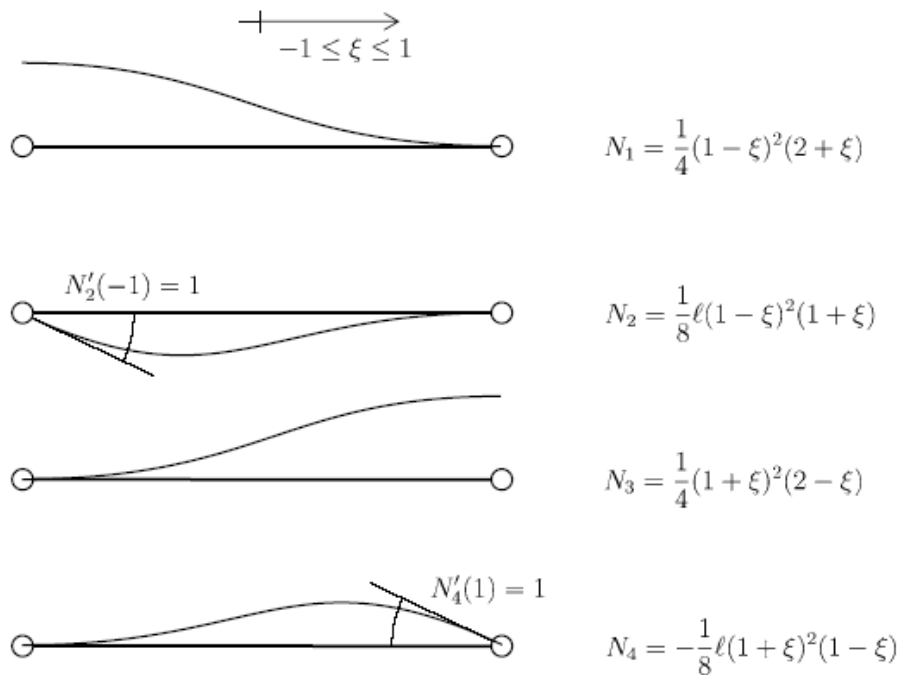
Figure 5.5: Cubic shape function

For this nonlinear problem, the governing equation in rectangular Cartesian coordinates is derived using the principle of minimum total potential energy, i.e.

$$W_i^{(e)} = \int_{x_a}^{x_b} \underline{\sigma}_g \bullet \underline{\varepsilon}_g^* dx = \mathbf{F}_{ext} \bullet \tilde{\mathbf{q}}^*$$

$$\underline{\varepsilon}_g^* = \mathbf{B}_{NL} \tilde{\mathbf{q}}^* \tag{5.17}$$

$$\underline{\sigma}_g = f\left(\underline{\varepsilon}_g\right)$$

where $\underline{\sigma}$ and $\underline{\varepsilon}$ are given in (5.2).Using (5.17) the incremental finite element equation of equilibrium can be written as:

$$\mathbf{R}(\mathbf{q}) = \mathbf{F}_{int}(\mathbf{q}) - \mathbf{F}_{ext} = 0 \tag{5.18}$$

where $\mathbf{q} = \left(u_1 \ w_1 \ \theta_1 \ u_{r1} \ u_2 \ w_2 \ \theta_2 \ u_{r2}\right)^T$. Implementing Newton-Raphson method to solve the Equation (18) leads to

$$\mathbf{q}_{n+1}^{k+1} = \mathbf{q}_{n+1}^k + \mathbf{k}_{tNL}^{-1}(\mathbf{q}_{n+1}^k)\left(\mathbf{F}_{ext}^{n+1} - \mathbf{F}_{int}(\mathbf{q}_{n+1}^k)\right) \tag{5.19}$$

where

$$\mathbf{k}_{tNL}(\mathbf{q}_{n+1}^k) = \int_V \mathbf{B}_{NL}^T \left.\frac{d\hat{\sigma}}{d\hat{\varepsilon}}\right|_{\hat{\varepsilon} = \mathbf{B}_{NL}\mathbf{q}_{n+1}^k} \mathbf{B}_{NL} \det \mathbf{J} \, dV \tag{5.20}$$

where

$$\mathbf{B}_{tNL}^{k+1}(\mathbf{q}_{n+1}^k) = \begin{bmatrix} \dfrac{2}{l} N_1' & k_{12} & \dfrac{2}{l^2} N_5'^2 \theta_{1_{n+1}}^k & 0 & \dfrac{2}{l} N_2' & k_{16} & k_{17} & 0 \\[2mm] 0 & N_3'' / \tau_{n+1}^k & N_5'' / \tau_{n+1}^k & 0 & 0 & N_4'' / \tau_{n+1}^k & N_6'' / \tau_{n+1}^k & 0 \\[2mm] 0 & 0 & 0 & \dfrac{l}{2} N_1' & 0 & 0 & 0 & \dfrac{l}{2} N_2' \end{bmatrix}$$

$$(5.21)$$

$$k_{12} = \frac{2N_3'}{l^2}(N_3' w_{1_{n+1}}^k + 2N_4' w_{2_{n+1}}^k + 2N_5' \theta_{1_{n+1}}^k + N_6' \theta_{2_{n+1}}^k) \qquad (5.22)$$

$$k_{16} = \frac{2N_4'}{l^2}(N_4' w_{2_{n+1}}^k + 2N_5' \theta_{1_{n+1}}^k + 2N_6' \theta_{2_{n+1}}^k) \qquad (5.23)$$

$$k_{17} = \frac{2N_6'}{l^2}(N_6' \theta_{2_{n+1}}^k + 2N_5' \theta_{1_{n+1}}^k) \qquad (5.24)$$

$$\tau_{n+1}^k = \left(1 + \left(N_3' w_{1_{n+1}}^k + N_4' w_{2_{n+1}}^k + N_5' \theta_{1_{n+1}}^k + N_6' \theta_{2_{n+1}}^k\right)^2\right)^{3/2} \qquad (5.25)$$

The derivation of the consistent tangent operator $\left. \dfrac{d\hat{\sigma}}{d\hat{\varepsilon}} \right|_{\hat{\varepsilon} = \mathbf{B}_{NL}\mathbf{q}_{n+1}^k}$ is given in [6].

87

5.5 Application to a cantilever riser subjected to an end bending moment

Consider a cantilever flexible riser with length 500 m which is subjected to an end bending moment (*1500 N.m*). Figure 5.6 depicts the result for this flexible riser for three different condition: Linear solution with constant EI=608108, nonlinear solution with constant EI=608108 and nonlinear solution with the inclusion of the constitutive model with initial value EI=608108 (the first EI value which is taken from the constitutive model's output). From Figure 5.6 it is noted that the presented constitutive model [6] is capable of capturing the energy dissipation in flexible riser structure due to frictional slip between layers and the hysteretic response. According to [67], finite element analysis of a details model of a flexible riser using finite element software on a cluster of parallel processors took many hours to arrive at the solution. Using the developed constitutive model and a generalized finite element formulation, however, we are able to study the nonlinear behavior of a long length of flexible risers by getting the results in seconds. This example shows the capability and importance of the proposed constitutive model
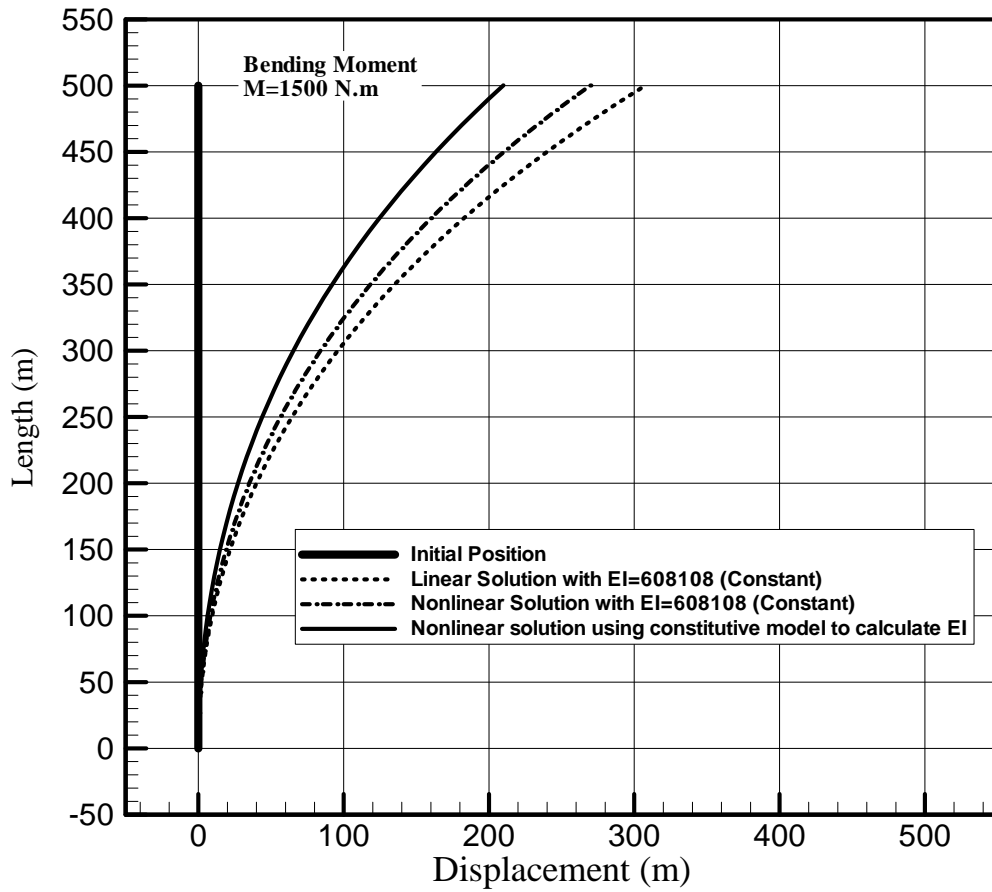
Figure 5.6: Cantilever riser subjected to an end bending moment

Chapter 6

Results Verification

6.1 Introduction

Based on the presented finite element formulation in previous chapters a finite element code has been developed. Using this code we study linear and nonlinear behavior of the riser structures subjected to various loading conditions. The results are verified by making comparisons to those available in the literature.

6.2 Curve pipe under end loading

A curved pipe structure subjected to a concentrated end load, F, as shown in Figure 6.1 is considered in this example. Mechanical properties and geometrical dimensions of this structure are shown in the figure. Figure 6.2 shows the results from linear solution of the structures those obtained from the proposed 3D annular section beam element and also from a 2D beam element of ABAQUS [69], where a good agreement is achieved.
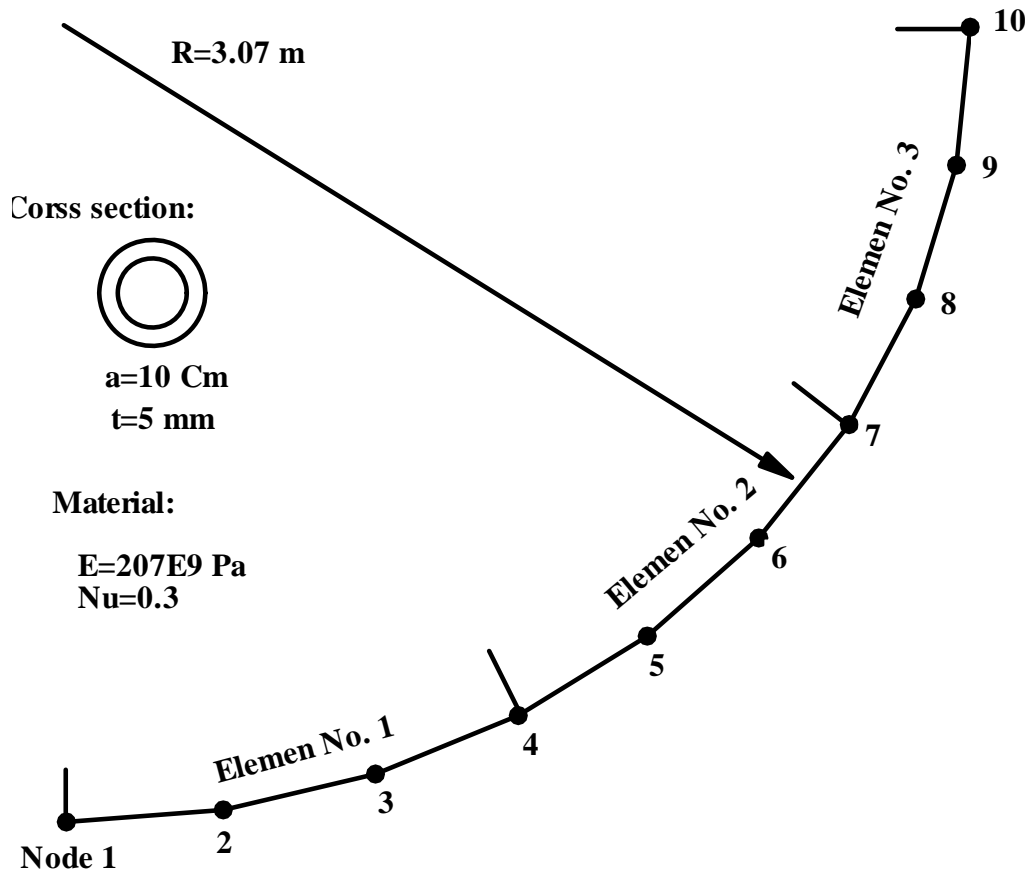
Figure 6.1: A curved pipe structure nodes, elements, geometry and material properties
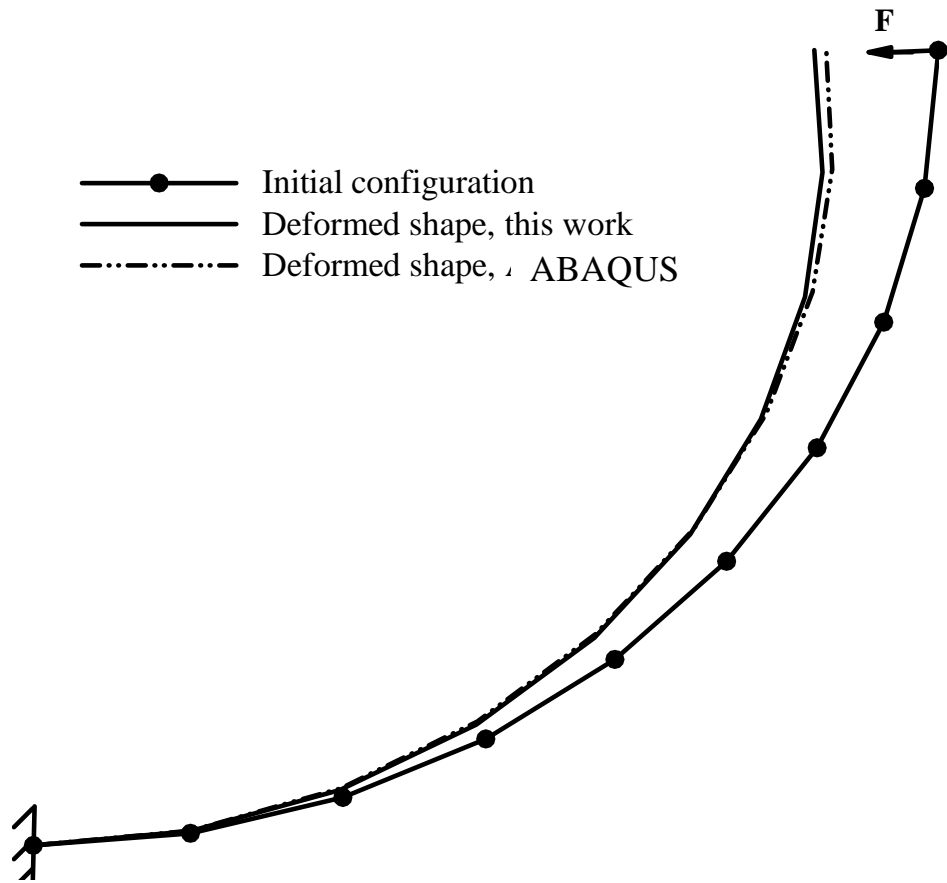
Figure 6.2: Configuration, initial and deformed

6.3 Large deformation analysis results

A cantilever pipe subjected to an end load with length 4.5 m is analyzed in this example. Results are depicted for load versus deflection in Figure 6.3. This figure shows the difference between linear and nonlinear solutions. In addition, the history of displacement during the incremental solution of the same cantilever pipe structure is shown in Figure 6.4. According to the results, there is a considerable difference between the results from the linear and nonlinear solutions in large deformation region. Also, it is noted that the proposed Algorithm gives convergence for nonlinear solution with less solution effort [15].

6.4 A cantilever beam loaded by a uniformly distributed displacement-dependent normal pressure

A cantilever beam which is loaded by a uniformly distributed displacement-dependent normal pressure P_l along its length (Figure 6.5) is considered. Therefore, as the beam deforms the load remains normal to the beam's centre-line. Figure 6.6 shows the horizontal and vertical displacements as well as the rotation at the central point of the free end versus non-dimensional load parameter $\beta = P_l l^3/(EI)$. Bathe et al. [70] used a standard linearization method which gave a limited range of deflections in vertical direction for low values of the load parameter β. Also, Argyris and Symeonidis [71] could not control the flutter problem after $\beta = 28$ when using their natural mode based theory. Using the presented finite element formulation with just three elements, we have managed to solve the same problem for up to $\beta = 52.6$. The history of the deformation of the beam is also shown in Figure 6.7.
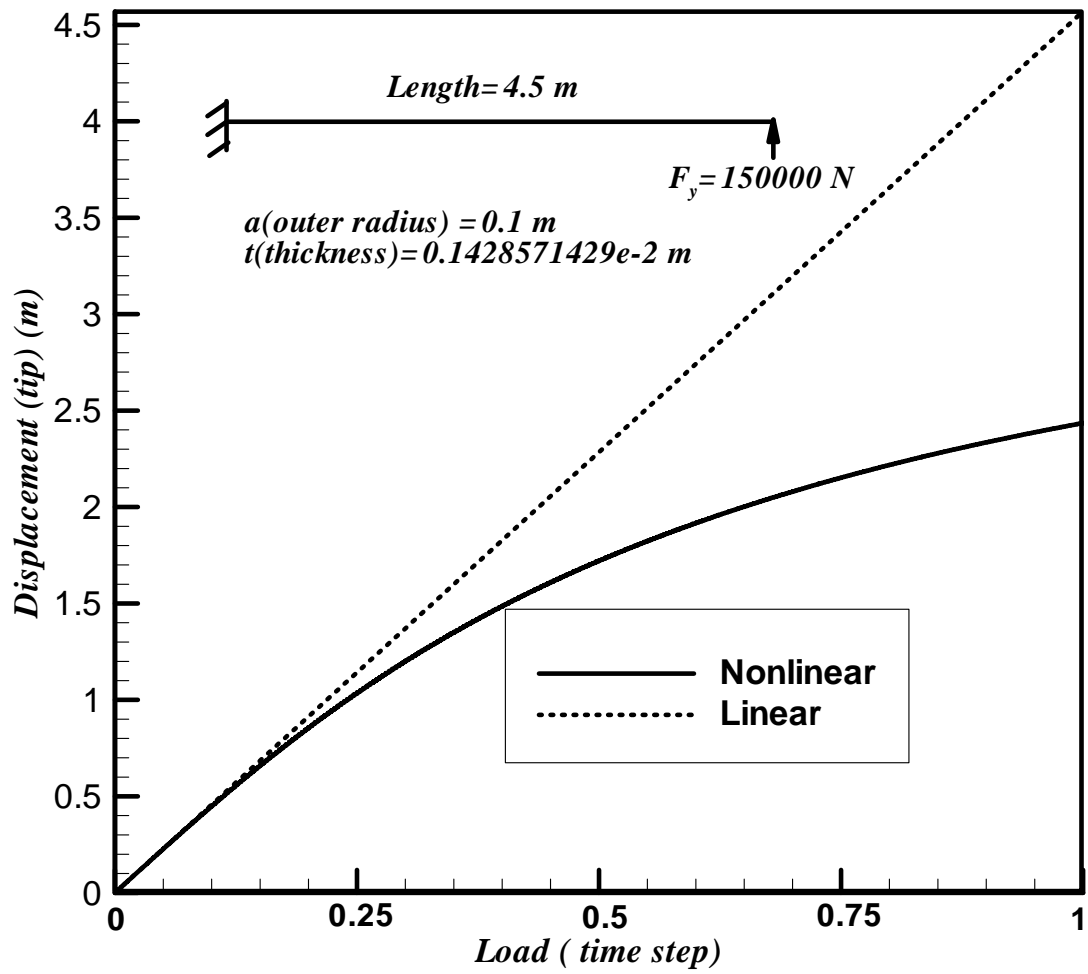
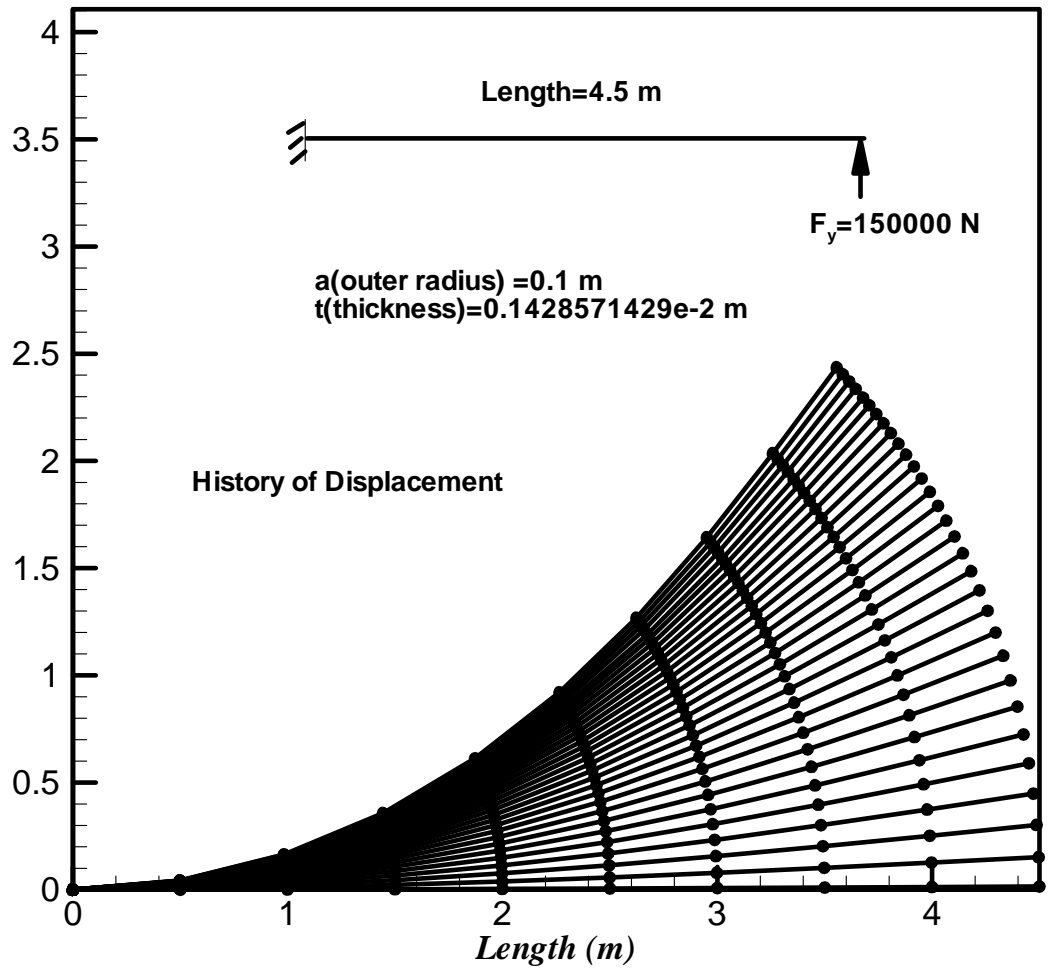Figure 6.3: Comparing the linear and nonlinear solution

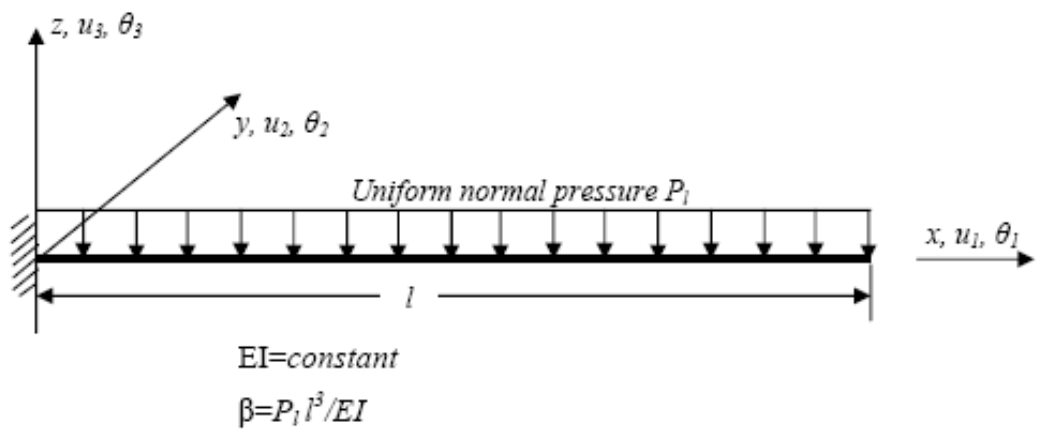Figure 6.4: History of displacement during incremental solution

Figure 6.5: Cantilever beam loaded by a uniformly distributed follower normal pressure P_l
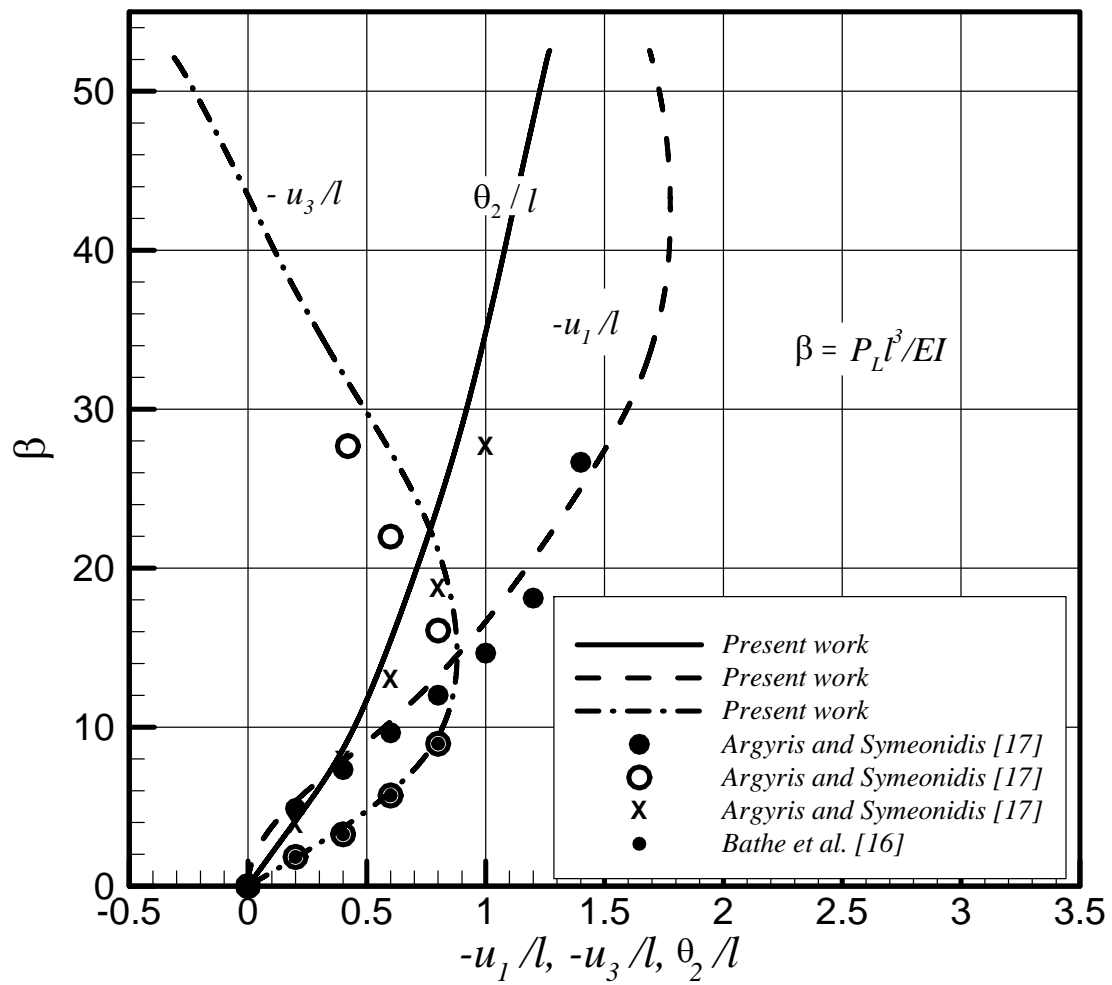
Figure 6.6: Large displacement and rotation at the free end of the cantilever beam
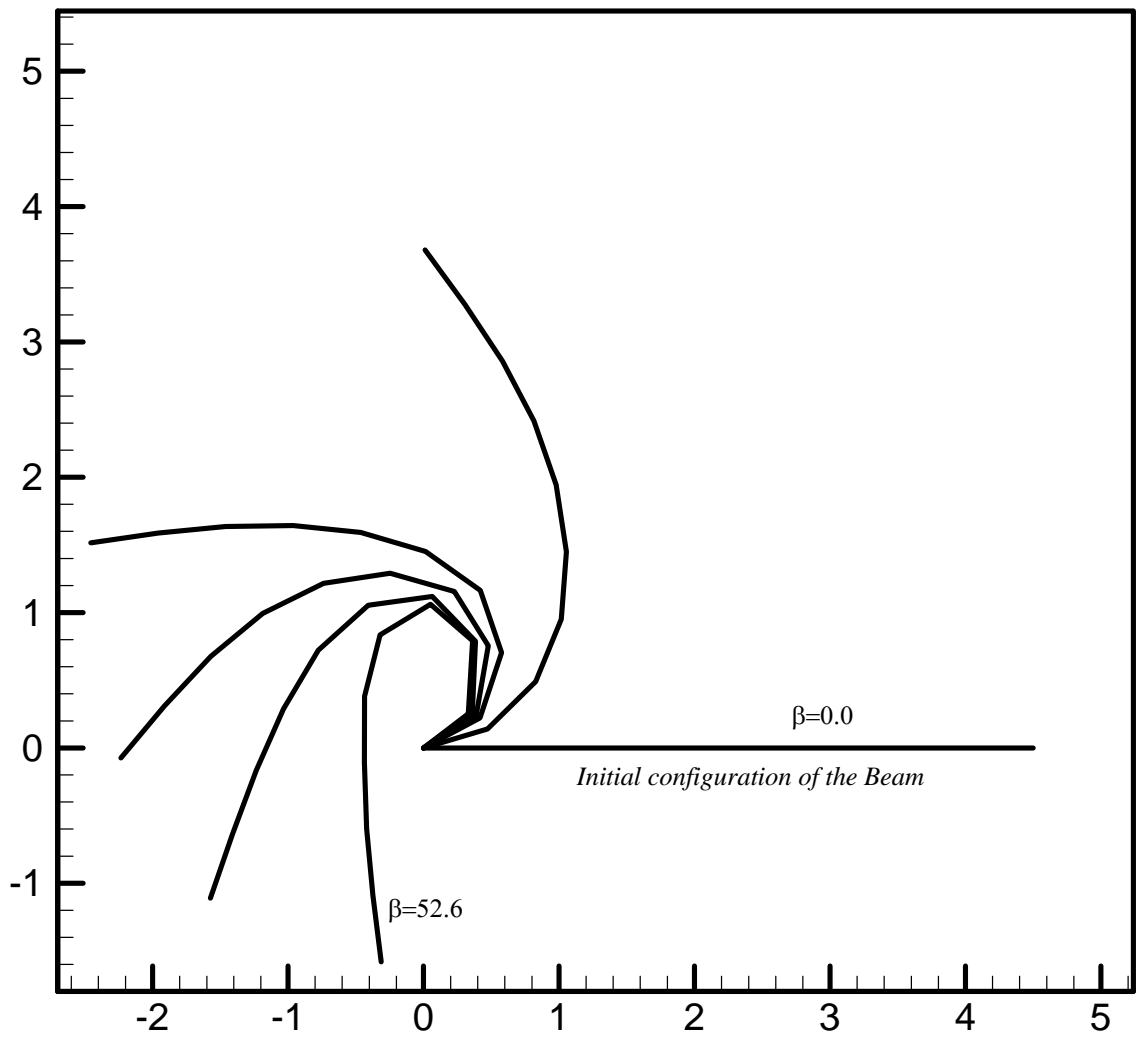
Figure 6.7: Deformed geometry of the beam mid-line

6.5 Flexible cantilever riser structure subjected to buoyancy force

Consider a flexible cantilever polyethylene riser structure with internal diameter $0.8\,m$, external diameter $0.85\,m$ and length $20.0\,m$. This structure is capped at both ends and is placed at $100.0\,m$ below the water surface. The riser is loaded with a vertical point load with value $510\ kN$ at the free end. The unit weight of the pipe and sea water are $\rho_{wp} = 12000\,N/m^3$ and $\rho_{ww} = 10250\,N/m^3$, respectively. Also, the pipe material properties used are: modulus of elasticity, $2.0\,GPa$ and Poisson's ratio 0.25. In the present work, the riser cross section is homogeneous and the slippage between layers is ignored.

Yazdchi and Crisfield [17] used a two dimensional model to analyze this problem. The purpose of the analysis is to find the final configuration of the beam under gravity combined with external and buoyancy loads. Figure 6.8 depicts the deformed configuration with and without consideration of buoyancy force. In this figure, the result from the presented formulation is compared with those given by [17]. As can be seen the two sets of predictions provide very close comparisons. Moreover, it is also observed that the maximum displacement values obtained from the present formulation are lower than those reported in literature. These differences may arise due the accuracy which is implied in the present finite element formulation during the linearization process. Also, from these results it is noted that buoyancy force has a significant effect on flexible riser behaviors. Figure 6.9 shows axial stress distribution at outer surface in the root of cantilever riser through the circumferential direction. According to this figure, the maximum axial stress value increases up to %65 when the buoyancy force has been considered. Figures 6.10 also illustrate the axial stress distribution contour in a cross section at the root of cantilever riser. From these results it is noted that buoyancy force has a significant effect on flexible riser behaviors. Also figures 6.9 and 6.10 demonstrate the capabilities of the present formulated element which gives the stress distribution around the pipe circumferences at each particular point in the riser.
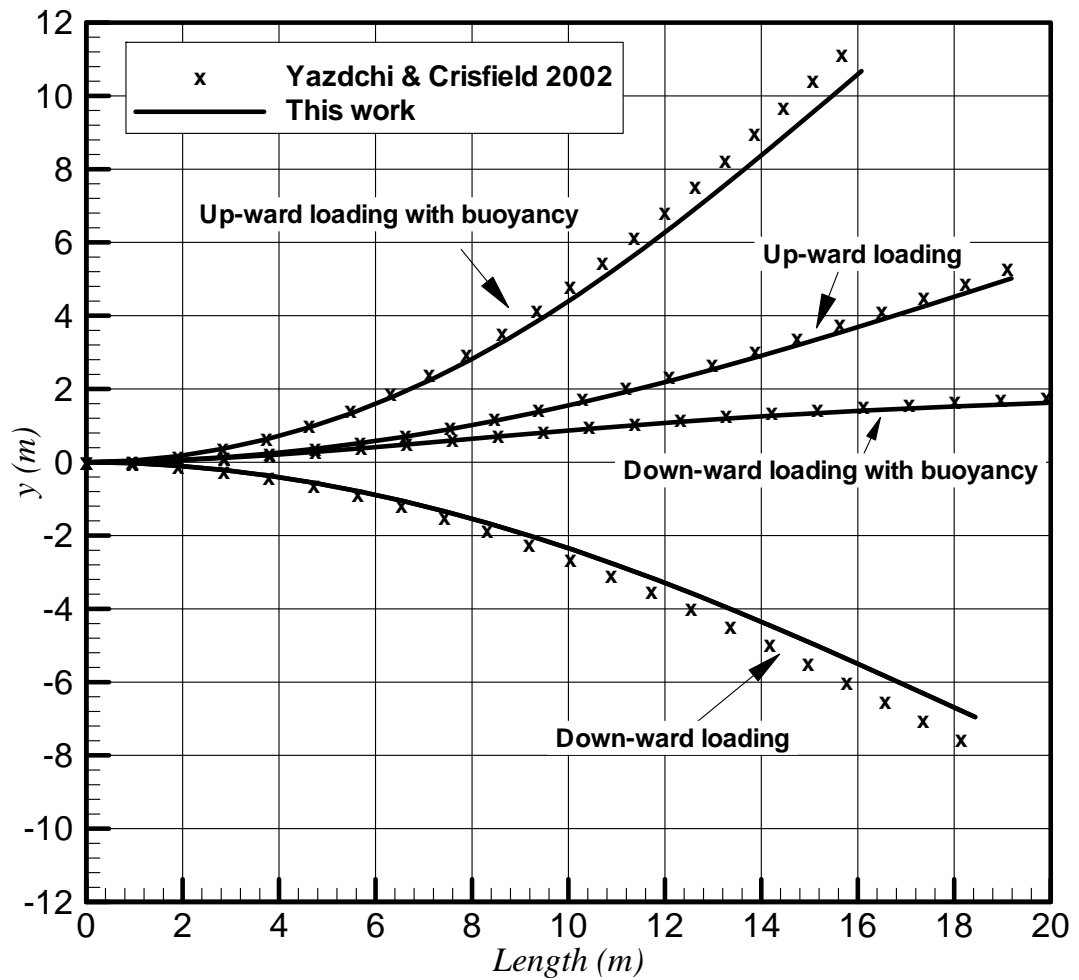
Figure 6.8: Deformed configuration of the flexible cantilever polyethylene pipe with and without considering buoyancy force
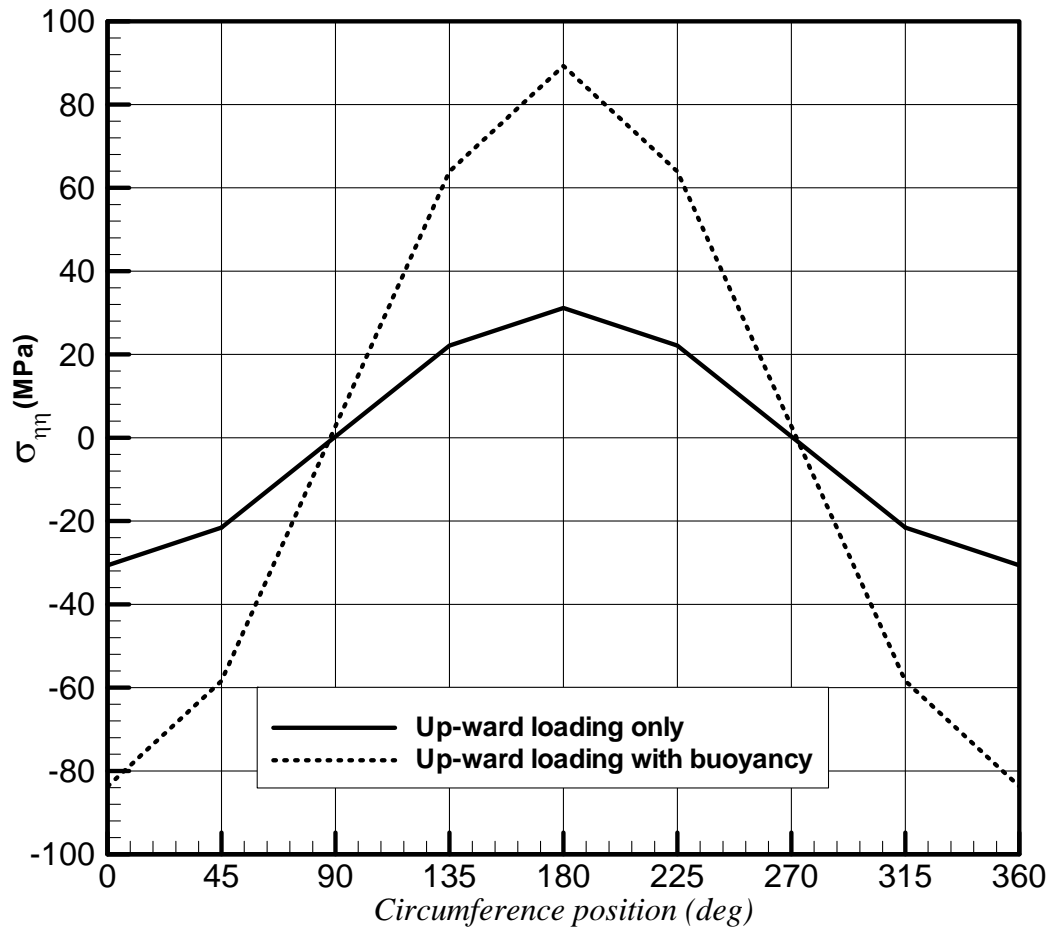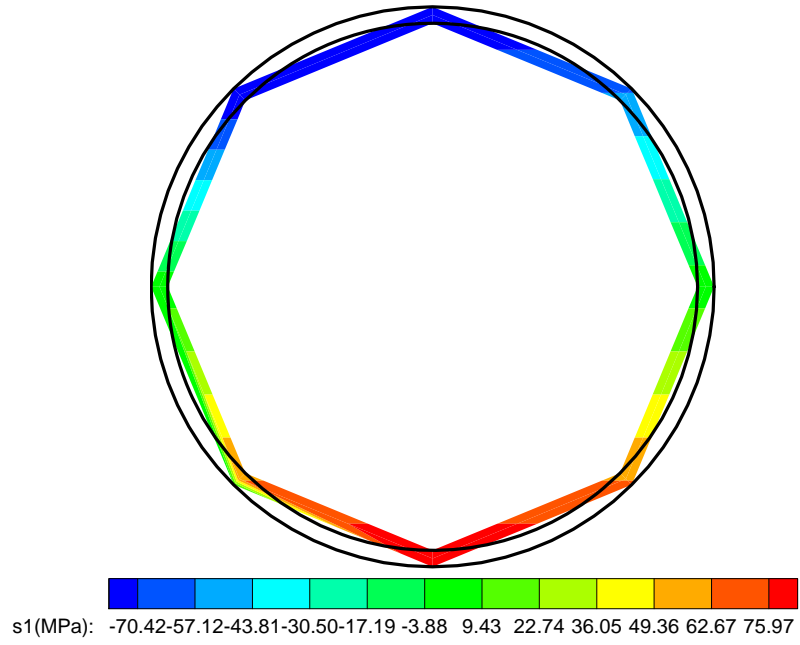
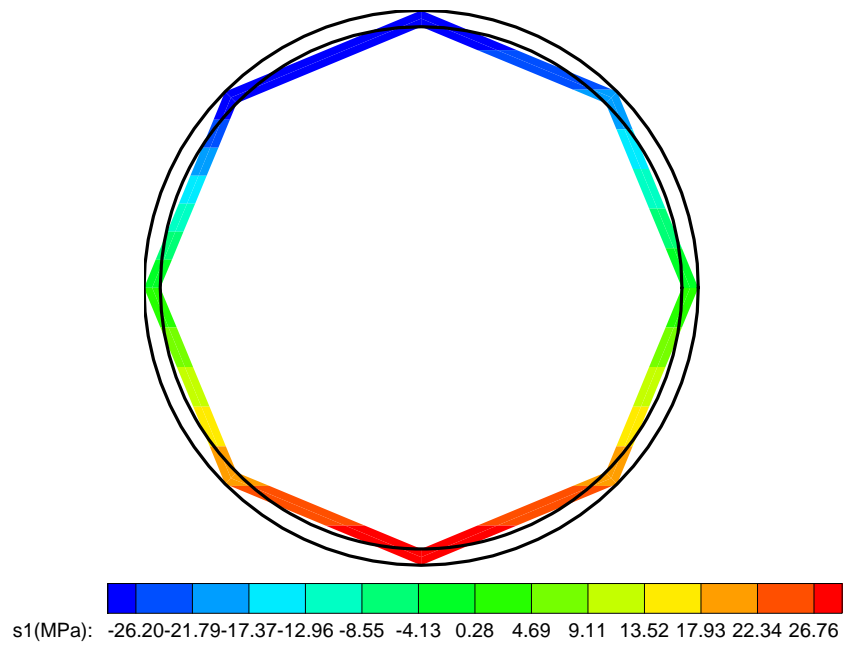Figure 6.9: Axial stress distribution at the root of cantilever riser in circumferential direction at the outer surface

s1(MPa): -70.42 -57.12 -43.81 -30.50 -17.19 -3.88 9.43 22.74 36.05 49.36 62.67 75.97

(a)

s1(MPa): -26.20 -21.79 -17.37 -12.96 -8.55 -4.13 0.28 4.69 9.11 13.52 17.93 22.34 26.76

(b)

Figure 6.10: Axial stress distribution contour in a cross section at the root of cantilever riser (a) Up-ward loading only (b) Up-ward loading with buoyancy force

6.6 A vertical riser subjected to a riser top-tension and current loading

A 320.0 m length riser (Figure 6.11) with internal and external diameters 0.21 m and 0.25 m is considered. In this example the behavior of a riser top-tension, which is attached to a floating system, with top tension force 510.0 kN is evaluated. A modulus of elasticity 2.0 × 10^{11} N/m^2 and a Poisson's ratio of 0.25 is used for this riser. The water depth is taken as 300.0 m and the unit weight of pipe and sea water are 77000.0 N/m^3 and 10250.0 N/m^3, respectively. Also, for steady state current, the transverse and tangential drag coefficients are 1.0 and 0.01, respectively.

The riser is modeled with thirty elements equally spaced below the water level and four elements equally spaced above it. It is assumed that the riser is initially vertical with the bottom node being hinged and the top-tension force being applied to the top point vertically. Figure 6.12 presents the deformed configuration for two different magnitudes for the uniform current profile, namely 1.0 and 2.0m/s. Yazdchi and Crisfield [17] have used a two-dimensional finite element analysis of flexible risers to solve this problem. As can be observed in Figure 6.12, a very good agreement is obtained between the results in moderately large displacement region but in the very large displacement region, the two sets of results diverge due to the accuracy which is implied in the present finite element formulation during the linearization process.
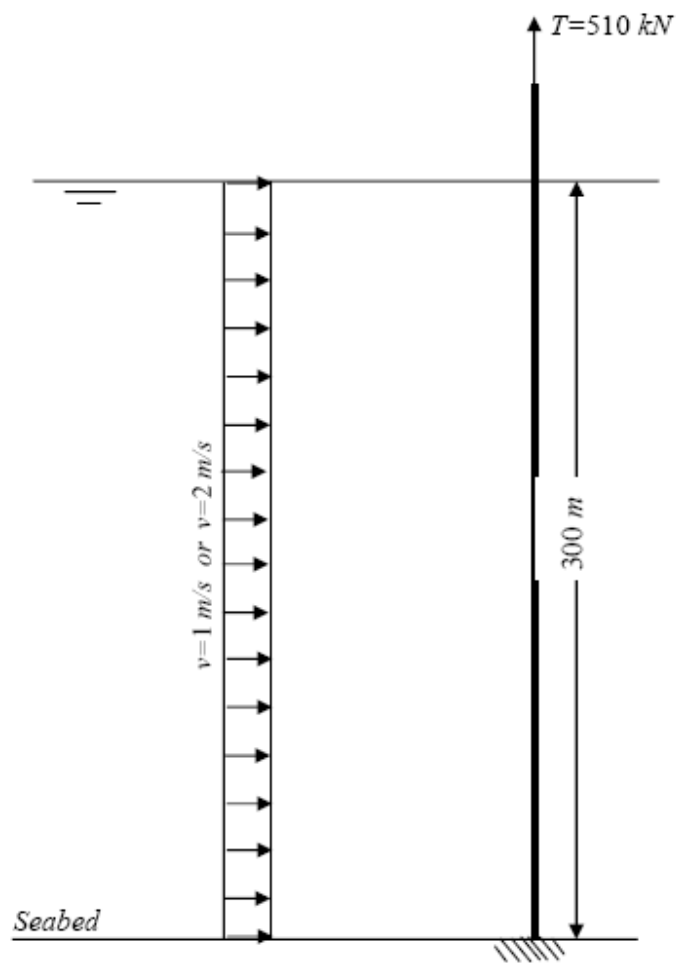
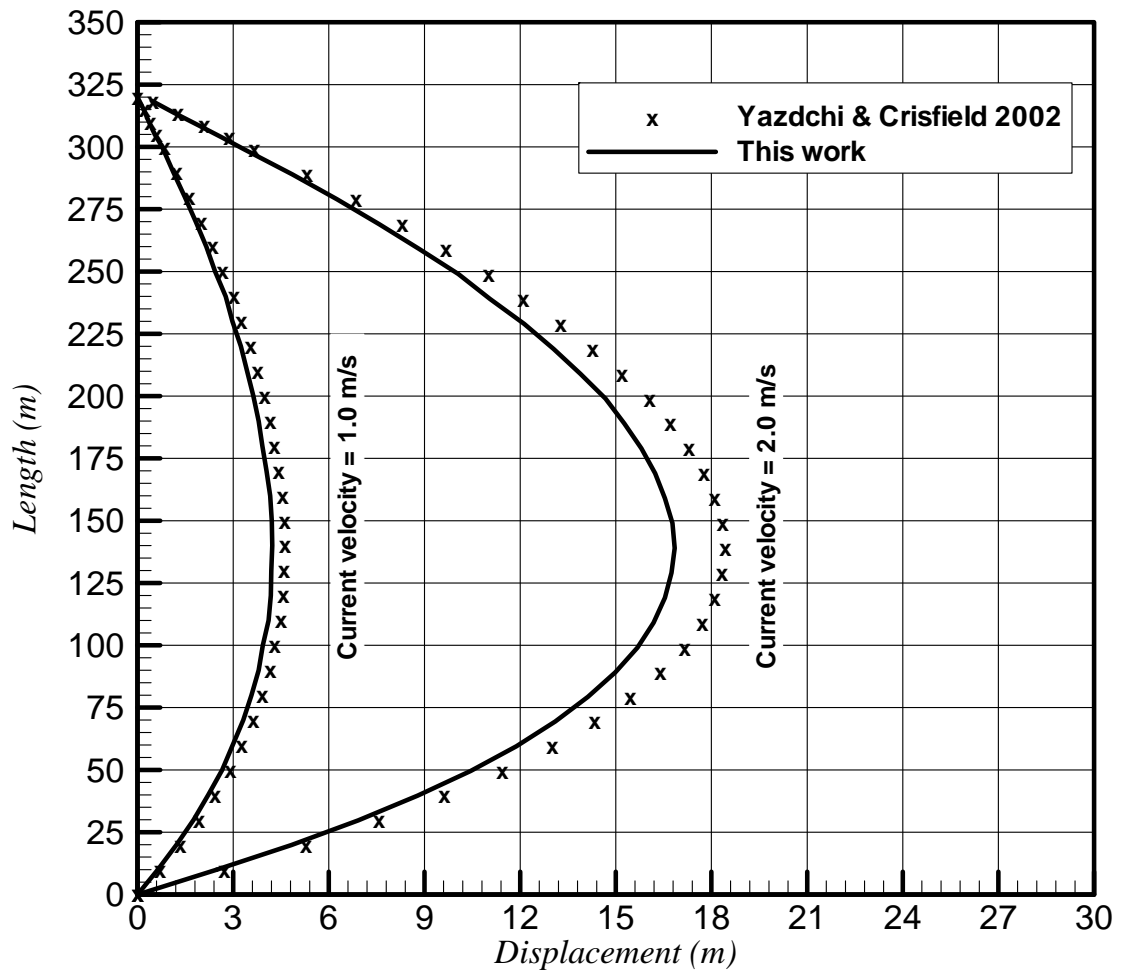Figure 6.11: a vertical riser which is attached to the floating system (top tensioned)

Figure 6.12: Deformed configuration of riser considering two different magnitudes for the uniform current profile, namely 1.0 and 2.0m/s

6.7 Riser subjected seabed boundary condition

In order to study the effects of using pipe-soil interaction model to identify seabed boundary condition on flexible riser behavior, in this example the same polyethylene pipe example 4 is considered to be laid down at the seabed. The calculated initial penetration depth for this riser on the seabed with a given material properties is 0.28 m (Figure 6.13). For this example an onsoy clay seabed with undrained shear strength $S_u = 50 \times 10^3 \, kPa$, $F_C = 10^3 \, N$ and $c_V = 0.7 \, m^2 / year$ is considered. Also the pull-out velocity assumes $V_p = 0.05 \, m/s$. Figure 6.14 represents deformed configuration of the flexible cantilever polyethylene pipe with and without the seabed boundary condition. From these results it is concluded that including a suitable model for the pipe-soil interaction obtains a more realistic and accurate results for deep water flexible riser structures.

6.8 Flexible riser subjected to a horizontally boundary movement

For this example a horizontal flexible riser structure with simply supported boundary condition at both ends is considered. This riser has an initial length of L=142.5 m, first configuration span l=130 m, cross sectional area $A^0 = 8 \times 10^{-3}$ m^2, moment of inertia $J^0 = 5.1 \times 10^{-6}$ m^4 and modulus of elasticity E=100 GPa.

A static analysis is conducted to move the right end boundary of this riser structure horizontally to the left by 105 m. Figure 6.15 shows the configurations of this riser structure at three different stages of the boundary movement. Lacarbonara and Pacitti [54] solved this problem using an exact analytical formulation with flexural stiffness effects. It can be seen in this figure that the results from the presented finite element formulation are in very good agreement with those from the exact analytical solution [54].
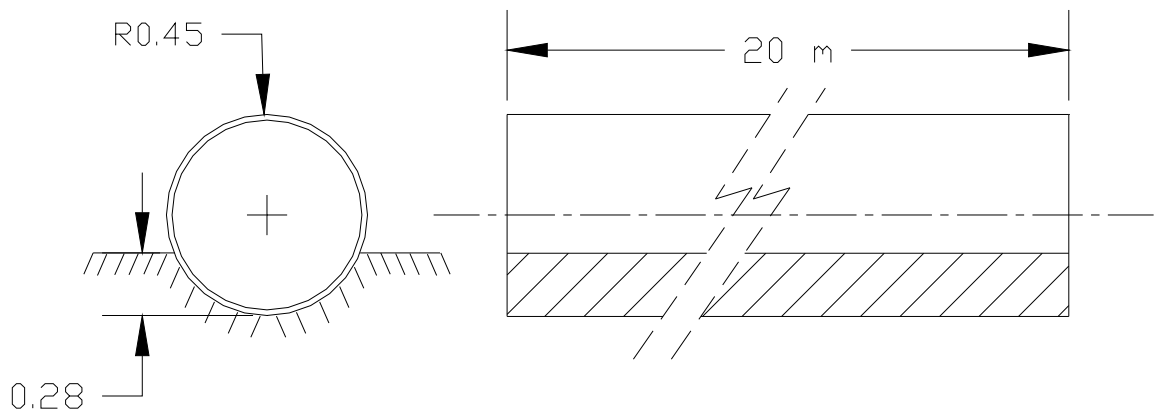
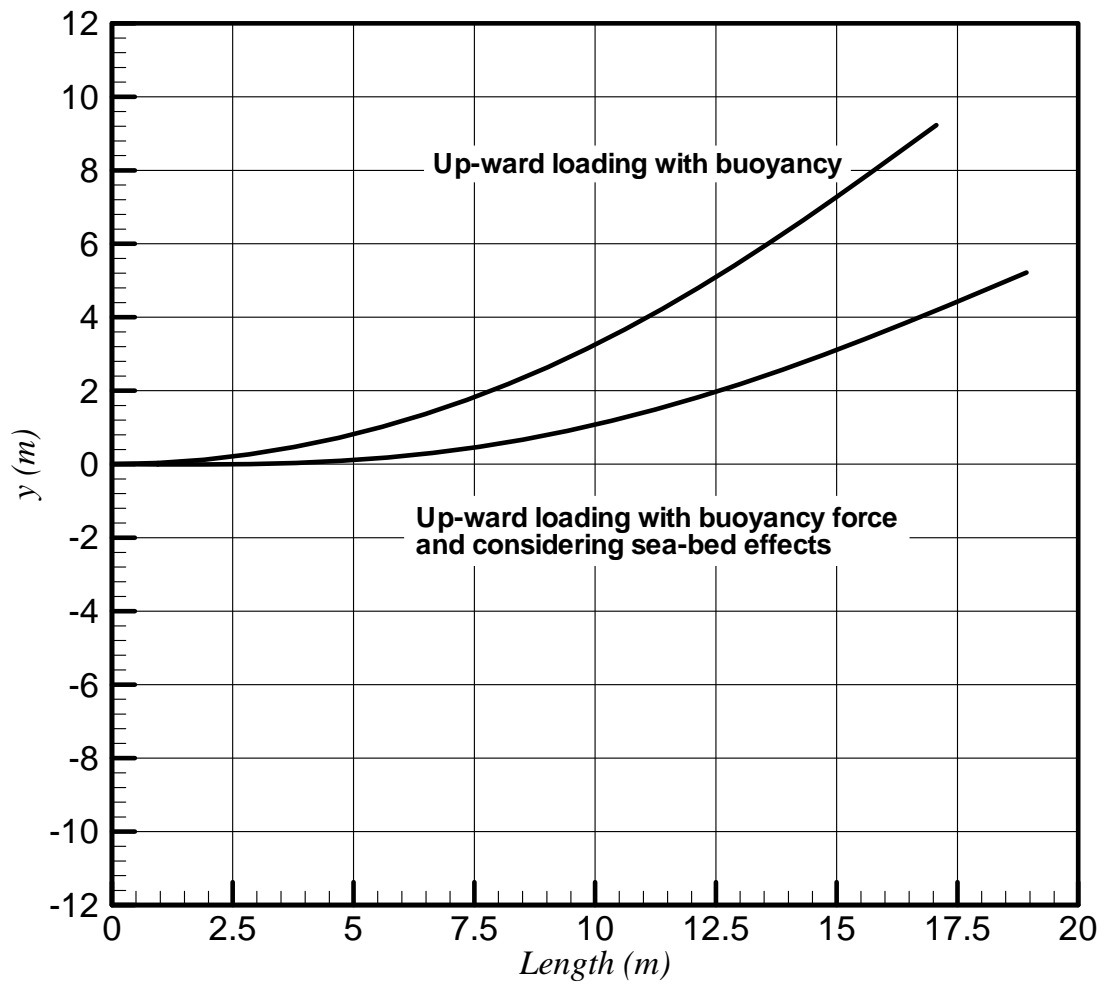Figure 6.13: The calculated initial penetration depth (0.28 *m*)

Figure 6.14: Deformed configuration of the flexible cantilever polyethylene pipe with and without including seabed boundary condition
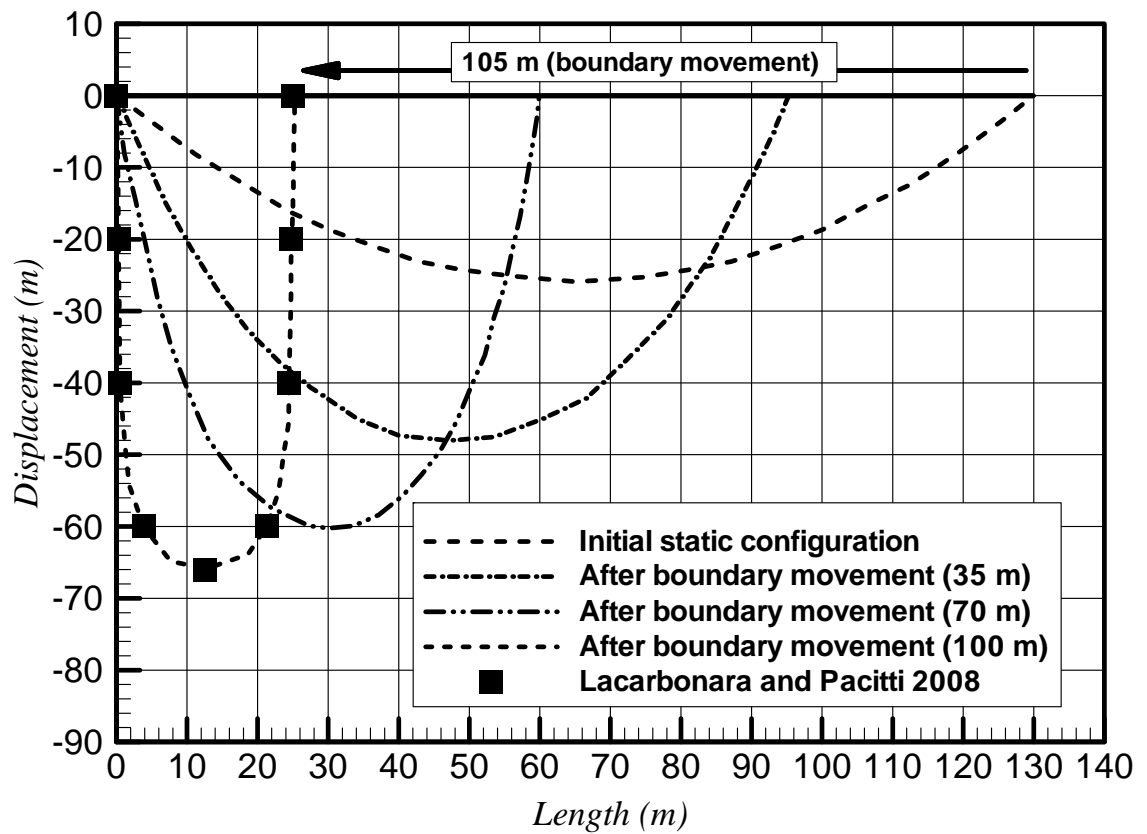
Figure 6.15: Deformed configuration of horizontal flexible riser

6.9 Flexible riser subjected to a periodically ship movement

For this example a flexible riser system with external diameter 0.26 *m*, internal diameter 0.2 *m* and bending stiffness 20.96 x 10^3 *N-m²* at 150 *m* water depth is analyzed (Figure 6.16). The upper point is to be connected to a surface floating vessel which is displaced 150 *m* horizontally and the other end is fixed to a sub-sea tower at a depth of 150 *m*. Both ends can rotate freely. The riser length is 350 *m*. The riser is divided into twenty elements. Details of element discretization can be found in reference [16]. It is assumed that the riser is filled with seawater. Mass density of seawater is 1025 *kg/m³* and mass per unit length of the riser is considered to be 57.5 *kg/m*. This particular riser system has already been analyzed by Yazdchi and Crisfield [16] using a 3D beam element. The transverse and tangential drag coefficients are 1.0 and 0.0, respectively. The loading condition includes a steady state current load together with buoyancy force effects.

A static analysis has initially been conducted to move the pipe from its horizontal configuration at a depth of 150 *m* to its final shape as shown in Figure 6.16 using both force and displacement controls, sequentially. The bending moment diagram of the flexible riser in its final configuration is plotted in Figure 6.17 which is shown to be consistent with that reported by Yazdchi and Crisfield [16]. Subsequently, the riser is analyzed dynamically for forces due to ship movement with amplitude of 2.01 *m* and a corresponding period of 14.0 *s*. The results of this analysis for the sub-sea connected node are shown in Figure 6.18. As ship movement imposes moderately large displacement to the flexible riser, there is a good agreement between the results from present formulation and those presented in [16].
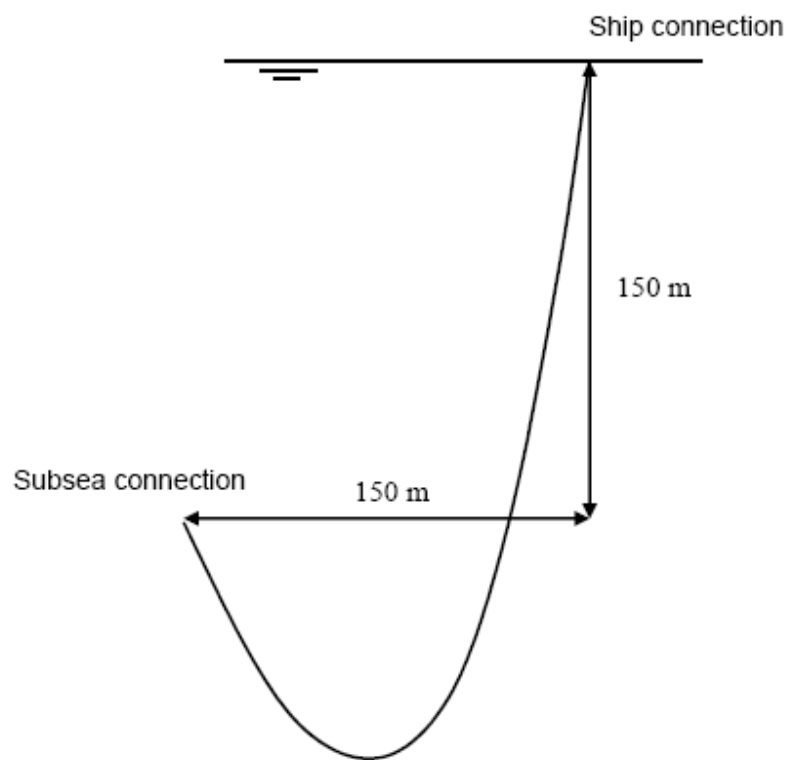
Figure 6.16:. Deep water flexible riser
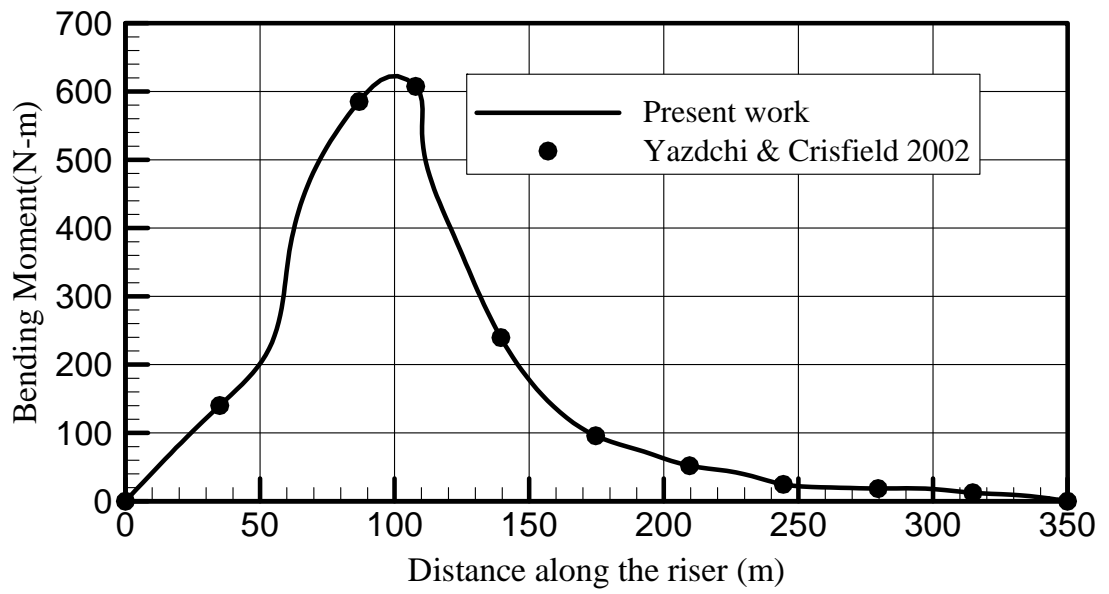
Figure 6.17: Bending moment diagram
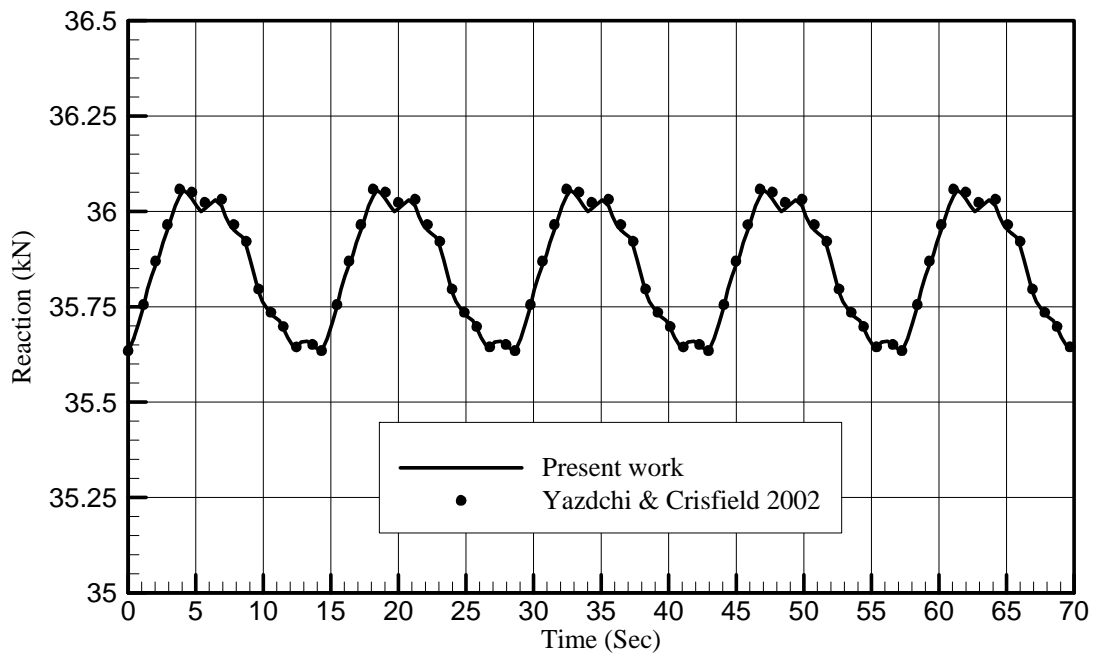
Figure 6.18: Reaction at the sub-sea connected node

Chapter 7

Conclusions and recommendations for future work

7.1 Conclusions

A finite element formulation was presented for geometrically nonlinear dynamic analysis of flexible riser structures in presence of steady state current, riser-soil interaction and buoyancy forces.

The formulation has been derived using an incremental updated Lagrangian approach together with a modified linearization scheme for a three-dimensional flexible riser element. Decomposing the Green-Lagrange strain and the 2nd Piola-Kirchhoff stress into two second-order six termed functions of through-the-thickness parameters, made it possible to explicitly account for the nonlinearities in the direction along the thickness. Moreover, these decompositions led to a particular linearization scheme using Taylor series expansion. It is noted that the employed efficient linearization scheme avoids inaccuracies normally associated with other linearization methods.

The proposed nonlinear finite element formulation has been implemented in a finite element code using a proper nonlinear algorithm. This code is then used to model and analyze some typical riser configurations subjected to the various loading conditions.

Some examples of flexible riser were solved and the results have been compared with those available in the literature. Concerning a flexible cantilever riser subjected by a follower distributed pressure; it has been shown that displacements are in good agreements for moderate range of displacements. According to the results the difference between the results from the present formulation and those in the literature gradually increases when we deal with larger displacements and rotations in flexible riser structures. It is considered that the difference between the two sets of results diverges due to the accuracy which is implied in the present finite element formulation because the linearization process.

 The fluid-solid interaction problem is a significant concern in flexible riser structures where there is a strong coupling between the fluid motion and the risers dynamics behavior. Chapter 4 has therefore been devoted to developing an efficient riser problem fluid-solid interaction algorithm. Two different approaches have been proposed to modify the fluid mesh flow governing elasticity equation matrices. From the result it is noted that both two approaches keep the smaller cells from distortions while the fluid mesh is moved in accordance with the riser's motion.

In view of the fact that the equivalent modeling scheme for simulation of the various layers of a flexible riser fails to model multi layer flexible riser behavior properly, using a more accurate constitutive model for flexible riser structures Using detailed finite element simulation of the risers unbonded layers the constitutive model characterizes the behavior of various riser's layers subjected to different modes of loading. In Chapter 5 this constitutive model is implemented into a generalized finite element formulation which has been developed based on Euler-Bernoulli beam element formulation together with two new degrees of freedom. From the result it is noted that using the constitutive model together with the developed generalized finite element formulation, capability is developed to study the nonlinear behavior of a long length of flexible risers in a very short time.

7.2 Recommendations for future work

The following suggestions are put forward for future investigations.

- Development of a flexible riser constitutive model for proposed nonlinear flexible riser element
- Implementation of the proposed approaches for fluid mesh movement in a fluid code and developing an ALE formulation for the riser problem
- Implementation of the developed flexible riser element together with constitutive model in a fluid code to study VIV

Bibliography

1. O'Brien, P. J. and McNamara, J. F. (1988). 'Analysis of flexible riser systems subject to three-dimensional sea state loading', *Proceedings of the international conference on behaviour of offshore structures, BOSS 88*, Trondheim, Norway, 6 1373-1388.

2. Machado, Z.L. and Dumay, J.M. (1980). 'Dynamic production riser on Enchova field offshore Brazil', *Offshore Brazil conference, Latin America Oil Show*, Rio de Janeiro.

3. Out, J.M.M., Kronemeijer, D.A., van de Loo, P.J. and de Sterke, A. (1995). 'The integrity of flexible pipe: search for an inspection strategy', *Engineering structures*, 17, 4 305-314.

4. Kraincanic, I. and Kebadze, E. (2001). 'Slip initiation and progression in helical armouring layers of unbonded flexible pipes and its effect on pipe bending Behaviour', *Journal of Strain Analysis*, 36, 3 265-275.

5. Kagoura, T., Ishii, K., Abe, S., Inoue, T., Hayashi, T., Sakamoto, T., Mochizuki, T., and Yamada, T. (2003). Development of a Flexible Pipe for Pipe-in-pipe Technology, *Furukawa Review* 24: 69-75.

6. Bahtui A., Hosseini-Kordkheili S.A., Bahai H., Alfano G. (2008e). 'A multi-scale computational model for unbonded flexible risers', *Under development*.

7. Hosseini Kordkheili S.A., Naghdabadi R. (2007), Geometrically Nonlinear Thermoelastic Analysis of Functionally Graded Shells Using Finite Element Method, *International Journal for Numerical Methods in Engineering*, 72, 964-986.

8. Arciniega R.A., Reddy J.N. (2007), Tensor-based finite element formulation for geometrically nonlinear analysis of shell structures, *Computer Methods in Applied Mechanics and Engineering,* 196, 1048–1073.

9. Arciniega R.A., Reddy J.N. (2007), Large deformation analysis of functionally graded shells, *International Journal of Solids and Structures,* 44, 2036-2052.

10. Yu W., Hodges D.H.(2004), A geometrically nonlinear shear deformation theory for composite shells, *Journal of Applied Mechanics,* 71, 1-9.

11. Woo J., Meguid S.A. (2001), Nonlinear analysis of functionally graded plates and shallow shells, *International Journal of Solids and Structures,* 38, 7409-7421.

12. Yoo S.W., Choi C.K. (2000), Geometrically nonlinear analysis of laminated composites by an improved degenerated shell element, *Structural Engineering and Mechanics,* 9, 99-110.

13. A. Masud, C.L. Tham, W.K. Liu (2000), A stabilized 3-D corotational formulation for geometrically nonlinear analysis of multi-layered composite shells, *Computational Mechanics*, 26, 1–12.

14. C.L. Tham, Z. Zhang, A. Masud (2005), An elastoplastic damage model cast in a corotational kinematic framework for large deformation analysis of laminated composite shells, *Computational Methods in Applied Mechanical Engineering*, 194, 2641–2660.

15. Hosseini Kordkheili S.A., Bahai, H. (2008), Non-linear finite element analysis of flexible risers in presence of buoyancy force and seabed interaction boundary condition, *Archive of Applied Mechanics,* 78, 765-774.

16. Yazdchi M., Crisfield M.A. (2002), Nonlinear Dynamic Behaviour of flexible marine pipes and risers, *International Journal for Numerical Methods in Engineering,* 54, 1265–1308.

17. Yazdchi M., Crisfield M.A. (2002), Buoyancy forces and the 2D finite element analysis of flexible offshore pipes and risers, *International Journal for Numerical Methods in Engineering*, 54, 61–88.

18. Hosseini Kordkheili S.A., R. Naghdabadi and M. Jabbarzadeh (2008), A Geometrically Nonlinear Finite Element Formulation for Shells Using a Particular Linearization Method, *Journal of Finite Element in Analysis and Design*, 44, 123-130.

19. Zielinski A.P., Frey F. (2001), On linearization in non-linear structural finite element analysis, *Computers and Structures,* 79, 825-838.

20. Bathe K.J. (1982), Finite element procedures in engineering analysis, *Prentice Hall*.

21. Bathe K.J., Ramm E., Wilson E.L. (1975), Finite element formulation for large deformation dynamic analysis, *International Journal of Numerical Methods in Engineering,* 9, 353-389.

22. Bathe K.J., Almeida C.A. (1980), A simple and effective pipe elbow element – linear analysis, *Journal of Applied Mechanics*, 47, 93-100.

23. Bathe K.J., Almeida C.A., Ho L.W. (1983), A simple and effective pipe elbow element, some nonlinear capabilities, *Computers and Structures*, 17, 659-667.

24. Massin P., Al Mikdad M. (2002), Nine node and seven node thick shell elements with large displacements and rotations, *Computers and Structures* 80, 835–847.

25. Jiang L.C., Michael W., Pegg Neil G. (1994), Corotational updated Lagrangian formulation for geometrically non-linear finite element analysis of shell structures, *Finite Element in Analysis and Design*, 18, 129-140.

26. Lee S.J., Kanok-Nukulchai W. (1998), A nine-node assumed strain finite element for large-deformation analysis of laminated shells, *International Journal of Numerical Methods in Engineering,* 42, 777-798.

27. Moita G.F., Crisfield M.A. (1996), A finite element formulation for 3-D continua using the corotational technique, *International Journal of Numerical Methods in Engineering,* 39, 3775-3792.

28. Kanok-Nukulchai W., Taylor R., Hughes T.J.R. (1981), A large deformation formulation for shell analysis by the finite element method, *Computers and Structures,* 13, 19-27.

29. Crisfield M.A. (1981), A fast incremental/iterative solution procedure that handles snap-through, *Computers and Structures,* 13, 55-62.

30. Peng X., Crisfield M.A. (1992), A consistent corotational formulation for shells using the constant stress/constant moment triangle, *International Journal of Numerical Methods in Engineering,* 35, 1829-1847.

31. Djoudi M.S., Bahai H. (2003), A shallow shell finite element for the linear and nonlinear analysis of cylindrical shells, *Engineering Structures,* 25, 769-778.

32. Prema Kumar W.P., Palaninathan R. (1994), Explicit through-thickness integration schemes for geometric nonlinear analysis of laminated composite shells, *Finite Element in Analysis and Design,* 18, 129-140.

33. Brack, M., Troina, L.M.B. and Sousa, J.R.M. (2005). 'Flexible riser resistance combined axial compression, bending, and torsion in ultra-deep water depths', *Proceedings of 24th International Conference on Offshore Mechanics and Arctic Engineering, OMAE05*, June 12-17, Halkidiki, Greece.

34. API Recommended Practice 17B. (2002). *Recommended Practice for Flexible Pipe,* American Petroleum Institute.

35. API Specification 17J. (2002). *Specification for Unbounded Flexible Pipe,* 2nd Ed. American Petroleum Institute.

36. Knapp, R.H. (1979). 'Derivation of a new stiffness matrix for helically armoured cables considering tension and torsion', *International Journal for Numerical Methods in Engineering*, 14, 4 515-529.

37. Felippa, C.A., Chung, J.S. (1980), Nonlinear Static Analysis of Deep-ocean Mining Pipe EM DASH 1. Modeling and formulation, *American Society of Mechanical Engineers,* 80, 48: 6pages.

38. Felippa, C.A., Chung, J.S. (1981), Nonlinear Static Analysis of Deep-ocean Mining Pipe EM DASH 1. Modeling and formulation, *Journal of Energy Resources Technology, Transactions of the ASME*, 103, 11-15.

39. McNamara, J.F., Lane, M. (1984), Practical Modelling for Articulated Risers and Loading Columns, *Journal of Energy Resources Technology, Transactions of the ASME*, 106, 444-450.

40. McNamara, J.F., Lane, M. (1992), 3D Frequency Domain Analysis of Offshore Structures, *Proceedings of the 9th Conference on Engineering Mechanics*, College Station, TX, USA, 192-195.

41. O'Brien, P.J., McNamara, J.F. and Dunne, F.P.E. (1988), Three-dimensional Nonlinear Motions of Risers and Offshore Loading Towers, *Journal of Offshore Mechanics and Arctic Engineering*, 110, 232-237.

42. McNamara, J. F., and O'Brien, P. J. and Gilroy, S. G. (1988). 'Nonlinear analysis of flexible risers using hybrid finite elements', *Journal of Offshore Mechanics and Arctic Engineering*, 110, 3 197-204.

43. Hoffman, D., Ismail, N., Nielsen, R. and Chandwani, R. (1991), Design of Flexible Marine Riser in Deep and Shallow Water, *Proceedings 23rd Annual Offshore Technology Conference, OTC91*, Houston, TX, USA, 253-265.

44. Atadan, A.S., Calisal, S.M., Modi, V.J., and Guo, Y. (1997), Analytical and Numerical Analysis of the Dynamics of a Marine Riser Connected to a Floating Platform, *Ocean Engineering,* 24, 111-131.

45. Chai Y.T., Varyani K.S., and Barlt N.D.P. (2002), Three-dimensional Lump-mass Formulation of a Catenary Riser with Bending, Torsion and Irregular Seabed Interaction Effect, *Ocean Engineering,* 29, 1503–1525.

46. Ong, P.P.A. and Pellegrino, S. (2003). 'Modelling of seabed interaction in frequency domain analysis of mooring cables', *Proceedings of 22nd international conference on offshore mechanics and arctic engineering ASME, OMAE03*, Cancun, Mexico, 1-9.

47. Zhang, Y., Chen, B., Qiu, L., Hill, T. and Case, M. (2003). 'State of the art analytical tools improve optimization of unbonded flexible pipes for deepwater environments', *The 2003 Offshore Technology Conference*, Houston ,Texas, USA, May 5-8.

48. Willden, R.H.J. and Graham, J.M.R. (2005). 'CFD simulations of the Vortex-induced Vibrations of model riser pipes', *Proceedings of the 24th International Conference on Offshore Mechanics and Arctic Engineering, OMAE05*, Halkidiki, Greece, 3, 837-846.

49. Hibbitt, H.D., Becker, E.B. and Taylor, L.M. (1979), Nonlinear analysis of some slender pipelines, *Computer Methods in Applied Mechanics & Engineering*, 17, 203-25.

50. Nielsen, R., Colquhoun, R.S., McCone, A., Witz, J.A. and Chandwani, R. (1990). 'Tools for predicting service life of dynamic flexible risers', *Proc First European Offshore Mechanics Symposium*, Trondheim, Norway, 449-456.

51. Witz, J.A. and Tan, Z. (1989). 'An analysis method for the prediction of the long term mechanical degradation of unbonded flexible pipes', *BPP Report*, No. 7419A for Wellstream Corporation, Houston, USA.

52. Patel, M.H. and Seyed, F.B. (1995). 'Review of flexible riser modelling and analysis techniques', *Engineering structures*, 17, 4 293-304.

53. Smith, R., O'Brien, P., O'Sullivan, T. and Weibe, C. (2007). 'Fatigue analysis of unbonded flexible risers with irregular seas and hysteresis', *The 2007 Offshore Technology Conference, OTC07*, Houston, Texas, USA, April 30-May 3.

54. Lacarbonara, W., Pacitti, A. (2008), Nonlinear Modeling of Cables with Flexural Stiffness, *Mathematical Problems in Engineering*, Available online (doi:10.1155 /2008/370767).

55. Hosseini Kordkheili S.A., Bahai (2007), Non-Linear Finite Element Analysis of Flexible Risers with a Touch down Boundary Condition, *OMAE2007, June 10-15, San Diego ,California, USA*.

56. Hosseini Kordkheili S.A., Bahai (2008), Nonlinear Dynamic Analysis of Flexible Riser Structures, *OMAE2008, June 15-20, Estoril, Portugal*.

57. Hosseini Kordkheili S.A., Bahai (2008e), An updated Lagrangian finite element formulation for large displacement dynamic analysis of three-dimensional flexible riser structures, *Computers and Structures (Under review)*.

58. Hosseini Kordkheili S.A., Bahai (2008e), Nonlinear Dynamic Analysis of Flexible Riser Structures, *Journal of Offshore Mechanics and Arctic Engineering (Under review)*.

59. Bathe K.J. et al. (1978), Some computational capabilities for nonlinear finite element analysis, *Nuclear Engineering and Design,* 46, 429-455.

60. Laver K., Clukey E. and Evans T. (2004), Steel catenary touchdown point vertical interaction models, *OTC 16628*.

61. Chu J., Bo M.W., Chang M.F., Choa V. (2002), Consolidation and permeability properties of Singapore marine clay, *Journal Of Geotechnical And Geoenvironmental Engineering*, Sep., 725-732.

62. Farahani K., Naghdabadi R. (2003), Bases free relations for the conjugate stresses of the strains based on the right stretch tensor, *International Journal of Solids and Structures,* 40, 5887-5900.

63. Zielinski A.P., Frey F. (2001), On linearization in non-linear structural finite element analysis, *Computers and Structures*, 79, 825-838.

64. Ross, M.R. (2006), Coupling and Simulation of Acoustic Fluid-Structure Interaction Systems Using Localized Lagrange. Multipliers, *Thesis directed by Prof. Carlos Felippa*, *University of Colorado.*

65. Belytschko T., Liu W.K. (2001), Moran B., Nonlinear finite elements for continua and structures, *John Wiley and Sons, LTD.*

66. De Boer A., VAN Zuijlen A.H., Biji H. (2007), Review of coupling methods for non-matching meshes, *Computer methods in applied mechanics and engineering*, 196, 1515-1525.

67. Bahtui A. (2008), Development of a Constitutive Model to Simulate Unbonded Flexible Riser Pipe Elements, *Thesis directed by Dr. H. Bahai*, *Brunel University.*

68. Alfano G., Bahtui A., Bahai H. (2008). Numerical Derivation of Constitutive Models for Unbonded Flexible Risers, *Submitted to International Journal of Mechanical Sciences.*

69. BACUS (2001), ABAQUS theory and user's manuals, Version 6.2, Hibbitt, Karlsson & Sorenen, Inc., Pawtucke, Rhode Island, USA.

70. Bathe K.J., Ramm E., Wilson E.L. (1975), Finite element formulation for large deformation dynamic analysis, *International Journal of Numerical Methods in Engineering,* 9, 353-389.

71. Argyris J.H., Symeonidis Sp. (1981), Nonlinear finite element analysis of elastic systems under nonconservative loading – natural formulation. Part I. Quasistatic problems, *Computer Methods in Applied Mechanics and Engineering,* 26, 75-123.

Appendix A – List of all publications resulted from this work

Journal Papers

1. Hosseini Kordkheili S.A., Bahai, H. (2008), Non-linear finite element analysis of flexible risers in presence of buoyancy force and seabed interaction boundary condition, *Archive of Applied Mechanics,* 78, 765-774.

2. Hosseini Kordkheili S.A., Bahai H. (2009), Nonlinear Dynamic Analysis of Flexible Riser Structures, To be published in *Journal of Offshore Mechanics and Arctic Engineering.*

3. Hosseini Kordkheili S.A., Bahai H. (2008e), An updated Lagrangian finite element formulation for large displacement dynamic analysis of three-dimensional flexible riser structures, Submitted for *Computers and Structures.*

4. Bahtui A., Hosseini-Kordkheili S.A., Bahai H., Alfano G. (2008e). A multi-scale computational model for unbounded flexible risers, *Under development.*

Conference Papers

5. Hosseini Kordkheili S.A., Bahai H. (2008), Nonlinear Dynamic Behavior of Flexible Risers, *WCCM8-ECCOMAS2008, June 30 – July 5, Venice, Italy.*

6. Hosseini Kordkheili S.A., Bahai H. (2008), Nonlinear Dynamic Analysis of Flexible Riser Structures, *OMAE2008, June 15-20, Estoril, Portugal.*

7. Hosseini Kordkheili S.A., Bahai H. (2007), Non-Linear Finite Element Analysis of Flexible Risers with a Touch down Boundary Condition, *OMAE2007, June 10-15, San Diego ,California, USA.*

8. Hosseini Kordkheili S.A., Bahai H. (2006), Nonlinear Finite Element Modelling of Flexible Risers Using Pipe Elbow Element, *CST2006, Sep. 12-15, Las Palmas, Spain.*

9. Hosseini Kordkheili S.A., Bahai H. (2006), A Finite Element Formulation for Analysis of Flexible Risers Structures, *MAFELAP2006, June 13*-16**,** *London, UK.*